NRL REPORT 3652

DESIGN OF THE ANTENNA FOR AN/SPS-3 (XDK) HEMISPHERIC RADAR

NAVAL RESEARCH LABORATORY
WASHINGTON, D.C.

[redacted]

NRL REPORT 3652

DESIGN OF THE ANTENNA FOR AN/SPS-3 (XDK) HEMISPHERIC RADAR

P. A. Lantz, J. R. Shoemaker
and
R. J. Adams

April 17, 1950

Approved by:

Mr. A. A. Varela, Head, Search Radar Branch
Mr. L. A. Gebhard, Superintendent, Radio Division II

NAVAL RESEARCH LABORATORY
CAPTAIN F. R. FURTH, USN, DIRECTOR
WASHINGTON, D.C.

DISTRIBUTION

BuShips	
Attn: Code 823A	5
Attn: Code 816	1
OpNav	
Attn: Op-413B2	5
Attn: Op-342E	1
ONR	
Attn: Code 470	2
BuOrd	
Attn: Code Re3	1
Attn: Code Re4a	1
BuAer	
Attn: Code TD-4	1
Dir., USNEL	2
Attn: Dr. T. J. Keary	1
CDR, NADC, Johnsville	1
Attn: Dr. H. Krutter	1
CDR, NATC, Patuxent	1
Attn: Mr. R. L. Hensell	1
CDR, USNOTS	
Attn: Reports Unit	2
SNLO, USNELO, Ft. Monmouth	3
Ch. of Staff, USAF	1
OCSigO	
Attn: Ch. Eng. & Tech. Div., SIGTM-S	1
CO, SCEL	
Attn: Dir. of Eng.	2
Dir., ESL, Belmar, N. J.	2

CONTENTS

ABSTRACT

. This report summarizes the development work accomplished to date on an 80-degree, dual-beam Foster scanner antenna for the hemispheric radar set AN/SPS-3. The scheme of operation is explained with reference to the MIT Radiation Laboratory sketches which accompanied the original proposal for this system. The basic design changes incorporated during development are:

(1) Reorientation of the two pillboxes to permit placing them on a single level in the cone.

(2) Introduction of choke-type, back-to-back toothed mirrors.

(3) Substitution of magnesium for Fiberglas construction.

(4) Use of an integral intermediate shell to provide the necessary strength.

The design of a parabolic cylindrical reflector for collimation of the beams in azimuth is discussed. Wind drag and r-f leakage data are presented for tubing-type and edgewise-strip-type surfaces. The latter requires an unusual strip configuration because of the reflector inclination.

A flat pillbox has been used to determine proper dimensions for the pillbox feed horns, toothed mirrors, and output horns. The construction and r-f characteristics of an experimental scanner are described; the vertical pattern side lobes do not exceed 18 decibels through most of the scanning range; the match is good; and the gain, while 3.5 decibels below theoretical, is reasonably independent of elevation angle.

A description is given of two prototype AN/SPS-3 antennas under construction at the American Machine and Foundry Company.

Magnesium protective coatings are of the greatest importance in view of the salt-water atmosphere to which this antenna will be exposed. Accordingly, salt-spray tests have been made on a number of treated panels, and r-f attenuation measurement studies on treated magnesium waveguide are projected. The results will appear in a forthcoming NRL report.

PROBLEM STATUS

This is an interim report; work is continuing.

AUTHORIZATION

NRL Problem R02-23R
NR 502-230

DESIGN OF THE ANTENNA FOR AN/SPS-3 (XDK) HEMISPHERIC RADAR

INTRODUCTION

The development of a scanning antenna for a hemispheric search radar was begun at the Radiation Laboratory at Massachusetts Institute of Technology, where Gordy [1] showed that a Foster scanner could be made to generate two beams covering a total elevation angle of 80 degrees. This Panoramic Radar project was assigned to the Naval Research Laboratory [2] at the close of the war and given the title AN/SPS-3 (XDK) Hemispheric Radar. Although early plans were for a model suitable for systems tests ashore, the problem was later expanded to include the development of two complete prototype antennas with stable bases.

Summary of System Design

The operational need for this radar and the considerations leading to the choice of its system parameters have been described at length in an earlier report,[3] but are summarized here for convenience. The AN/SPS-3 is intended for installation on destroyers and larger ships, where it will perform one or more of the following functions:

(1) Hemispheric search to a range of at least 15 miles for small aircraft.

(2) Target indication to guns and missiles.

(3) Surface search.

(4) Air traffic control in the landing pattern of carriers.

Of these, hemispheric search is of the greatest importance, and has dictated the use of a narrow-beam, high-speed scanner capable of covering the complete hemisphere once in 4 seconds.

---

[1] *Gordy, W. O. "Proposed Antenna for Panoramic Radar," Report S-55 Radiation Laboratory, Massachusetts Institute of Technology, 22 May 1945 (Secret)*

[2] *BuShips ltr. S-S67-5, (Confidential) Serial 1427 (938) 004190, to NRL, 27 November 1945, requesting assignment of Problem S1192*

[3] *Blake, L. V. "Interim Report on Development of Model SPS-3 (XDK) Shipborne Hemispheric-Search Radar," NRL Report R-3165, 27 August 1947 (Confidential)*

The sensitivity of a radar set drops rapidly if the number of pulses received from a target during each scan is permitted to fall below 4 or 5. In the present case, where the range requirement limits the pulse repetition frequency to 3000 per second, and accuracy requirements limit the antenna beam widths to the order of 2 degrees, a single radar system would need 8 seconds or more to cover the hemisphere. Accordingly, the solid angle to be searched has been divided into two 40-degree elevation sectors and assigned to two separate radar sets, as suggested by Gordy. This results in a single antenna structure, consisting of a dual Foster scanner and a parabolic cylindrical reflector mounted on a stable base. All r-f components, which include a pulse transformer, two high power X-band magnetrons, duplexers, and receiver pre-amplifiers, are to be mounted on the antenna to avoid transmission losses.

The indicator system includes a G scope for tactical evaluation as well as a number of PPI and RHI scopes.

The system parameters relative to normal scanning operation are:

	Lower Beam	Upper Beam
Elevation Coverage	0 - 40°	40 - 80°
Vertical Scan Rate	30/sec	30/sec
Azimuth Coverage	360°	360°
Azimuth Rotation	15/min	15/min
Vertical Beam Width	1.7°	2.5°
Horizontal Beam Width	2.9°	2.9°
Wavelength	3.2 cm ± 1/3%	3.3 cm ± 1%
Pulse Length	2/3 microsecond	
Pulse Rate	3000/sec	
Pulse Power	150 - 200 kw per beam	
Receiver Noise Factor	11 db	
Stabilization Limit, Roll	± 25° (9 sec period)	
Stabilization Limit, Pitch	± 8° (8 sec period)	
Stabilization Accuracy	± 15 min	

When Moving Target Indication is required, the azimuth and elevation scan rates must be cut by a factor of three to increase the number of pulses per target from 5 to 15. This is accomplished by the use of dual speed motors. For surface search operation, the scanner must be stopped with the lower beam on the water.

It was originally planned that the AN/SPS-3 antenna would be mounted at the top of a mast; such a condition fixed the permissible topside weigth at 1000 to 1400 lbs.[4] Present estimates of the weight of the prototype are approximately 750 lbs for the antenna proper, 250 lbs for the r-f components, and 1000 lbs for the stable base, or a total of 2000 lbs. As this is too great a load for the mast of a destroyer, it is planned to use a tripod mast mounting instead. It is possible that a study of the operation of the prototype antenna will lead to a substantial weight reduction.

Radiation Laboratory Model of Dual Foster Scanner

When the Panoramic Radar project was transferred to NRL, Radiation Laboratory furnished a number of preliminary sketches (S 14761 A through S 14761 F) for the dual Foster scanner. Two of these—a cross section and a development—have been modified slightly for clarity and reproduced as Figures 1 and 2 to illustrate the theory of operation. The scanner comprises an outer fixed cone and an inner rotating cone, separated by an annular scanning space. The inner cone carries two parabolic pillboxes on different levels. These are energized by H-flared horns that are fed through wave guide rotating joints at the upper and lower bearings. In the usual symmetrical pillbox, the feed horn obstructs the center of the aperture with the result that the side lobes of the radiation pattern are quite high. The Radiation Laboratory design avoids this defect by using only that part of the parabolic reflector that is included between the vertex and one end of the latus rectum. The feed horn is on the axis, clear of the emerging beam. While this type of construction doubles the focal length required for a given aperture, it seems worthwhile in view of the fact that high side lobes are an acute problem in the design of a Foster scanner.

The beams generated by the two pillboxes are reflected from opposite sides of a toothed double mirror, M_1, into the scanning space, where their paths are indicated by the parallel dotted and dot-dash lines of Figure 1. The rotation of the inner cone is clockwise as seen from the large end (Figure 2); this is equivalent, in Figure 1, to sweeping the output mirror, M_2, from right to left. The angle at which the beams strike M_2 at any given moment is equal to their angle of emergence from the scanner. For example, the lower beam (from the upper pillbox) is pointed up 10 degrees with respect to the output slot at the instant shown, while the upper beam (lower pillbox) is pointed up $22\frac{1}{2}$ degrees. Inspection of this figure shows that the lower beam scans from $27\frac{1}{2}$ degrees down to $22\frac{1}{2}$ degrees up, and the upper beam from 60 degrees up to 10 degrees up. Now the output slots of the scanner are mounted along the focal line of a parabolic cylindrical reflector which provides directivity in the horizontal plane. This assembly is mounted with the axis of the cylinder inclined $22\frac{1}{2}$ degrees back from the vertical (Figure 3), so that the nominal elevation coverage is -5 degree to + $82\frac{1}{2}$ degrees, with a $12\frac{1}{2}$ degrees region of overlap in the middle. A calculation of the "dead time" associated with the passage of M_1 through M_2 shows that the actual scan would be from -$2\frac{1}{2}$ degree to + 80 degrees, with about 8 degrees overlap.

Figure 4 indicates some of the constructional details of the proposed Radiation Laboratory model of the scanner. The inner cone comprises three coaxial conical shells of thin Fiberglas laminate, spaced by layers of polyfoam, while the outer cone is of 1/8 inch Fiberglas. Wherever conducting surfaces are required, aluminum foil is cemented to the Fiberglas. Leakage through the mirror is held to a minimum by the three-quarter-wave transformers at the top of the teeth. If b, h, and h_1 represent the three clearances indicated in

---

[4] *BuShips ltr. (XDK) (916b) Serial C-916-10635 to CNO, Military Characteristics for XDK Radar*

Figure 4, then the normalized series impedance[5] seen by either beam at the entrance to the gap between mirror and outer cone is

$$z = \frac{h^4}{b^2 h_1^2} \qquad (1)$$

with b = 0.300, h = 0.050, and h_1 = 0.175 inch, z = 0.0023; thus the leakage power should be some 26 db down.

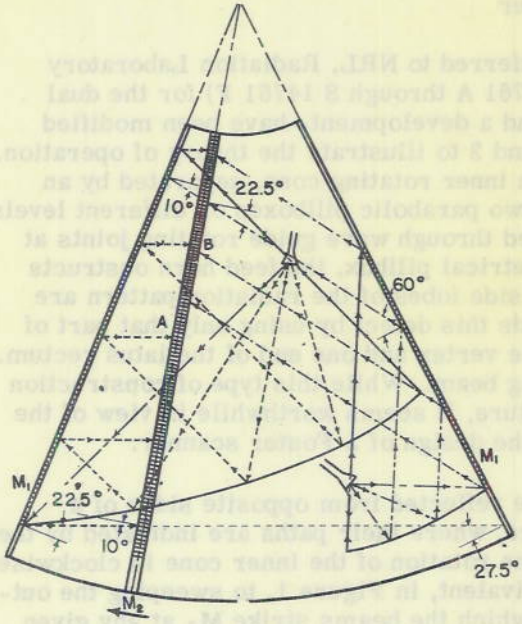

Figure 1 - Development of Radiation Laboratory inner cone
A - Beam from upper pillbox (50" aperture x f = 25")
B - Beam from lower pillbox (18" aperture x f = 9")

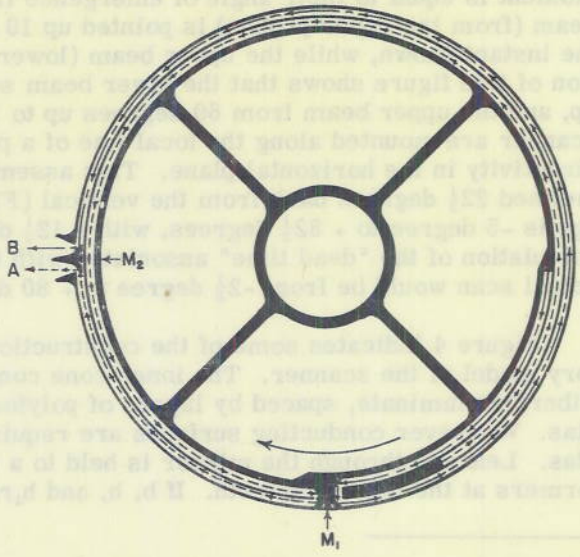

Figure 2 - Cross section of Radiation Laboratory scanner
A - Upper pillbox, lower beam
B - Lower pillbox, upper beam

[5] *Millett, W. E. et.al., "Survey of Foster Scanner Developments," Massachusetts Institute of Technology Radiation Laboratory Report 1074, p. 6, 25 April 1946 (Confidential)*

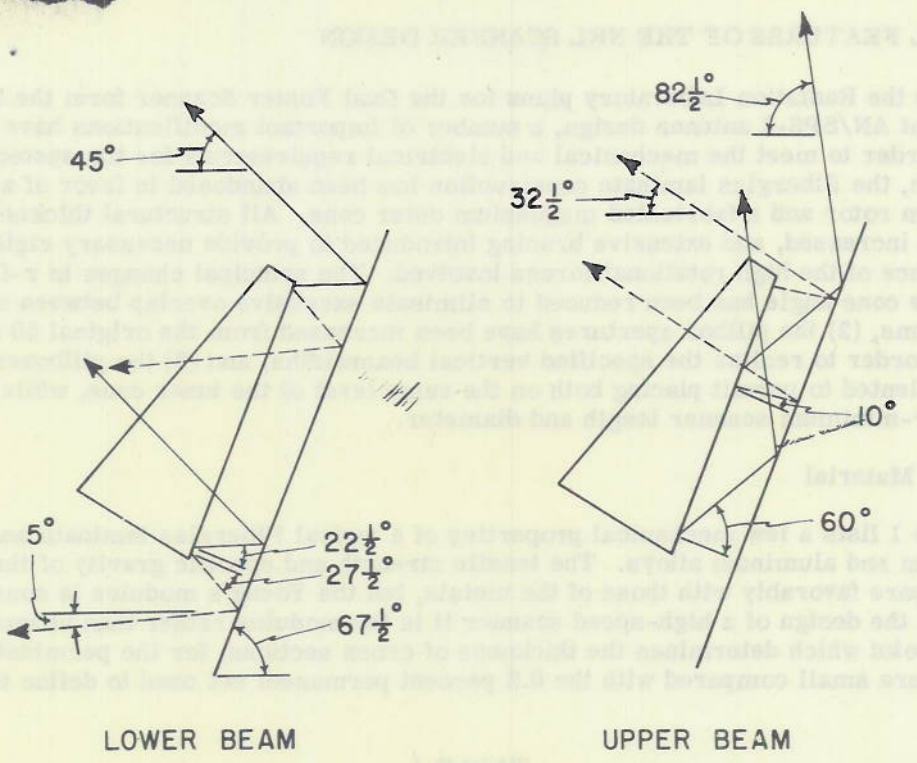

Figure 3 - Flevation coverage of Radiation Laboratory scanner

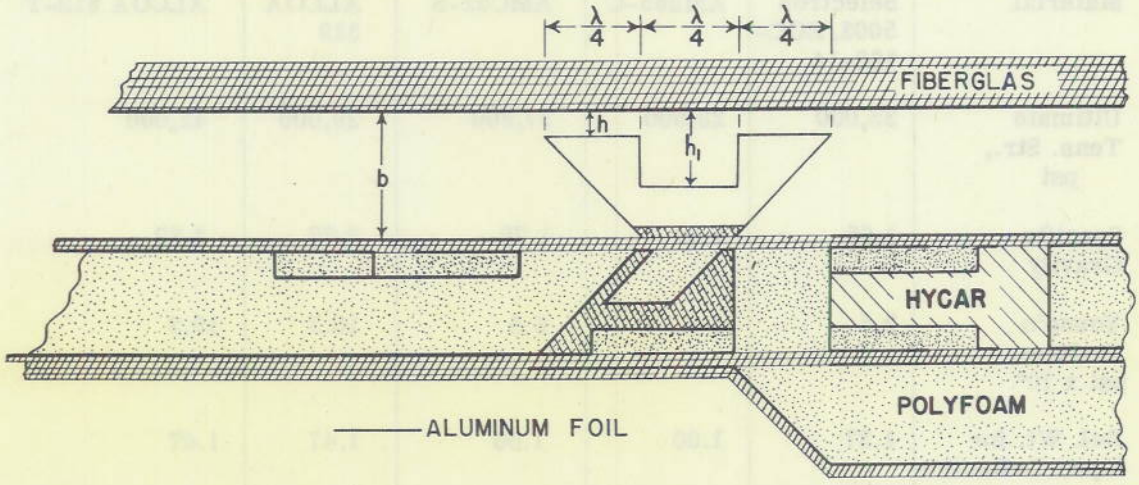

Figure 4 - Detailed cross section of a part of the Radiation Laboratory scanner

GENERAL FEATURES OF THE NRL SCANNER DESIGN

While the Radiation Laboratory plans for the Dual Foster Scanner form the basis of the present AN/SPS-3 antenna design, a number of important modifications have been made in order to meet the mechanical and electrical requirements for the system. In the first place, the Fiberglas laminate construction has been abandoned in favor of a cast magnesium rotor and a fabricated magnesium outer cone. All structural thicknesses have been increased, and extensive bracing introduced to provide necessary rigidity in the presence of the high rotational forces involved. The principal changes in r-f design are (1) the cone angle has been reduced to eliminate excessive overlap between upper and lower beams, (2) the pillbox apertures have been increased from the original 50 and 18 inches in order to realize the specified vertical beamwidths, and (3) the pillboxes have been reoriented to permit placing both on the same level of the inner cone, while attaining a near-minimum scanner length and diameter.

Choice of Material

Table 1 lists a few mechanical properties of a typical Fiberglas laminate and selected magnesium and aluminum alloys. The tensile strength and specific gravity of the Fiberglas compare favorably with those of the metals, but the Young's modulus is considerably lower. In the design of a high-speed scanner it is the modulus rather than ultimate strength or yield point which determines the thickness of cross sections, for the permissible deflections are small compared with the 0.2 percent permanent set used to define the yield point.

TABLE 1
Mechanical Properties of Materials Considered for Use in the Scanner
Type of Construction

	Fiberglas Laminate	Magnesium		Aluminum	
		Cast	Fabricated	Cast	Fabricated
Material	Selectron 5003, ECC-128-14	AM265-C	AMC52-S	ALCOA 319	ALCOA 61S-T
Ultimate Tens. Str., psi	35,000	28,000	37,800	29,000	42,000
Specific Gravity	1.65	1.84	1.79	2.77	2.70
Young's Modulus, psi x 10^6	2.5	6.5	6.5	10.3	10.3
Rel. Wt. for Equal Deflection	1.37	1.00	1.00	1.47	1.47

If the skin of the inner cone is considered as a beam, simply supported from internal ribs, the thickness required to hold the radial deflection within a certain limit is proportional to the square root of the ratio of specific gravity to Young's modulus, so that the over-all

weight of the rotor is roughly proportional to

$$\sqrt{\frac{(\text{Sp. Gr.})^3}{\text{Y. Mod.}}}. \qquad (2)$$

On this basis, magnesium enjoys a considerable weight advantage over Fiberglas (Table 1). There are other arguments against the use of a Fiberglas laminate construction. It is anticipated that some difficulty would be encountered in attempting to hold dimensional tolerances of 0.015 inch when curing a cone 7 feet long. Once the material has hardened, machining is difficult, and there is no satisfactory way of attaching other parts. In particular, it is doubtful if at 1800 rpm cement or glue will hold the rotating mirror to the inner cone.

The need for holding weight to a very minimum has dictated the use of magnesium rather than aluminum, even though use of the lighter metal introduces severe corrosion problems. The inner cone is of cast magnesium, because of the internal bracing, while the outer cone is fabricated from sheet magnesium.

Electrical Design

The pillbox apertures required to produce the specified vertical beamwidths were calculated as follows:

$$\text{Lower Beam: } D = 75^\circ \frac{\lambda}{(\theta_v)_l} = 75^\circ \frac{1.26}{1.7^\circ} = 55.6 \text{ inches}, \qquad (3)$$

$$\text{Upper Beam: } D_u = 75^\circ \frac{\lambda}{(\theta_v)_u} = 75^\circ \frac{1.30}{2.5^\circ} = 39.0 \text{ inches}. \qquad (4)$$

In order to allow for obstruction by a corner of the feed horn, these dimensions have been increased to 56 and 40 inches.

The angular extent of the scanning space on a development of the inner cone has been reduced, somewhat arbitrarily, from 50 to 41 degrees. Since the rotating mirror is included between two elements of the cone 1.61 degrees apart, the total developed cone angle is 42.61 degrees. It was hoped that when allowance had been made for the time lost at tooth passage, each beam would have a clear scanning angle of 40 degrees, but an exact calculation of dead time had to be deferred until the diameter of the upper end of the cone was known. When this had been determined, as described in the next paragraph, it was found that this cone angle was very nearly the smallest that would give 80 degrees coverage with a satisfactory overlap between beams.

Meanwhile the effective scanning angle of the cone was taken as 40 degrees for the purpose of laying out the pillboxes. The over-all length of the cone seemed to be the most critical dimension from a mechanical standpoint; it was minimized by computing the cone length required for each beam separately in terms of the angle, θ, between the aperture of the upper pillbox and the rotating mirror, then equating these two lengths and solving for θ. By reference to Figure 5, it is seen that the beam from the upper pillbox occupies a cone length

$$S_1 = (S + 56) \csc (50 + \theta) - S, \qquad (5)$$

where S is the slant height of the cone that is cut from the top of the scanner. In Figure 6, the lower pillbox is inclined at an angle $40 + \theta$ to the toothed mirror to make the beams overlap at the end of the scan. The upper beam requires a cone length

$$S_2 = (40 + S \cos\theta) \csc(50 - \theta) - S. \quad (6)$$

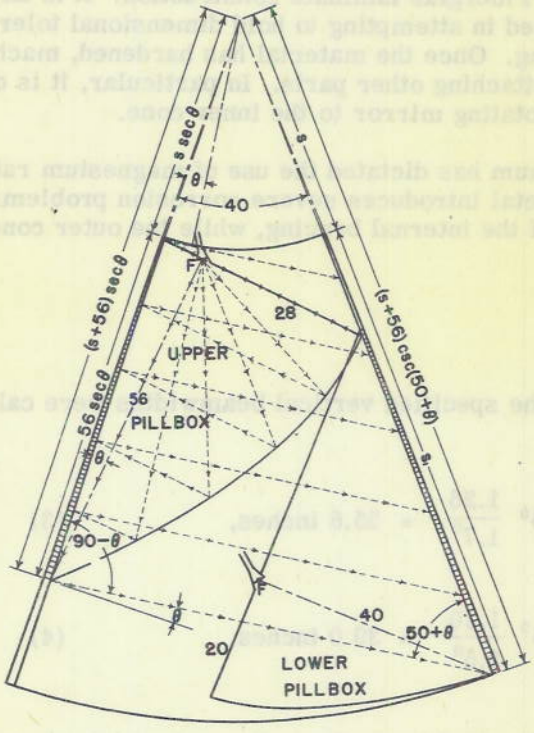

Figure 5 - Ray diagram of upper pillbox showing cone length required

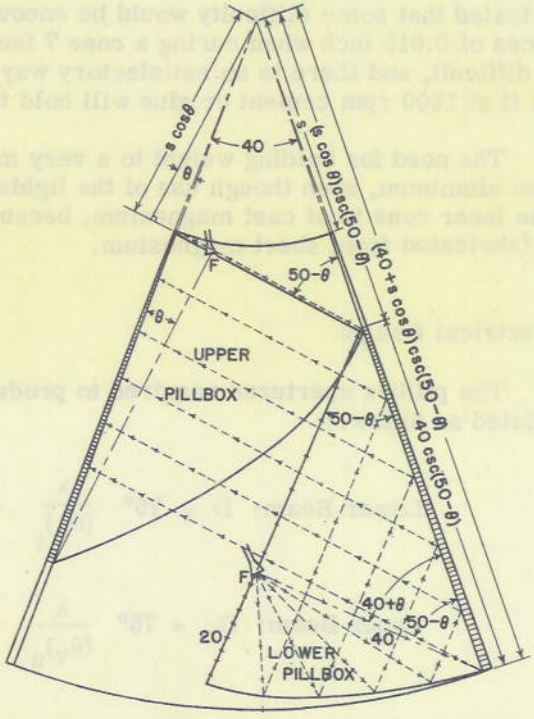

Figure 6 - Ray diagram of lower pillbox showing cone length required

In order to solve for θ, it is necessary to specify the dependence of S on θ. Now the diameter at the top of the scanner is

$$D = \frac{2}{9} S \quad (7)$$

so that S must be kept as small as possible. With this general arrangement of pillboxes, S is minimum when the vertex, V, of the upper pillbox falls at the edge of the scanning space, as shown in Figure 7. By applying the law of sines to triangle OVP, it is seen that

$$(S + 56) \sec\theta = \frac{62.610}{\sin 40} \sin(113.5 - \theta) \quad (8)$$

or

$$S = 97.403 \cos\theta \sin(113.5 - \theta) - 56. \quad (9)$$

In Figure 8, values D, S_1, and S_2 are plotted against θ, and the point of intersection of the latter two curves at $\theta = 6\frac{1}{2}$ degrees shows that the minimum cone length is 74.4 inches. However, Figures 5 and 6, which were drawn for this value of θ, indicate that in this compact arrangement, the pillboxes overlap and would have to be placed on separate levels, which is undesirable for mechanical reasons. By reducing θ to 6 degrees, the cone length is increased to 75.05 inches, but (Figure 9) the lower pillbox can be slid down to avoid interference with the upper one. This is the layout adopted for the present design. The diameter at the top of the cone is 8.09 inches.

It is interesting to note that if the upper pillbox were inverted as in Figure 10, the diameter of the scanner could be reduced by some 4-3/4 inches. This would mean a very great saving in weight, but would require two pillbox levels in the inner cone. In addition, an 8-inch diameter at the top of the cone is close to the minimum value required for mounting the upper bearing and waveguide rotating joint.

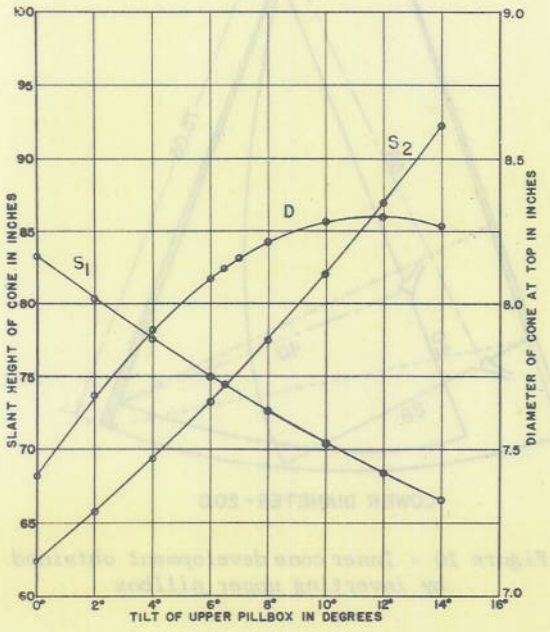

Figure 8 - Dependence of cone dimensions on tilt of upper pillbox
S_1 - *Cone length occupied by lower beam*
S_2 - *Cone length occupied by upper beam*
D - *Diameter of inner cone at top*

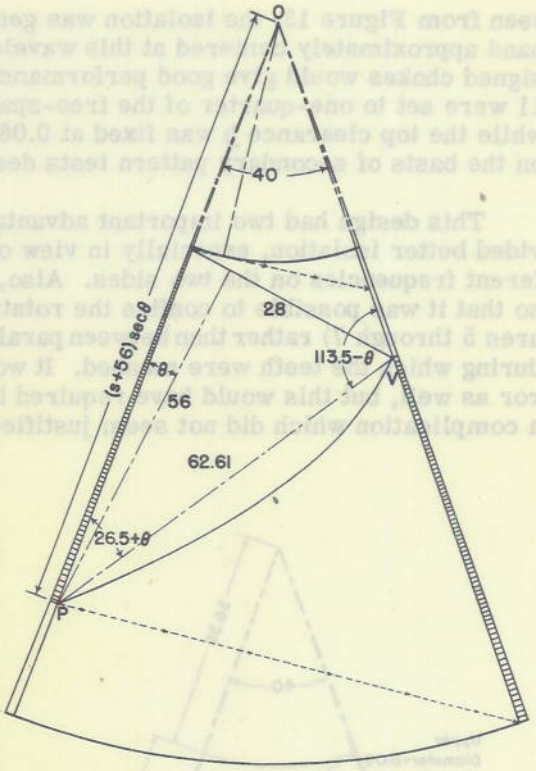

Figure 7 - Development showing how orientation of upper pillbox determines inner cone diameter

Design of Toothed Mirrors

The toothed mirrors of the NRL scanner (Figure 11) are based on the choke principle used in most Foster scanners, rather than on the impedance-step idea shown in Figure 4. The leakage across this type of mirror was checked with the aid of the small test box and probe-fed pillboxes seen in Figure 12. The teeth were 0.093 inch (0.07 wavelength) thick and spaced 0.156 inch (0.19 wavelength) on centers, while the top clearance was 0.060 inch. With output D terminated in a matched load, power was fed into A, and the difference in level at B and C was plotted in Figure 13. The left-hand chokes were cut for a guide wavelength of 3.3 cm, which was reached at a free-space wavelength of 3.265 cm in these $4\frac{1}{2}$-inch pillboxes. As may be

seen from Figure 13, the isolation was generally better than 40 decibels over a 4.7 percent band approximately centered at this wavelength. Thus it appeared that theoretically designed chokes would give good performance. Accordingly, dimensions a and b of Figure 11 were set to one-quarter of the free-space wavelengths 3.3 and 3.2 cm respectively, while the top clearance h was fixed at 0.060 inch. Dimensions c and d were determined on the basis of secondary pattern tests described in a later section of this report.

This design had two important advantages over the impedance-step mirror. It provided better isolation, especially in view of the fact that the chokes could be tuned to different frequencies on the two sides. Also, the over-all width of the teeth was arbitrary, so that it was possible to confine the rotating mirror between elements of the cone (Figures 5 through 7) rather than between parallel lines (Figure 1) and thereby reduce the time during which the teeth were meshed. It would have been desirable to taper the fixed mirror as well, but this would have required bending the output horns to bring them parallel, a complication which did not seem justified by the possible reduction in scanning dead time.

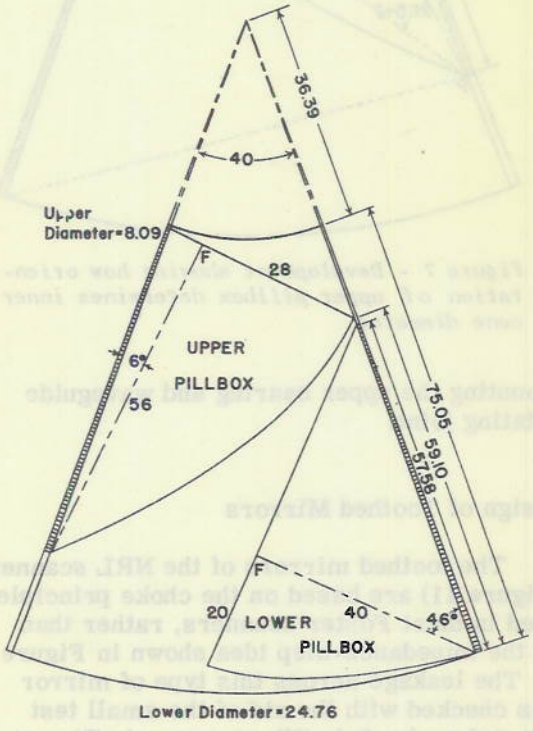

Figure 9 - Development of inner cone, showing layout used on NRL scanner

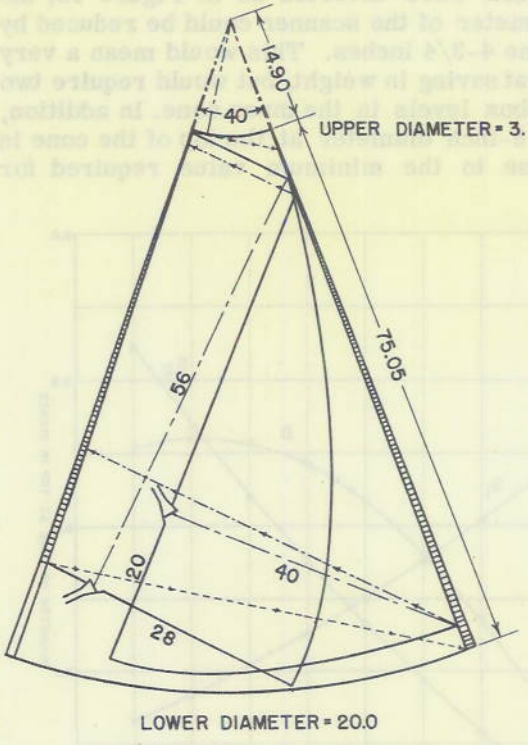

Figure 10 - Inner cone development obtained by inverting upper pillbox

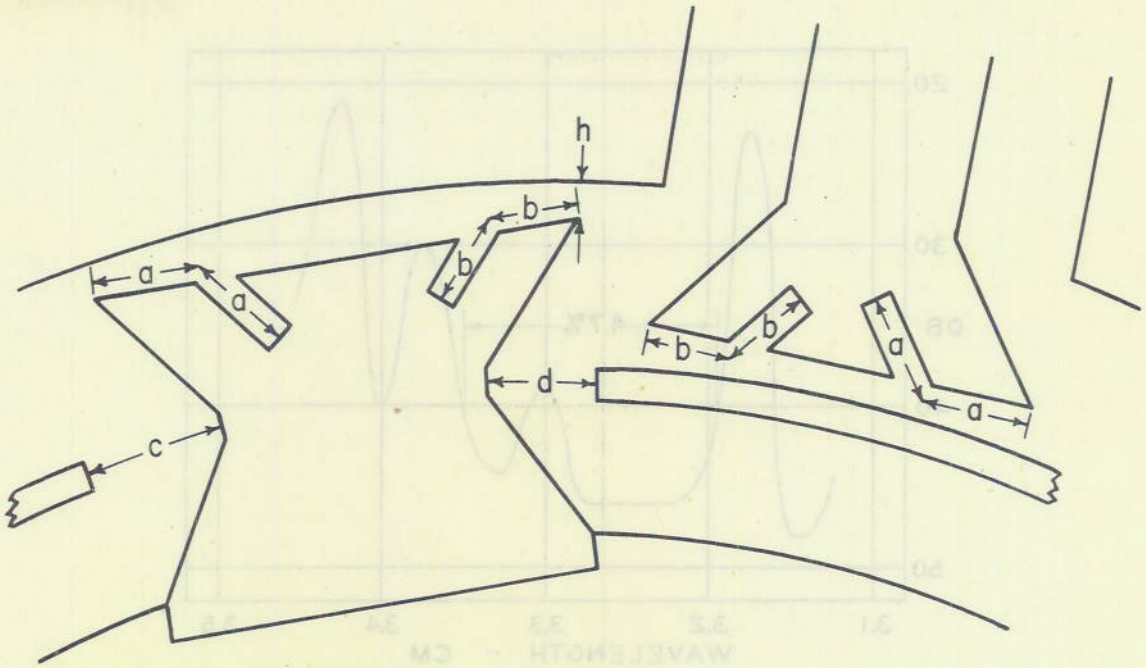

Figure 11 - Toothed mirrors of the NRL scanner, as seen from large end

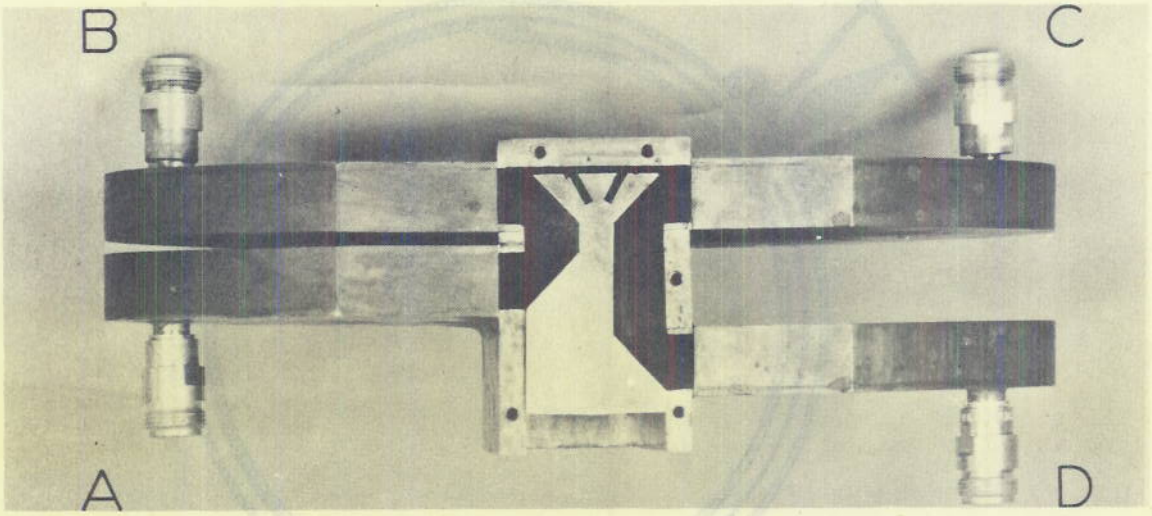

Figure 12 – Apparatus used for testing toothed mirrors. Each pillbox has an aperture of 4½ inches.

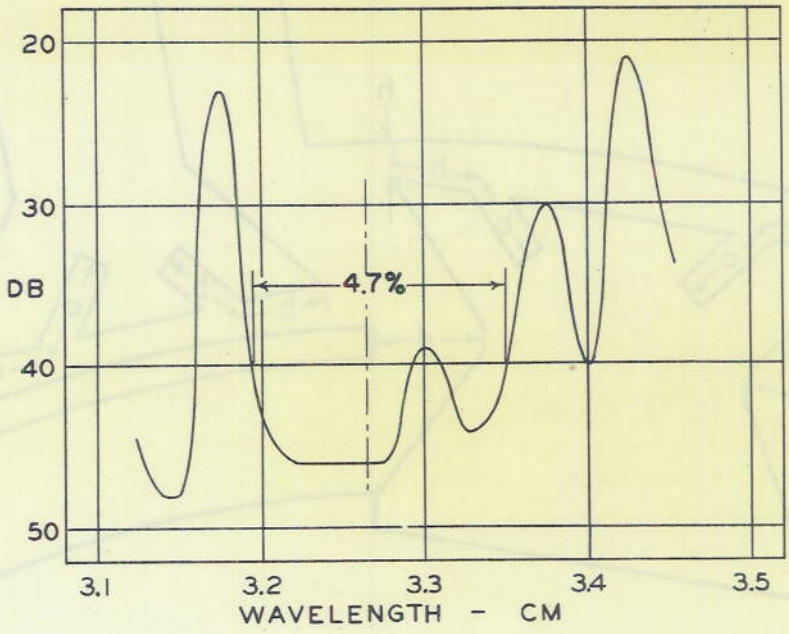

Figure 13 - Measured leakage of a choke-type toothed mirror

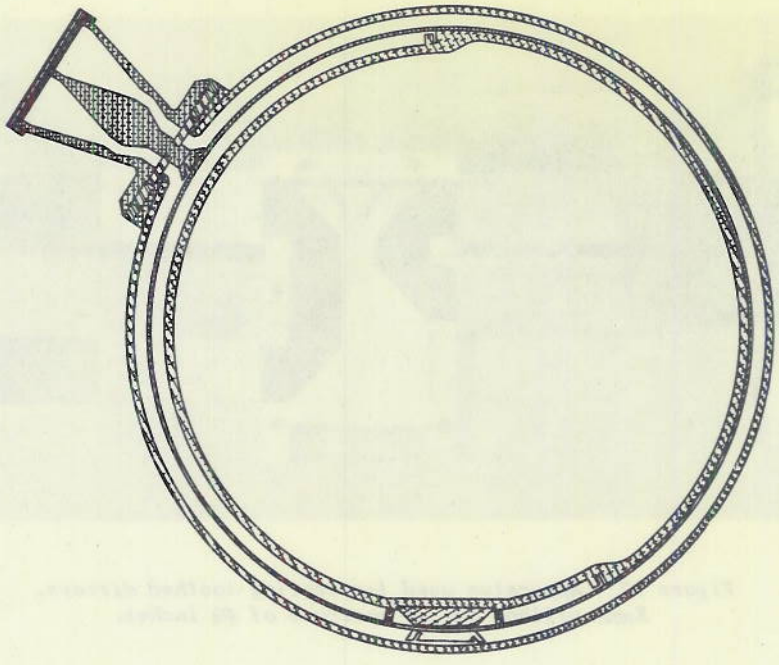

Figure 14 - Cross section of scanner

Constructional Details of Output Horns

Figure 14 is a cross section of the scanner showing the proposed construction of the output horns, in which 1/4-inch magnesium pins are used at 12-inch intervals to support the center web. The Fiberglas weatherizing cover provides additional rigidity.

In an earlier stage of the development, a considerable effort was made towards the design of dielectric windows to be clamped in at the throat of the horns. One of the configurations that was studied (Figure 15-a) consisted of a full-wave resonant Fiberglas window supported on 1/4-inch flanges, and choked to prevent leakage. This is the thinnest resonant window having the necessary mechanical strength, but electrical tests showed that its bandwidth was inadequate.

Figure 15-b shows a second design, based on the principle of the T-shaped dielectric plug.[6] In this scheme the two end sections act as quarter-wave transitions into a three-quarter-wave window to minimize reflection over a wide band. Electrical continuity through the flanges is provided by magnesium wires (B and S gauge 20) embedded in the laminate at 3/16-inch intervals. However, when a section was made up and tested in a parallel-plate region 56 inches wide, it caused severe deterioration of the pattern and gain. This was probably the result of poor contact between the wires and the metal plates. In the light of these experiments, dielectric windows were abandoned in favor of the metal pins described above. A further consideration was the dielectric loss of nearly 1 decibel inherent in either of these designs.[7]

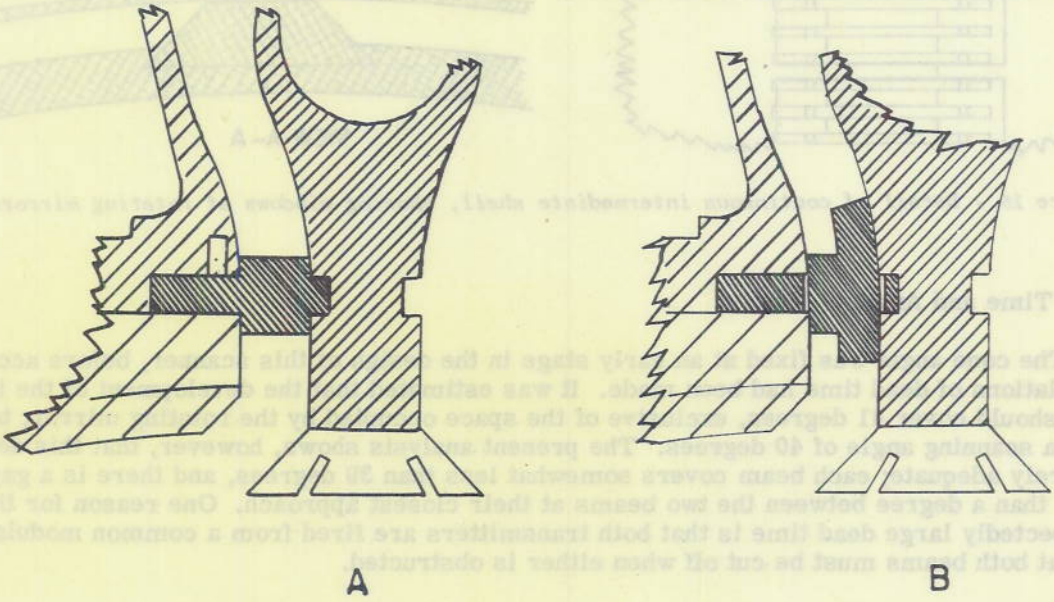

Figure 15 - Fiberglas r-f windows for supporting midsection of output horns

---

[6] *Ragan, G. L. "Microwave Transmission Circuits," Radiation Laboratory Series Vol. 9, Art. 4-21, New York, McGraw-Hill, 1948*

[7] *The Fiberglas used in these measurements, ECC 128-14 with Selectron 5003, had a dielectric constant of 4.07 and a loss tangent of 0.010.*

Construction Details of Intermediate Shell

Since the inner cone rotates at 1800 rpm, the stresses and deformation of the intermediate shell are major problems in the mechanical design. It was originally planned that the shell would be slotted to provide for passage of the beams at the rotating mirror. This would leave a free edge 57 inches long on either side, to be constrained against centrifugal force by a row of metal pins as indicated in Figure 14. However, a stress analysis based on analogy to a spoked flywheel indicates the shell would fail at the support points unless additional pins were distributed around the circumference. This would involve placing pins within the pillboxes, causing unusually severe pattern deterioration. On the other hand, if a continuous shell were used and all radial constraints removed, the resulting hoop tension and deflection would be well within allowable limits. This might be achieved without incurring excessive transmission losses by cutting out rectangular windows at the rotating mirrors (Figure 16), leaving 1/8-inch straps between. If the center-to-center spacing of the straps is 3/4 inch and the strap width is 1/8 inch, the tension in the straps will still be within limits; at the same time there will be no spurious diffraction lobes set up in either beam, and the gain reduction arising from the obstruction of the aperture should not be excessive. Alternatively a thin Fiberglas sheet might be molded across the gap, with slots to accommodate each of the teeth.

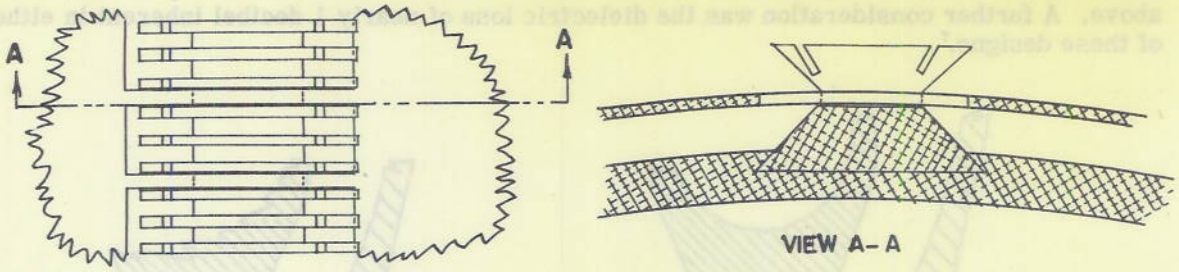

Figure 16 - Detail of continuous intermediate shell, showing windows at rotating mirrors

Dead Time and Angle of Scan

The cone angle was fixed at an early stage in the design of this scanner, before accurate calculations of dead time had been made. It was estimated that the development of the inner cone should cover 41 degrees, exclusive of the space occupied by the rotating mirror, to ensure a scanning angle of 40 degrees. The present analysis shows, however, that this design is barely adequate; each beam covers somewhat less than 39 degrees, and there is a gap of more than a degree between the two beams at their closest approach. One reason for the unexpectedly large dead time is that both transmitters are fired from a common modulator so that both beams must be cut off when either is obstructed.

By referring to View A-A of Figure 17, it is seen that at least one beam is obstructed from the time the leading edge of the fixed mirror (here thought of as moving) passes the edge of the intermediate shell (Condition 1) until the trailing edge clears the gap (Condition 2). The cone rotates through an angle of $360^0 \times (1.391/29.440) = 17.010$ degrees in going from Condition 1 to the fully meshed position, and a further angle of $360^0 \times (1.641/42.254) = 13.981$ degrees to reach Condition 2. These correspond to scanning angle losses of 2.013 and 1.655 degrees respectively, so that each beam covers 42.610 - 3.668 = 38.942 degrees. The dead time amounts to 8.6 percent.

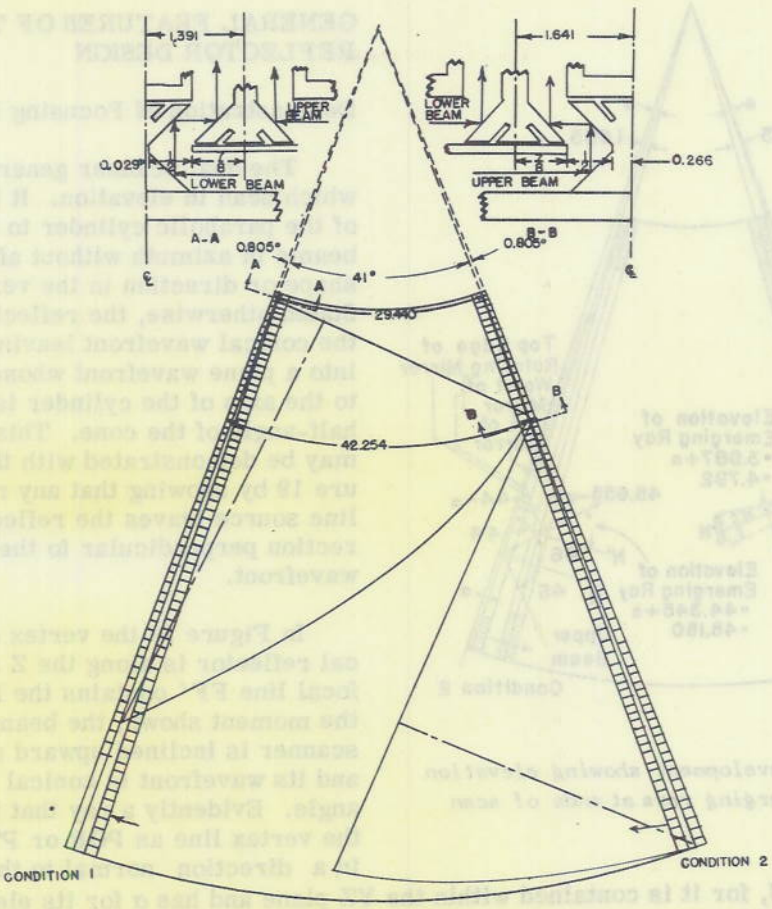

Figure 17 - Development of scanner, showing dimensions which determine the dead time

In order to determine the actual angles of scan with respect to the output slot, it is necessary to find the angle of emergence of the lower beam in Condition 1, and of the upper beam in Condition 2. These angles are 4.792 and 45.150 degrees up, respectively, as illustrated by Figure 18. Thus, the lower beam scans from 34.150 degrees down to 4.792 degrees up, while the upper scans from 45.150 degrees up to 6.208 degrees up. If the reflector is tilted back 33 degrees, the coverage will be from 1.15 degrees below the horizon to 78.15 degrees above with a gap of some 1.4 degrees between beams. Fortunately, the gap amounts to less than a beamwidth, so that the signal level at cross-over is down only 1.3 db.

The scanning angle could be extended by increasing the cone angle, or by increasing its diameter and so reducing the dead time. The mechanical design of the antenna has now progressed to a point where neither of these changes can be contemplated. However, the present design seems to be adequate electrically, and has the advantage of a minimum size and weight.

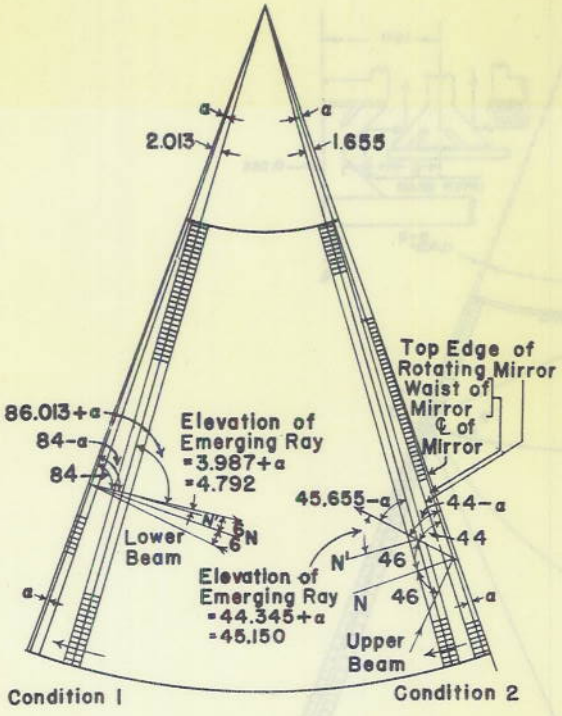

Figure 18 - Development showing elevation angle of emerging rays at ends of scan

GENERAL FEATURES OF THE NRL REFLECTOR DESIGN

Demonstration of Focusing Property

The dual scanner generates two beams which scan in elevation. It is the function of the parabolic cylinder to focus these beams in azimuth without affecting their shape or direction in the vertical plane. Stated otherwise, the reflector converts the conical wavefront leaving the scanner into a plane wavefront whose inclination to the axis of the cylinder is equal to the half-angle of the cone. This property may be demonstrated with the aid of Figure 19 by showing that any ray from the line source leaves the reflector in a direction perpendicular to the plane of this wavefront.

In Figure 19 the vertex of the cylindrical reflector is along the Z axis, while its focal line FF' contains the line source. At the moment shown, the beam leaving the scanner is inclined upward at an angle α, and its wavefront is conical with this half-angle. Evidently a ray that is reflected at the vertex line as POR or P' O' U, leaves in a direction normal to the assumed wavefront RSTU, for it is contained within the YZ plane and has α for its elevation angle. Any other ray PQS takes the same direction, for it (1) has an angle of elevation equal to α, and (2) a vertical plane through QS is parallel to the YZ plane. The first statement follows from the fact that the incident ray PQ and reflected ray QS are co-planar with the normal QN and make equal angles with it. Thus, the two right spherical triangles seen in Figure 19 are congruent, so that the elevation angle δ of QS is equal to α. To prove the second statement, it is noted that

$$\left.\begin{aligned} \phi &= \theta + (\theta + \beta - 90^0) = 2\left(\theta + \frac{\beta}{2}\right) - 90^0 = 90^0 \\ \text{for } \theta &= \tan^{-1}\left(\frac{2f'}{-x_1}\right) \text{and } \frac{\beta}{2} = \tan^{-1}\left(\frac{x_1}{2f}\right), \text{ where } Q = (x_1, y_1, z_1). \end{aligned}\right\} \quad (10)$$

It is easy to show that points R and S, in which rays POR and PQS pierce the wavefront, have equal Z coordinates, so that P maps into a horizontal line on the wavefront. This means the reflector has no effect on the vertical pattern, for it redistributes the energy in horizontal planes only.

Choice of Aperture and Focal Length

The horizontal aperture of the reflector was chosen as 31 inches to provide beam widths of 2.85 and 2.95 degrees at the two operating frequencies. This computation was based on an

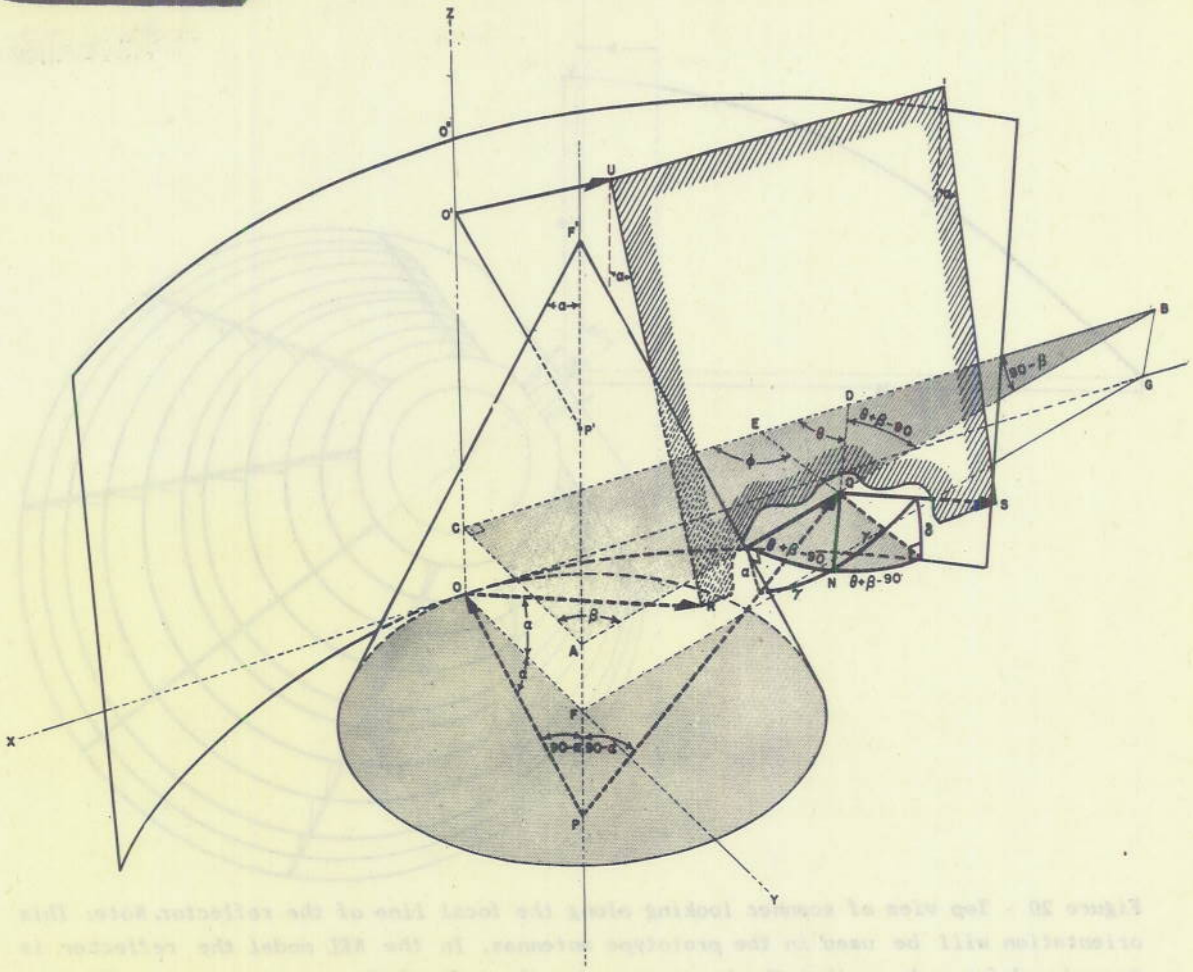

Figure 19 - Reflection of a conical wavefront from a cylindrical parabola

assumed illumination distribution for which the product of beamwidth and aperture in wavelengths would be 70 degrees—rather than 75 degrees as in the case of the pillboxes—in order to obtain more efficient use of the reflector.

It was necessary to remove a five-inch strip from the vertex edge of the reflector to be sure the beam would clear the bracing fins on the outer cone (Figure 20). Then, since the outer edge of the reflector was 36 inches from the axis, an 18 inch focal length was chosen.

Calculation of End Contours of Reflector

Although the vertical aperture of the larger pillbox in the scanner is only 56 inches, the cylindrical reflector must be on the order of 120 inches high to accommodate the wide angle of scan. The wind drag on such a large structure creates a troublesome overturning moment about the stabilization axis, so that it is of the greatest importance to hold the reflecting surface area to the minimum by proper design of the upper and lower contours.

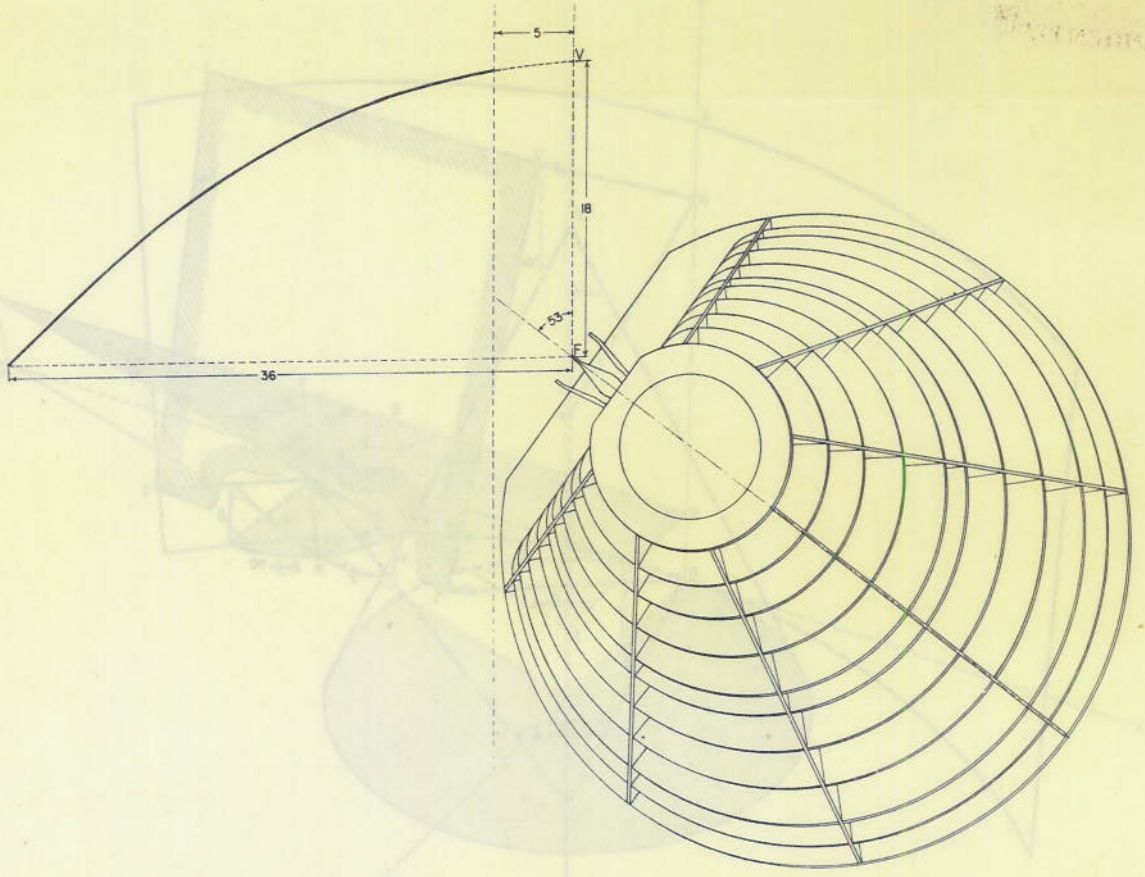

Figure 20 - Top view of scanner looking along the focal line of the reflector. Note: This orientation will be used in the prototype antennas. In the NRL model the reflector is turned end for end, so that the beams pass to the left of the scanner, as seen from the reflector.

The shape of the lower end of the reflector is determined by the lower beam in its extreme angle of scan, 34 degrees down, where the limiting cone of rays emerges from the lowest point of the output horn. As indicated in Figure 21A, it is the intersection of this cone and the parabolic cylinder that determines the lower contour of the reflector:

$$\left.\begin{aligned} x^2 + y^2 - (z - z_1)^2 \tan^2 \alpha_1 &= 0 \\ y &= \frac{x^2}{4f} - f \,. \end{aligned}\right\} \qquad (11)$$

The projection of this curve onto the XZ plane is obtained by eliminating y from Equation (11):

$$z = z_1 + \left(\frac{x^2}{4f} + f\right) \cot \alpha_1 \,. \qquad (12)$$

But $z_1 = d \cot \alpha_1$, where d is the normal path length through the output horn. Since d = 5 inches, f = 18 inches, and α_1 = 124 degrees, Equation (12) becomes

$$z = -(0.00937\ x^2 + 15.514), \qquad (13)$$

so that the lower contour is a simple parabola when viewed from the front.

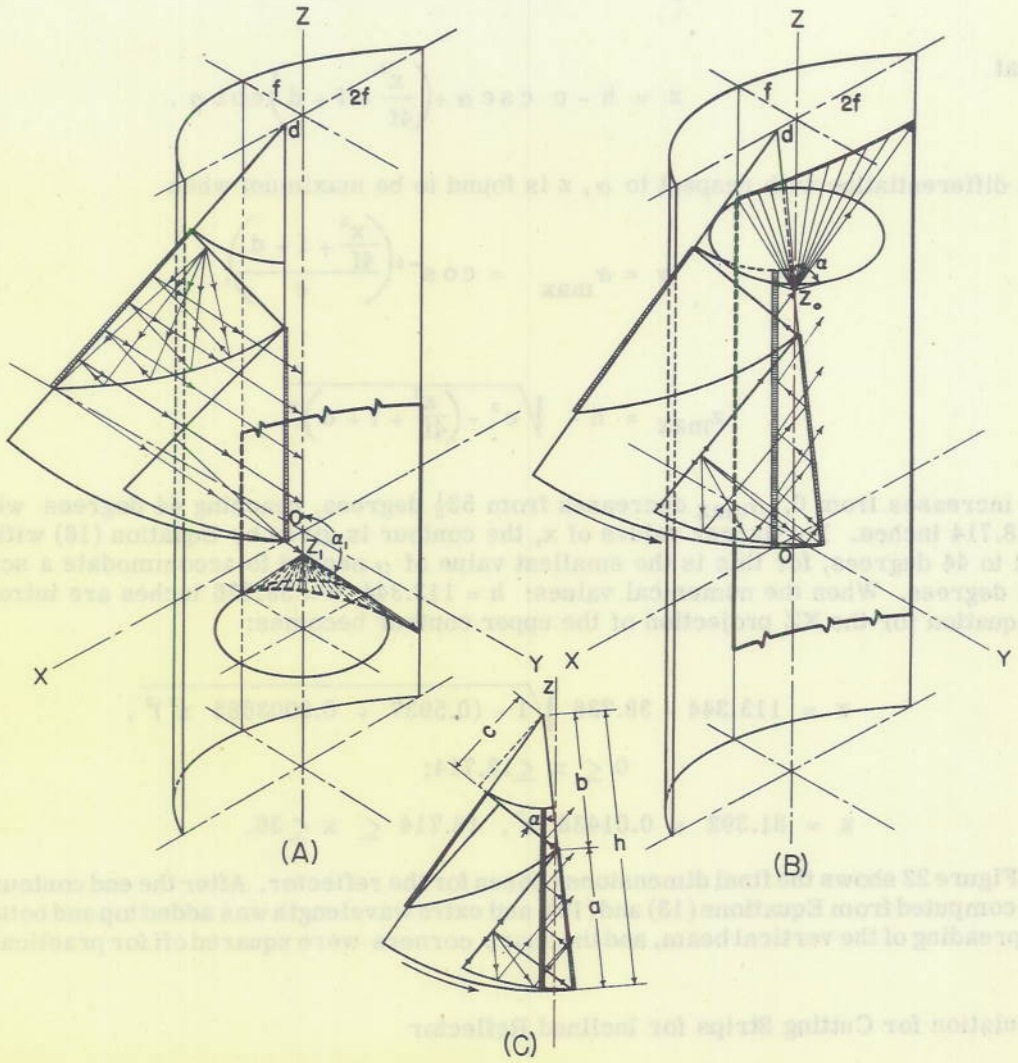

Figure 21 - Determination of reflector end contours, as a function of limits of beam scan

The upper contour is determined by the upper beam, but in this case all angles of scan must be considered, as may be seen from Figure 21B, because the point of emergence of the

limiting cone of rays moves down from the top of the output horn as the scanning angle increases upward. Accordingly, z_o and α are left variable in the XZ plane projection:

$$z = z_o + \left(\frac{x^2}{4f} + f\right)\cot\alpha. \tag{14}$$

Figure 21C shows that

$$z_o = h - c\csc\alpha + d\cot\alpha \tag{15}$$

so that

$$z = h - c\csc\alpha + \left(\frac{x^2}{4f} + f + d\right)\cot\alpha. \tag{16}$$

Upon differentiation with respect to α, z is found to be maximum when

$$\alpha = \alpha_{max} = \cos^{-1}\left(\frac{\frac{x^2}{4f} + f + d}{c}\right), \tag{17}$$

and

$$z_{max} = h - \sqrt{c^2 - \left(\frac{x^2}{4f} + f + d\right)^2}. \tag{18}$$

As x increases from 0, α_{max} decreases from $53\frac{1}{2}$ degrees, reaching 44 degrees when x = 18.714 inches. For larger values of x, the contour is given by Equation (16) with α set equal to 44 degrees, for this is the smallest value of α needed to accommodate a scan up to 46 degrees. When the numerical values: h = 113.344, c = 38.736 inches are introduced, the equation for the XZ projection of the upper contour becomes:

$$z = 113.344 - 38.736\sqrt{1 - (0.5937 + 0.0003585\ x^2)^2},$$

$$0 \leq x \leq 18.714;$$

$$z = 81.392 + 0.01438\ x^2,\quad 18.714 \leq x \leq 36. \tag{19}$$

Figure 22 shows the final dimensions chosen for the reflector. After the end contours had been computed from Equations (13) and (19), and extra wavelength was added top and bottom to allow for spreading of the vertical beam, and the sharp corners were squared off for practical reasons.

Calculation for Cutting Strips for Inclined Reflector

Since low wind drag is particularly important in the design of the SPS-3 cylindrical reflector, an edgewise-strip-type construction may be used. In most X band applications the strips lie in horizontal planes, and so the grating presents a large percentage of open area to the wind. However, the SPS-3 screen is inclined 33 degrees to the vertical, so that horizontal strips cannot be expected to support the currents required for efficient reflection. On the other hand, strips set in planes perpendicular to the axis of the cylinder are effective electrically, but the grating does not appear open from the front. Both objectives may be realized, however, if the strip shape is generated by a horizontal line segment whose length is equal to the depth of the strip which is kept parallel to the fore-and-aft line of the antenna while its forward end traces the curve of intersection of the

parabolic cylinder and a plane perpendicular to the axis. This surface is developable; the strips can be cut from a flat sheet and rolled up to conform to the reflector (Figure 23). If η and x are coordinates in the sheet and θ = 33 degrees is the tilt angle of the reflector, the equation for the front edge of the developed strip (Appendix I) is

$$\eta = x\sqrt{\tan^2\theta + \frac{f}{x}\sec\theta} + f\csc\theta\sinh^{-1}\sqrt{\frac{x}{f}\sin\theta\tan\theta}\,.$$

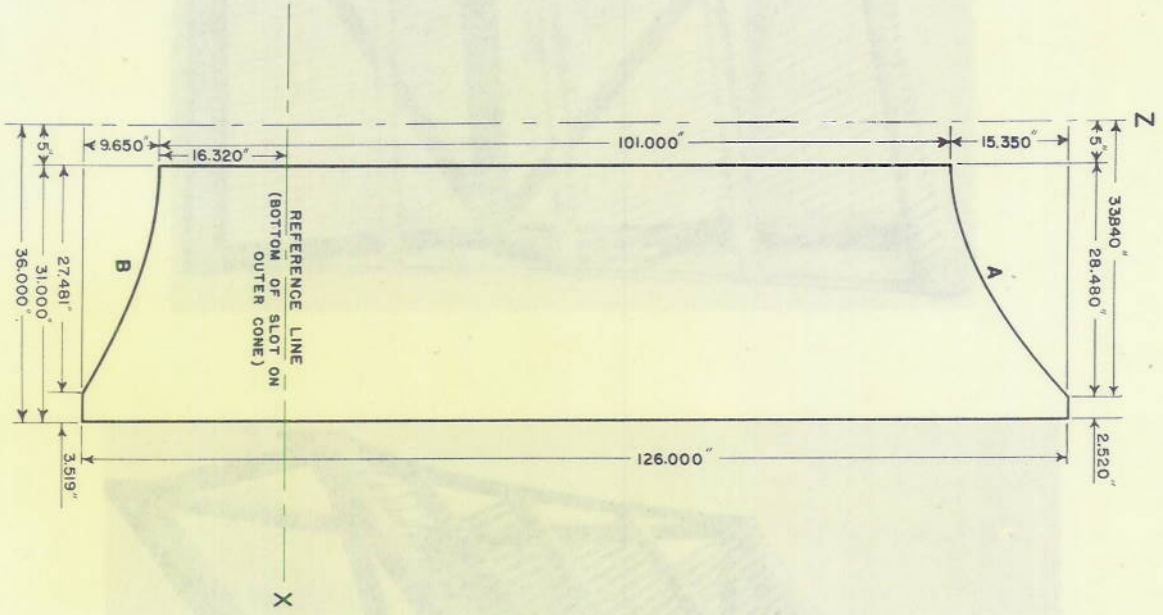

Figure 22 - Projected view of reflector

Wind Drag and Transmission Tests on Edgewise-Strip Reflectors

It was estimated that the r-f power transmission through the reflector should not exceed 1 percent if the back lobe were to be held to 30 db, since the gain of the antenna is only 10 db greater than that of the scanner. Three combinations of strip depth and spacing were selected from the Hayes report[8] to give 20 db leakage at 3.2 cm wavelength, and four test sections were constructed, three with these gratings and one with a solid reflector (Figure 24). These were full-scale models, in cross section, of the SPS-3 reflector, but were only two feet high. The David Taylor Model Basin made wind tunnel tests on all four sections at a wind velocity of 80 knots, measuring the six aerodynamic forces and moments at 20 degree intervals of azimuth. The maximum value of drag relative to that of the solid screen and other data are listed in Table 2 for each of the reflectors.

---

[8] *Hayes, W. D. "Gratings and Screens as Microwave Reflectors," Massachusetts Institute of Technology Radiation Laboratory Report 54-20, 1 April 1943 (Unclassified)*

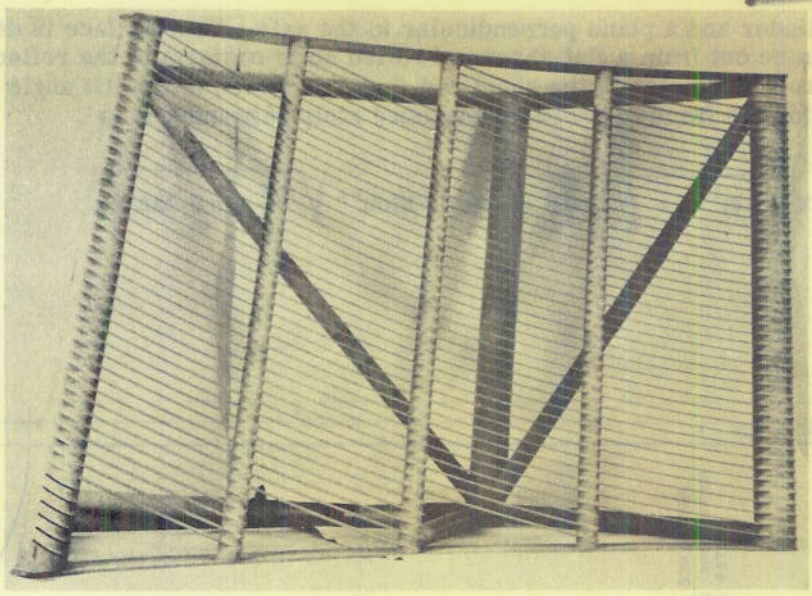

Figure 23 - Front and side views of an inclined, strip-type reflecting screen

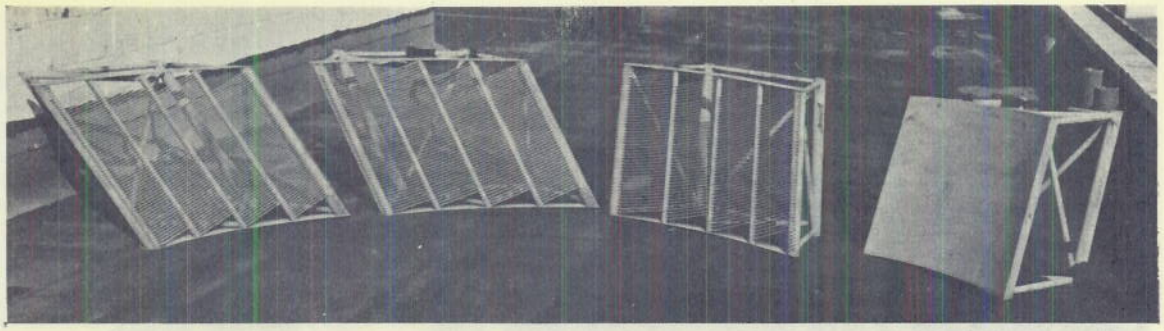

Figure 24 - Various reflecting screen models built for measuring air drag

TABLE 2
Wind Drag and R-F Attenuation of Edgewise-Strip Reflectors

Model	Strip Depth (inch)	Strip Spacing (inch)	Strip Thickness (inch)	Relative Drag (percent)	R-F Attenuation (decibels)
1	--	Solid	--	100.0	50
2	0.350	0.458	0.062	52.3	28
3	0.437	0.534	0.062	53.5	26.4
4	0.591	0.610	0.062	54.4	25.5

The r-f attenuation was measured by mounting the screens at such an angle that the front edges of the strips were in horizontal planes, and then inserting them between two horizontally polarized paraboloidal antennas of 18-inch aperture (Figure 25). An absorbing screen with a 12-inch round aperture was placed between the transmitting antenna and the reflector under test, so that a small area would be illuminated in a uniform manner. The leakage results were considerably better than anticipated. This is undoubtedly explained by the fact that the strips are inclined some 33 degrees to the direction of propagation in this normal incidence case. It is evident from Table 2 that the narrow strip design is superior on the basis of both drag and leakage.

Wind Drag and Transmission Tests on Tubing-Type Reflectors

The reflector used for the SX height finder[9] is constructed from half-inch tubes, spaced 1-3/8 inches on centers, and operates at a mean wavelength of 8.5 cm (3.35 in). From a mechanical standpoint such a reflector has important advantages over one using edgewise strips. It requires less bracing since tubes are inherently stronger than strips, and may therefore achieve a required degree of rigidity with less weight and drag.

---

[9] *Robinson, C. V. et. al., "The SCI Rapid Scan Height Finding Antenna," Massachusetts Institute of Technology Radiation Laboratory Report 688, 9 July 1945 (Restricted)*

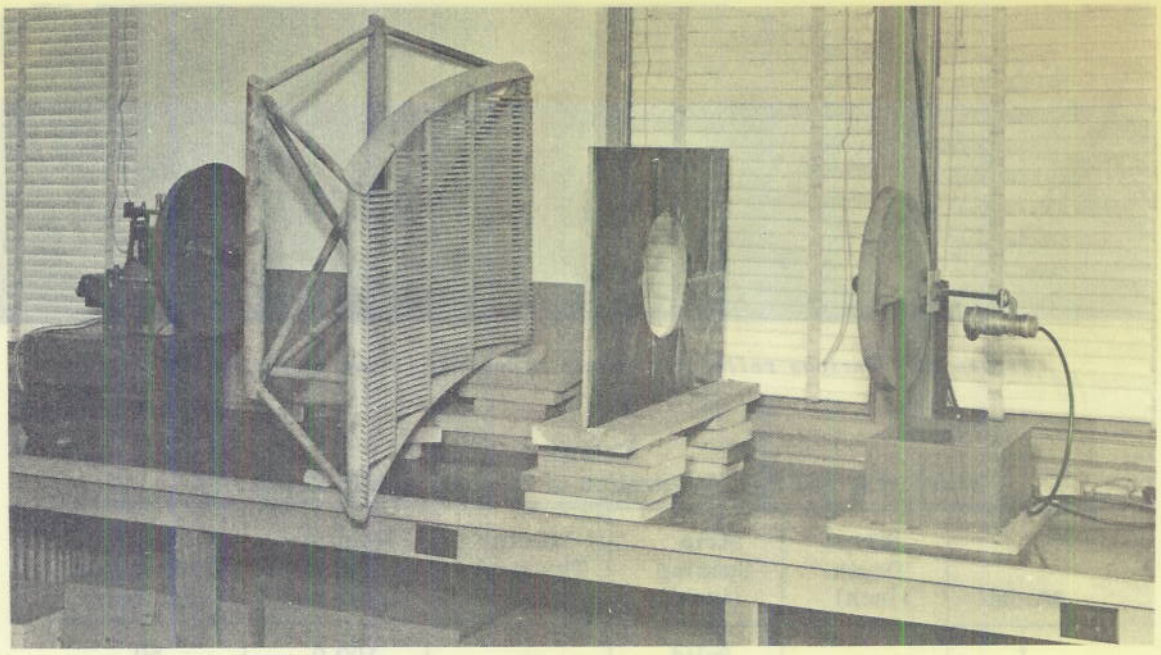

Figure 25 - Arrangement for measuring leakage through reflector gratings

Further, it is easier to manufacture, for tubes may be attached with screws, while the strips are usually welded into slotted members, a process which requires great care if warping is to be avoided.

In order to study the properties of this type of screen, three test sections were constructed, with 1/4-inch aluminum tubes mounted on a wooden frame at 1/2-, 9/16-, and 5/8-inch spacing on centers. Since these screens were not sufficiently rugged for testing in a wind tunnel, their drag was determined with an ordinary room fan. They were swung from three ball bearings mounted along their upper edge, and the horizontal force required to return them to a vertical position was measured. The results are given in Table 3. The attenuation was measured as described in the preceding section.

TABLE 3
Wind Drag and R-F Attenuation of Tubing-Type Reflectors

Model	Tubing Diameter (inch)	Tubing Spacing (inch)	Relative Drag (percent)	R-F Attenuation (decibels)
1	--	Solid	100.0	40
2	0.250	0.500	56.6	27
3	0.250	0.562	44.1	23
4	0.250	0.625	31.6	17

While the half-inch spacing provided the best attenuation, a wider spacing reduced the drag, as might be expected. However, if quarter-inch tubing is to be used in the SPS-3 reflector, the center-to-center spacing should be 9/16 inch. The transmission will not be excessive, and the relative drag will probably lie between 50 and 60 percent when the necessary braces are added. A final choice between strip- and tubing-type reflectors has not been made.

FLAT PILLBOX EXPERIMENTS

Purpose of Experiments with Flat Pillbox

When work on the Hemispheric Radar was started at the Naval Research Laboratory, it was realized that much design information could be obtained by experimenting with a flat pillbox. A unit of this type was considerably easier to build than a conical pillbox, and was readily adaptable to experimental design changes. Accordingly, a flat model of the upper pillbox was constructed with an aperture of 56 inches, a focal length of 28 inches, and a plate spacing of 1/2 inch. Figure 26 shows the pillbox mounted on a pedestal and fitted with output horn and a cylindrical reflector. Radiation patterns were observed by receiving a signal from a megnetron source 300 feet away.

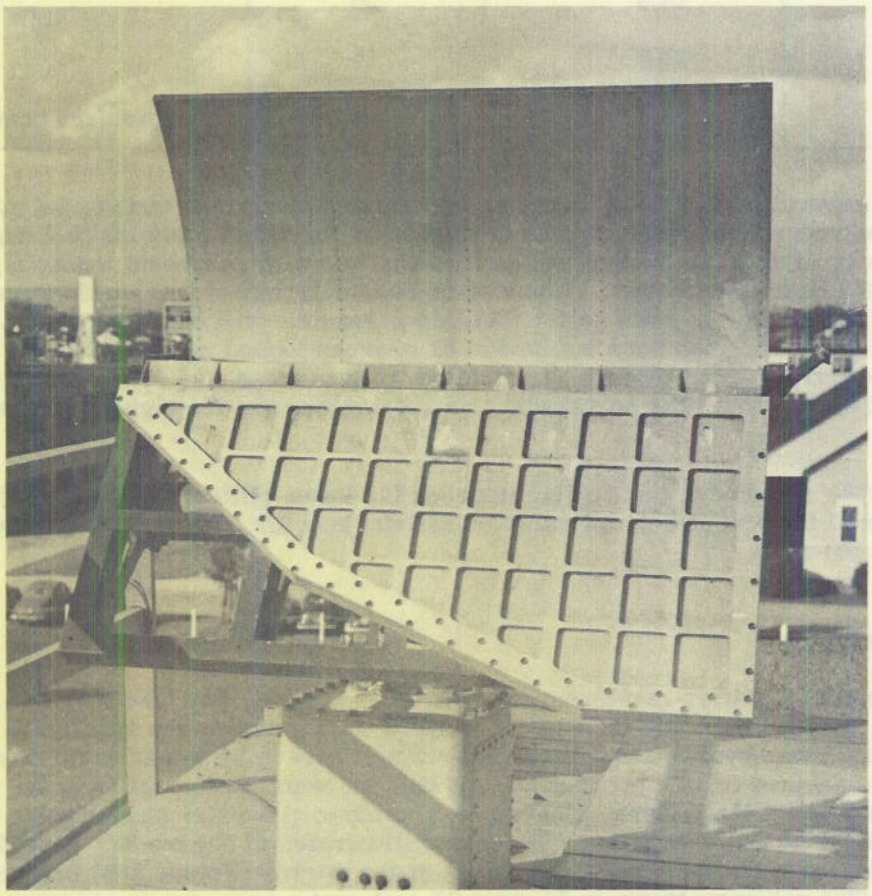

Figure 26 - Flat model of upper pillbox

Design of Pillbox Feed

In passing through the scanner, the pattern of the pillbox suffers deterioration in the process of reflection from the toothed mirrors and because of scattering from the pins or straps used to prevent deflection of the intermediate shell. It was therefore considered desirable to keep the initial side lobe level well below 30 db.

Four experimental feed horns were constructed for the flat upper pillbox on 1 x 1/2 inch waveguide, each 4 inches long and flared in the H-plane to 1-1/2, 2, 2-1/2, and 3 inches respectively. No E-plane flare was used. Free space primary patterns of these feeds were taken at a mid-band wavelength of 3.250 cm to determine the illumination taper that each would provide across the pillbox aperture (Table 4).

TABLE 4
Illumination Characteristics of Feed Horns

Feed Aperture	Illumination Taper	Tilt Angle	Notes
$1\frac{1}{2}$ in	9.8 db	48	Shoulders occurred
2	13.5	53	
$2\frac{1}{2}$	17.5	51	
3	19.0	55	Shoulders occurred

The proper angle of horn tilt for balancing the illumination on the ends of the aperture has also been recorded. These figures are based on the assumption that a 4 degree sector of the parabola adjacent to the vertex has been blanked with absorbent material, to prevent reflection back into the feed. It has since been determined that the illumination at the edges of the mirror is down so far that this precaution will be unnecessary. It can be seen that the 2-1/2-inch horn inclined at 51 degrees looked most promising. However, the best secondary pattern (Figure 27) resulted when the feed was inclined 52-1/2 degrees with respect to the axis. The beamwidth was 1.8 degrees and the highest side lobe was 31 db down.

It should be noted here that no flat model of the lower pillbox was constructed because it was assumed that the same feed would be satisfactory for any similar parabolic reflector of the same f/D ratio.

Design of Barriers

The secondary pattern mentioned above (Figure 27) was observed with a 3-1/2-inch gap between the feed horn and the end of the metal barrier along the axis of the parabola (Figure 28a). It was realized that the barrier would have to be joined to the horn when the pillbox was machined from a metal cone, and that its exact configuration in the vicinity of the feed would affect the pattern. Therefore, a number of barrier shapes were investigated to determine the best arrangement. These are illustrated in Figure 28. Extending the barrier from the corner of the feed to the vertex of the mirror (Figure 28b) produced 26 db side lobes. The schemes shown in Figures 28 c, d, and e gave rise to objectionable shoulders at about the 20 db level. Finally, it was decided to investigate the plan shown in Figure 28f,

varying the taper angle α of the end of the barrier. When this angle was such that the end of the barrier became an extension of one wall of the feed horn, the shape of the beam was somewhat distorted, and the beamwidth was too great. Decreasing the angle α improved the beamwidth, and the best pattern (Figure 29) resulted when the distance, x, was 3-1/2 inches. The beamwidth was 1.70 degrees and the side lobes were down 33 db (at λ = 3.2 cm), which was quite satisfactory. The configuration used to obtain this pattern was therefore adopted as the proper barrier design. The secondary pattern at the lower pillbox frequency of λ = 3.3 cm is shown in Figure 30. Here the side lobes were 31.2 db and the beamwidth was 1.96 degrees. This means that a beamwidth of 56/40 x 1.960 = 2.740 degrees would be expected from the lower pillbox.

Illumination of Pillbox Aperture

The distribution of illumination across the aperture of the pillbox was checked by removing the parabolic reflector and probing the field along this curve as shown in Figure 31. The signal was measured at 5 degrees stations around the parabola and has been plotted against the function

$$\frac{x}{D} = \frac{\sin \theta}{1 + \cos \theta} \qquad (20)$$

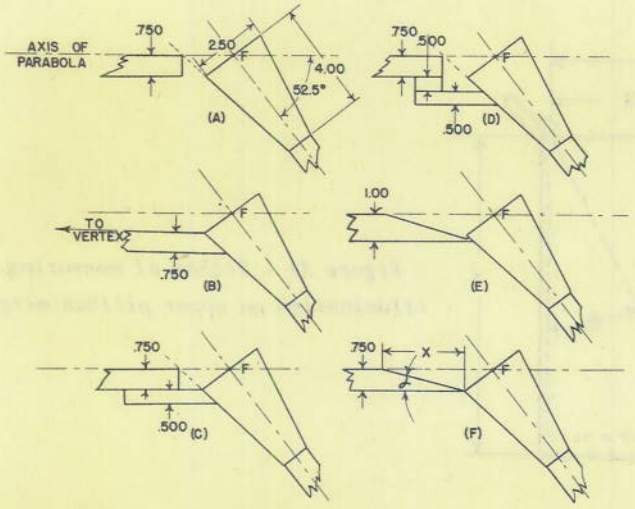

Figure 28 - Suggested arrangements of pillbox barriers adjacent to the feed horns

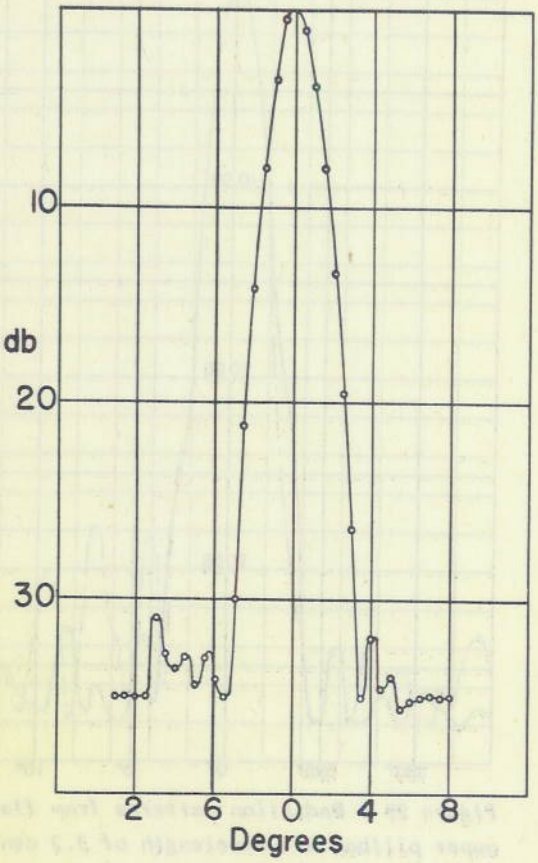

Figure 27 - Radiation pattern of flat upper pillbox

for wavelengths of 3.2 and 3.3 cm in Figures 32 and 33. While the illumination is not perfectly symmetrical, it reaches a satisfactory low level at the ends of the aperture. As a matter of interest, the illumination has been calculated from the free-space primary patterns (curve B). The agreement is fairly good except on the vertex side, where the barrier has a pronounced effect.

Effect of Rotating Mirror on Radiation Patterns

When a satisfactory pillbox design had been achieved, the next step in simulating the scanner in flat parallel plates was the introduction of the rotating mirror.

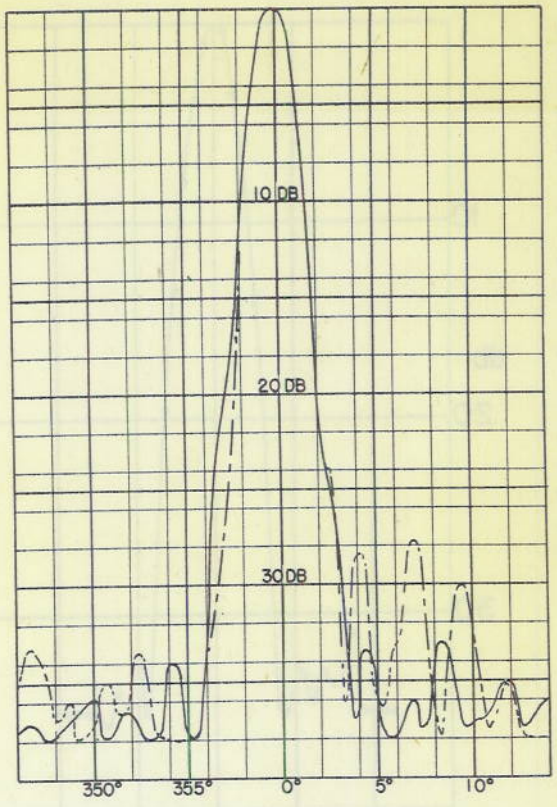

Figure 29 - Radiation patterns from flat upper pillbox at a wavelength of 3.2 centimeters. Dashed curve shows effect of reflection from rotating toothed mirror.

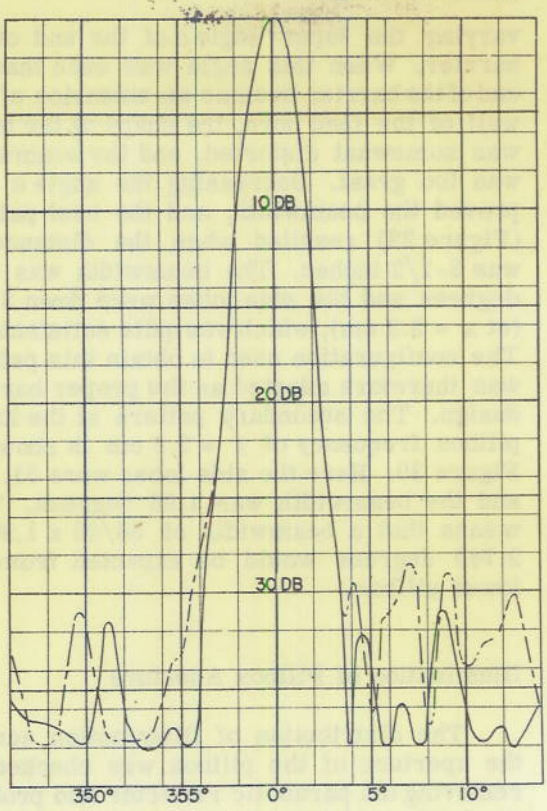

Figure 30 - Radiation patterns from flat upper pillbox at a wavelength of 3.3 centimeters. Dashed curve shows effect of reflection from rotating toothed mirror.

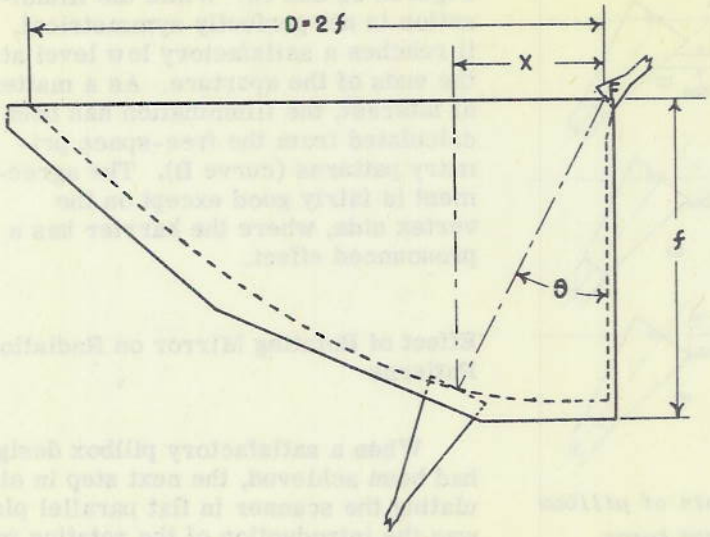

Figure 31 - Method of measuring illumination on upper pillbox mirror

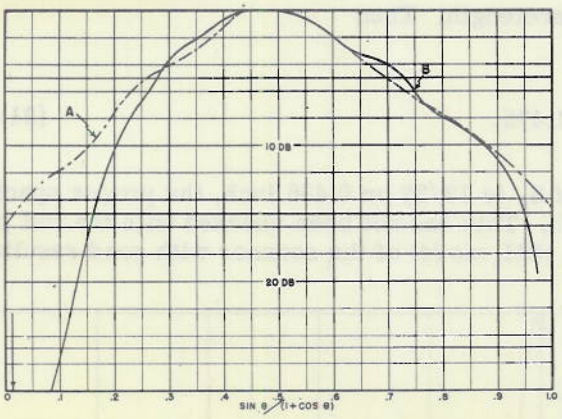

Figure 32 - Illumination of pillbox mirror at 3.2 centimeters. Arrow indicates portion of mirror shadowed by projecting feed.

Curve A - Measured illumination
Curve B - Illumination calculated from free-space pattern

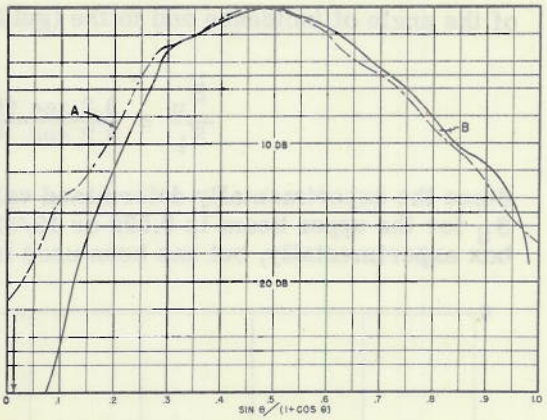

Figure 33 - Illumination of pillbox mirror at 3.3 centimeters. Arrow indicates portion of mirror shadowed by projecting feed.

Curve A - Measured illumination
Curve B - Illumination calculated from free-space pattern

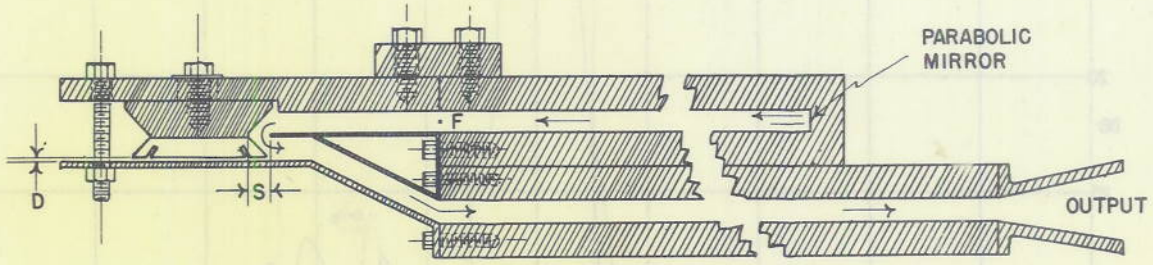

Figure 34 - Cross section of flat pillbox arrangement used for measuring effect of rotating toothed mirror on radiation pattern F - focal point of parabolic mirror

The arrangement shown in Figure 34 was used to study the radiation patterns as a function of the tooth clearance, d, and intermediate shell spacing, s. Figure 35 shows that as d was reduced, the side lobes improved slightly. From a mechanical standpoint, 1/16 inch seemed to be the minimum practical value, and this was adopted. The spacing, s, was somewhat more critical (Figure 37), with optimum performance occurring between 3/8 and 7/16 inch. The dashed curves of Figures 29 and 30 are the pillbox patterns at 3.2 and 3.3 cm wavelength, after reflection from the rotating mirror at optimum adjustment. The highest lobes are 28 and 27 db, as compared with 33 and 31 db without the mirror. Experiments with the arrangement shown in Figure 34 were limited to the case of normal incidence. However, in the scanner the upper beam strikes the mirror at an angle of incidence of 46 degrees (Figure 9), and it might be expected that a different spacing, s, would give the best pattern. Research done at the Radiation Laboratory[10] indicates that this spacing should be proportional to the secant

[10] *Taggart, M. A. and Fine, E. C. "Parallel Plate Bends," Massachusetts Institute of Technology Radiation Laboratory Report 760, 5 September 1945 (Unclassified)*

of the angle of incidence and to the (guide) wavelength. Thus

$$\frac{S_u}{S_l} = \frac{3.3 \sec 46^\circ}{3.2 \sec 6^\circ} = 1.475. \qquad (21)$$

Since the experimentally determined value of S_l is 13/32 or 0.406 inch, the proper spacing S_u for the upper beam is 0.599 or 19/32 inch. This has not been checked with the flat pillbox experimentally, but has been used in the NRL model of the scanner with good results.

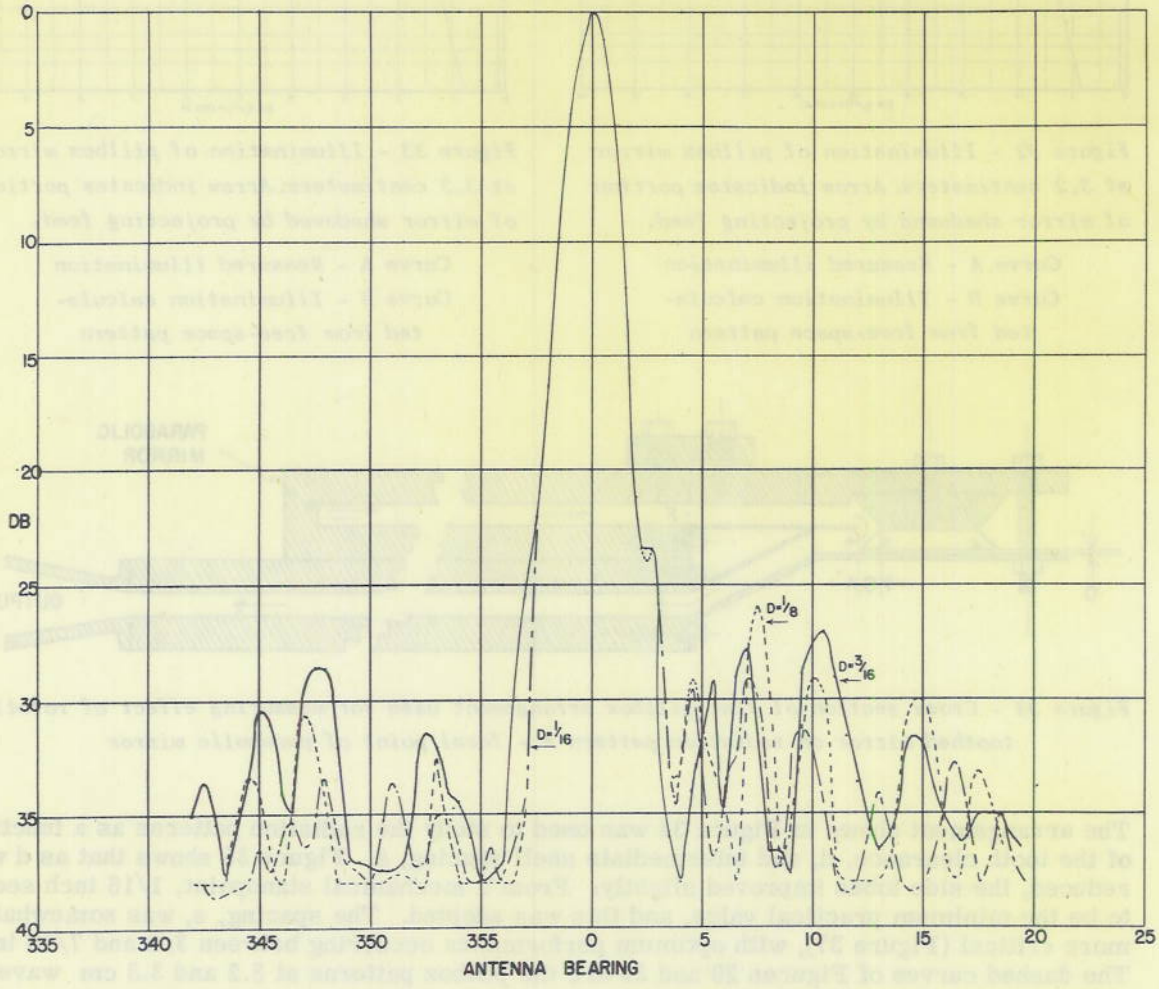

Figure 35 - Effect of tooth clearance on pillbox pattern at 3.2 cm - normal incidence

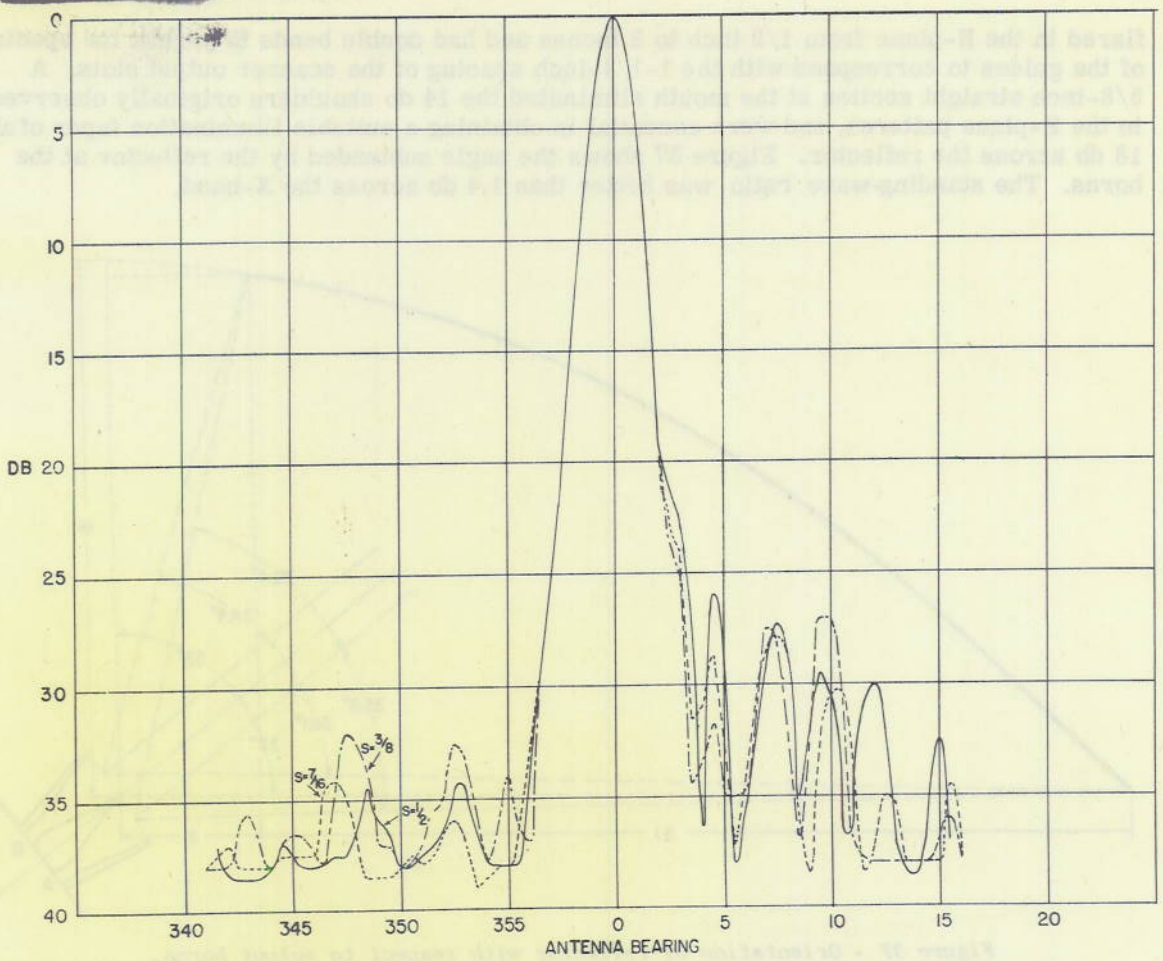

Figure 36 - Effect on pillbox pattern of varying the spacing between edge of intermediate shell and waist of toothed mirror at 3.2 cm - normal incidence

Effect of Output Support Pins on Patterns

As stated in an earlier section of this report, the mid-section of the scanner output horn is supported by 1/4-inch round pins spaced approximately 12 inches apart. In order to measure the effect of these pins on the radiation pattern, a flat pillbox has been constructed equal in size to the lower pillbox and having a 30-inch parallel plate region in front of the aperture. In this region it is possible to locate rows of pins such that the angles of incidence of the pillbox linear wave front are the same as would be expected at the scanner output (0° - 46°). It is planned to insert rows of pins at various angles and observe the resulting radiation pattern. No measurements have been made at this writing. Earlier experiments, conducted by drilling through the output horns of the 56-inch flat pillbox and inserting 3/16-inch diameter pins spaced 11-1/18 inches on centers, indicated that at normal incidence the side lobes came up about 3 db.

Electrical Design of Output Horns

The first experiments aimed at designing the output horns for the scanner were conducted using waveguide models. Each side of the double horn shown in Figure 26 was

flared in the E-plane from 1/2 inch to 2 inches and had double bends to permit the spacing of the guides to correspond with the 1-1/4-inch spacing of the scanner output slots. A 5/8-inch straight section at the mouth eliminated the 14 db shoulders originally observed in the E-plane patterns, and were essential in obtaining a suitable illumination taper of about 18 db across the reflector. Figure 37 shows the angle subtended by the reflector at the horns. The standing-wave ratio was better than 1.4 db across the X-band.

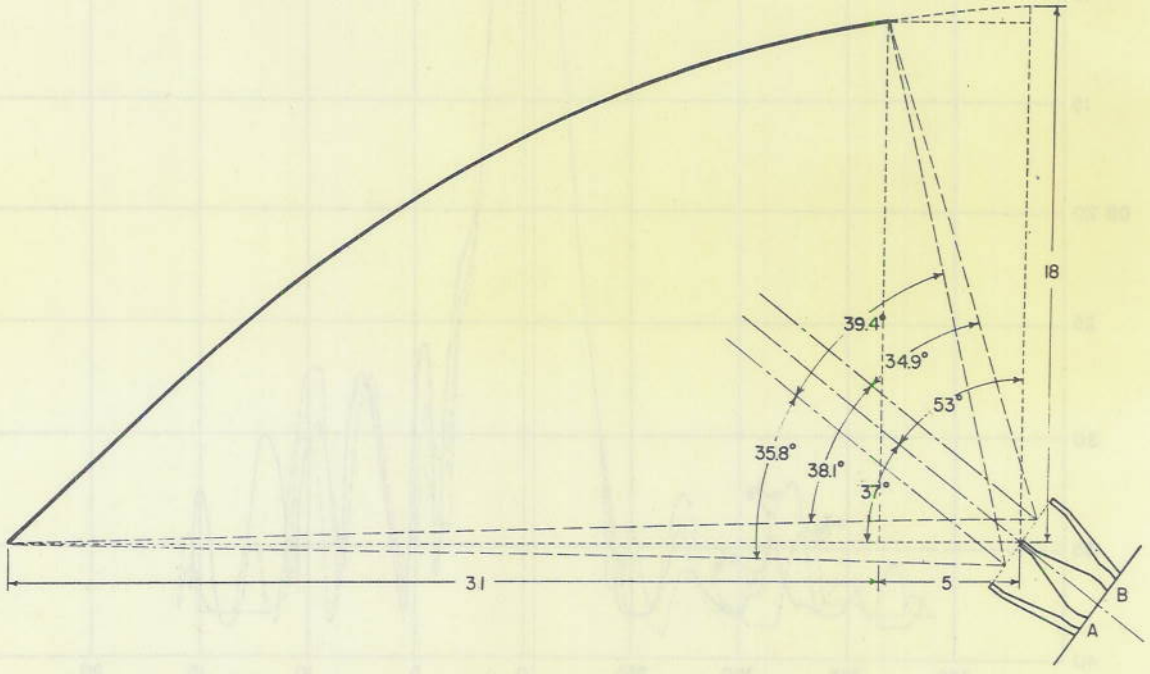

Figure 37 - Orientation of reflector with respect to output horns, as seen from small end of cone
A - Lower pillbox (Upper beam)
B - Upper pillbox (Lower beam)

Output horns based on this design were constructed for the flat upper pillbox and secondary patterns were observed with the arrangement shown in Figure 38. The beam-widths turned out to be excessively great, and investigation showed that the primary patterns were much too narrow. When the horn apertures were reduced to 1-11/16 inches, satisfactory secondary patterns were obtained. The final design must be carried out with the scanner itself.

CONSTRUCTION OF NRL SCANNER

An experimental hand-operated model of the AN/SPS-3 antenna has been constructed at the Naval Research Laboratory. It consists of five basic parts: a cast aluminum outer shell, a wooden inner cone, an aluminum intermediate shell, fixed and rotating toothed mirrors, and a cylindrical reflector 31 x f (= 18) x 144 inches. Each of these is discussed separately in this section. The assembled scanner is shown mounted horizontally in Figure 39, and vertically in Figure 40.

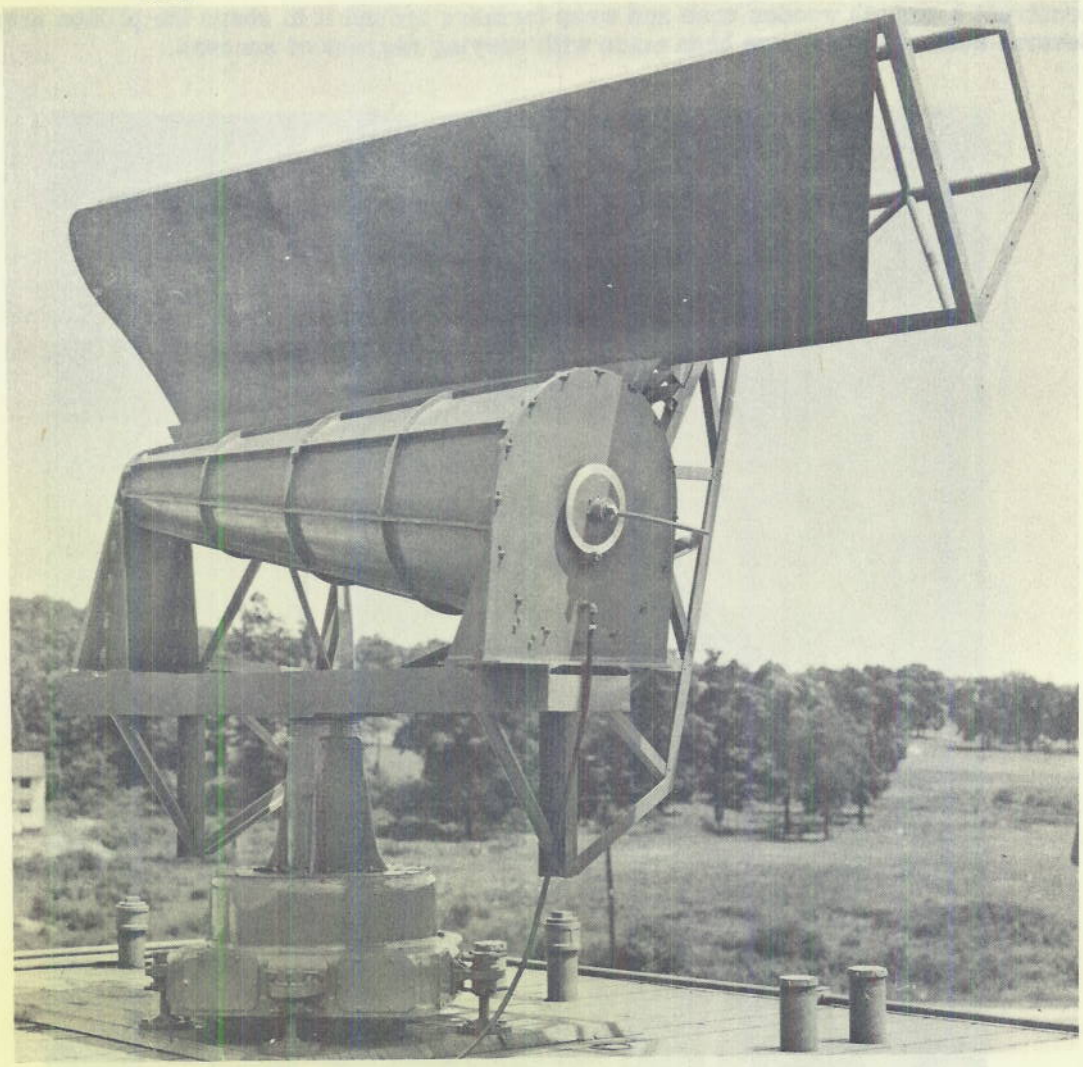

Figure 38 - Flat pillbox mounted for observing horizontal plane pattern

Outer Cone

The outer cone of the scanner was cast from aluminum alloy 3S at the NRL Foundry and machined at the Naval Gun Factory. When completed (Figure 41) it had a wall thickness of about one-quarter inch and weighed 168 lbs. The end bells seen in Figure 39 were machined from aluminum alloy 61 ST and attached to the cone by means of Rosan inserts. The cast aluminum output horns visible in this photograph have since been replaced by horns fabricated of sheet brass.

Inner Cone

It was thought impractical to make the inner cone of aluminum, since the NRL shop was not equipped to machine the parabolic mirrors and straight barriers. The alternative was to

construct a smooth wooden cone and wrap formers around it to shape the pillbox areas. Several such attempts have been made with varying degrees of success.

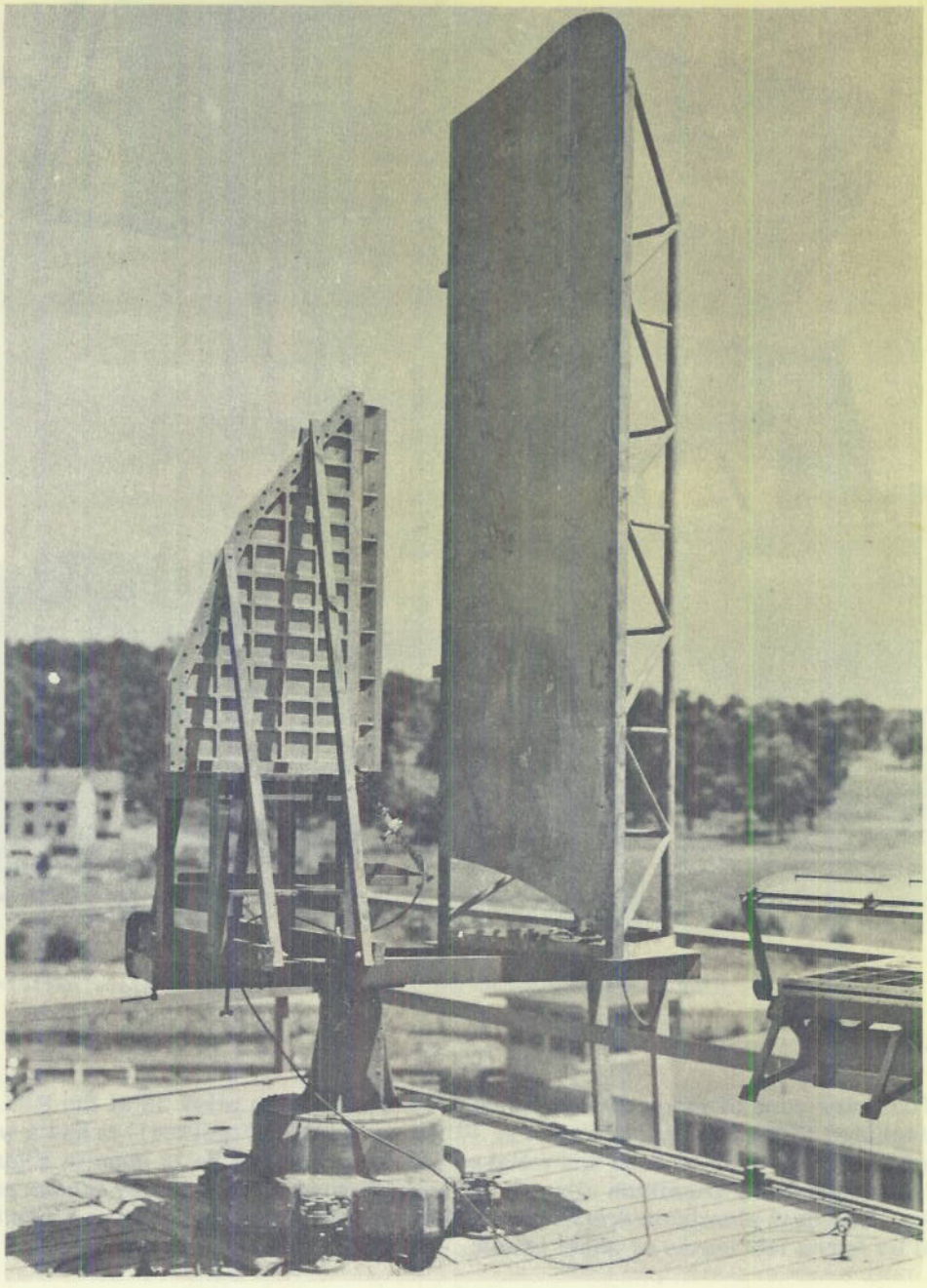

Figure 39 - NRL scanner mounted for observing vertical plane patterns

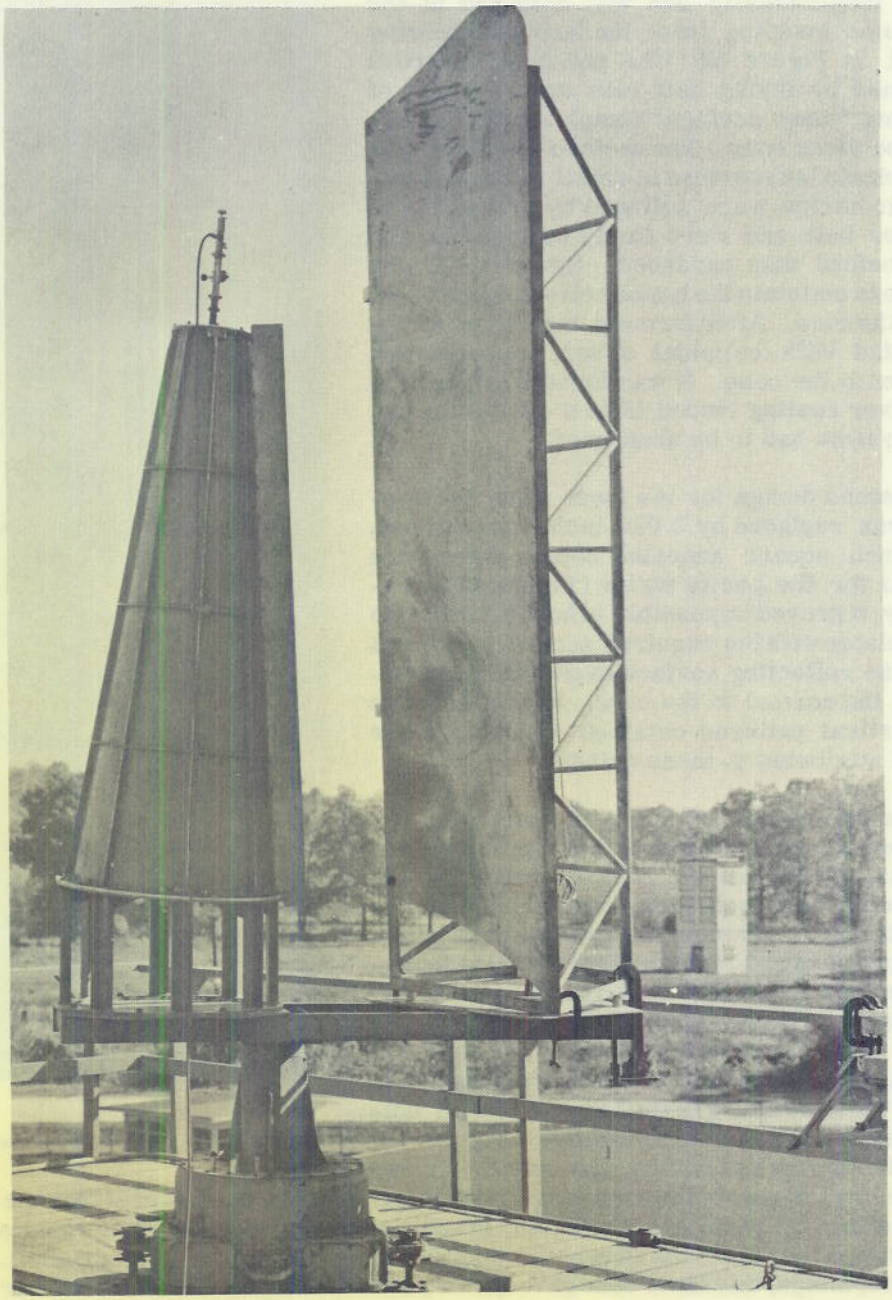

Figure 40 - NRL scanner mounted for observing horizontal plane patterns. The antenna is tilted 6 degrees forward

The first wooden inner cone was covered with copper foil 0.002 inch thick in strips which were stretched longitudinally and soft soldered at the seams. Some buckling from the heat of soldering is evident in Figure 42. The parabolic mirrors were formed by laying half-inch square strips of Lucite along "inner surface" templates of the pillboxes on the inner cone. The method of calculating these templates is described in detail in Appendix I. The plastic strips were softened by preheating in a hot water bath and were easily wrapped around the cone before they hardened. However, it was impossible to maintain the inside reflecting surfaces normal to the cone. After forming, the plastic strips were painted with colloidal silver, copperplated, and screwed to the cone. It was found that the copper and silver coating tended to peel off the Lucite, and this scheme had to be abandoned.

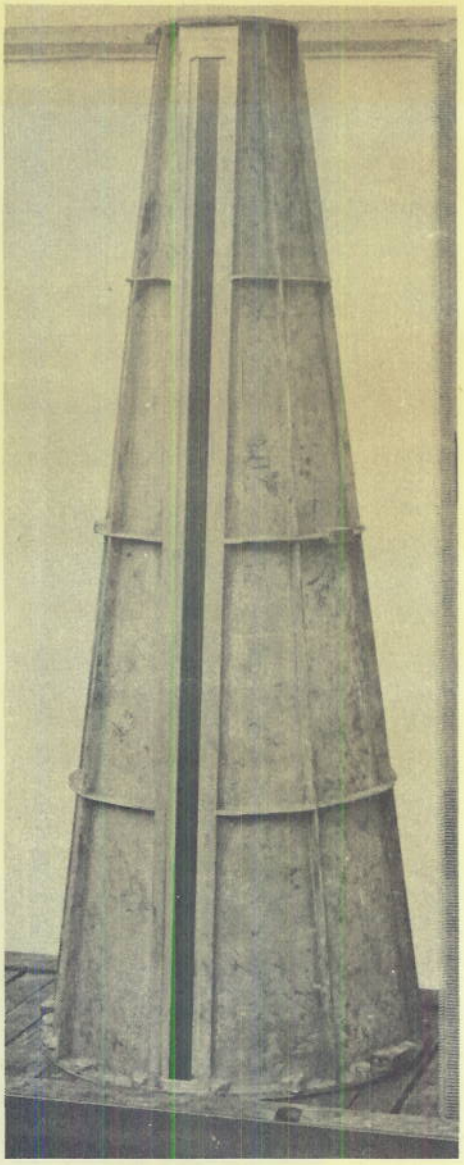

Figure 41 - NRL outer cone casting

In a second design for the inner cone, the copper foil was replaced by 0.020-inch copper sheet, and half-inch square annealed copper bars were substituted for the Lucite strips (Figure 43). Unfortunately, it proved impossible to hold the mirrors to the templates with the required accuracy of 0.031 inch, and the reflecting surface departed considerably from the normal to the cone. High side lobes in the vertical patterns obtained with this inner cone were attributed to these defects.

At the completion of these experiments, the wooden cone was no longer usable, and a new one was made up. This time the pillboxes were formed by (1) glueing half-inch thick, hand-shaped blocks of wood to the cone, covering the general area of the parabolic mirrors and straight barriers, (2) transferring the "outer surface" pillbox templates to the upper surface of these blocks, and (3) cutting the reflecting edges by running a router bit along the templates. Very accurate curves were obtained in this way. Then the entire unit was sprayed with colloidal silver to make it conducting (Figure 44). Although the surface resistivity was only 0.17 ohms per square, the low gain of the assembled scanner proved to be the result of leakage through the silvered walls of the parallel plate region. In addition some cross-coupling resulted from the poor contact between the tops of the silvered wooden formers and the intermediate shell. But in spite of these shortcomings, this inner cone gave better patterns than had been obtained previously.

To improve the gain and provide better isolation between channels, the pillbox walls were covered with preformed sheets of 0.020 inch annealed copper, and the top surfaces of the mirrors, barriers and feed horns with 1-1/2-inch strips of thin corrugated beryllium

copper (Figure 45). Since the corrugations were a half-inch apart and perpendicular to the boundaries, the channels between them were expected to simulate waveguides below cut-off frequency and in this way minimize the leakage.[11] On a metal inner cone, it would be more satisfactory to mill choke slots down into the barriers and mirrors a quarter wavelength back from the inside edges. This was not possible in the wooden model with the available facilities.

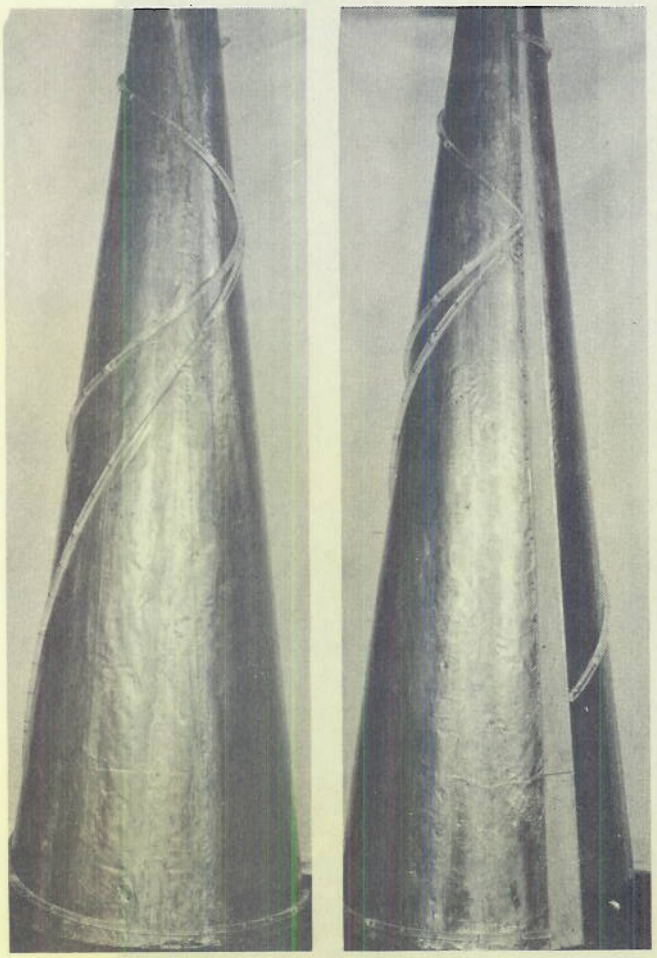

Figure 42 - Lucite formers on foil-covered inner cone

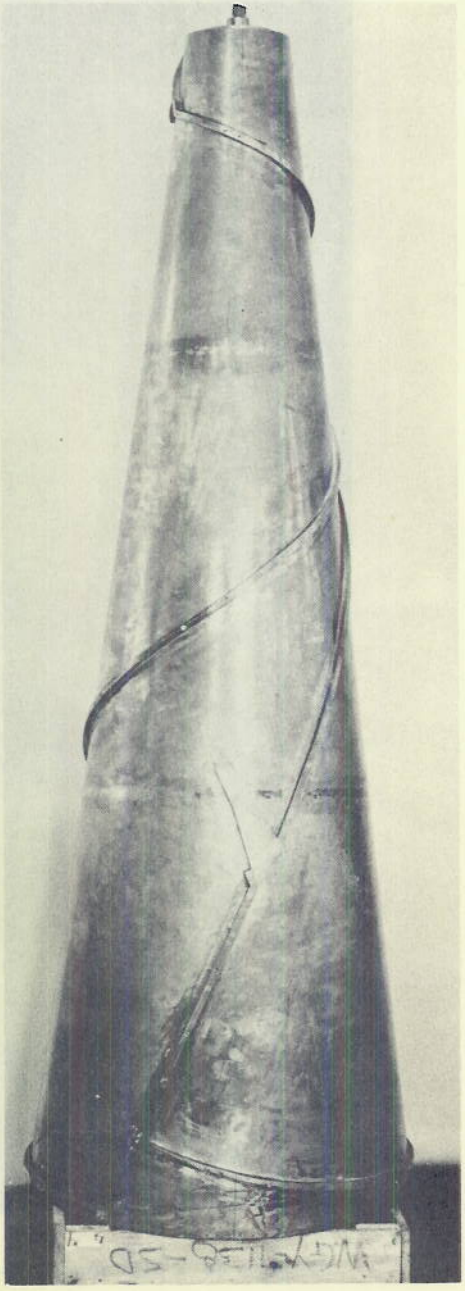

Figure 43 - Copper bar formers on copper sheet covered inner cone

[11] *This idea was developed by K. S. Kelleher of the Search Radar Branch, Naval Research Laboratory.*

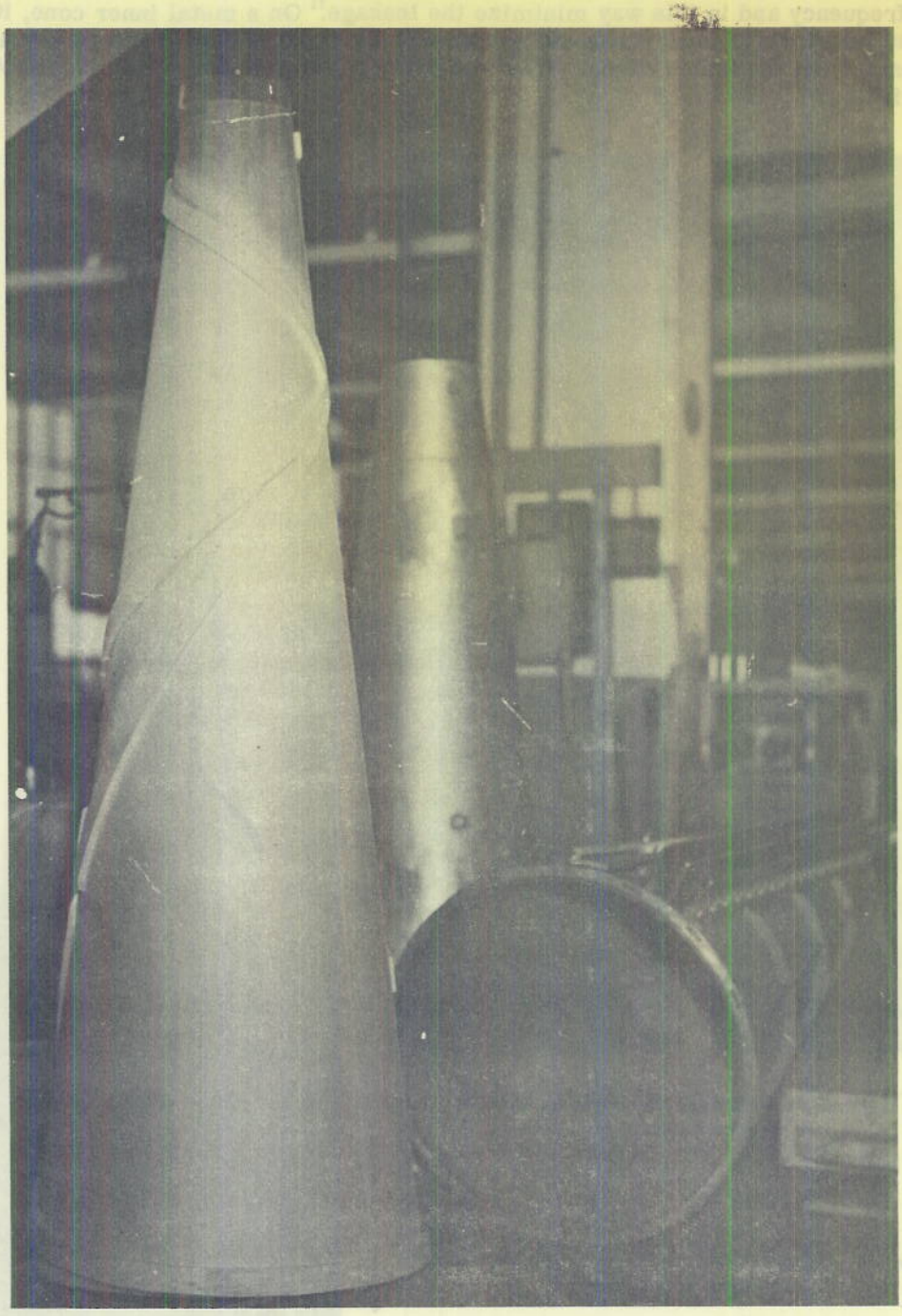

Figure 44 - NRL scanner - outer cone, intermediate shell, and silver sprayed wooden inner cone

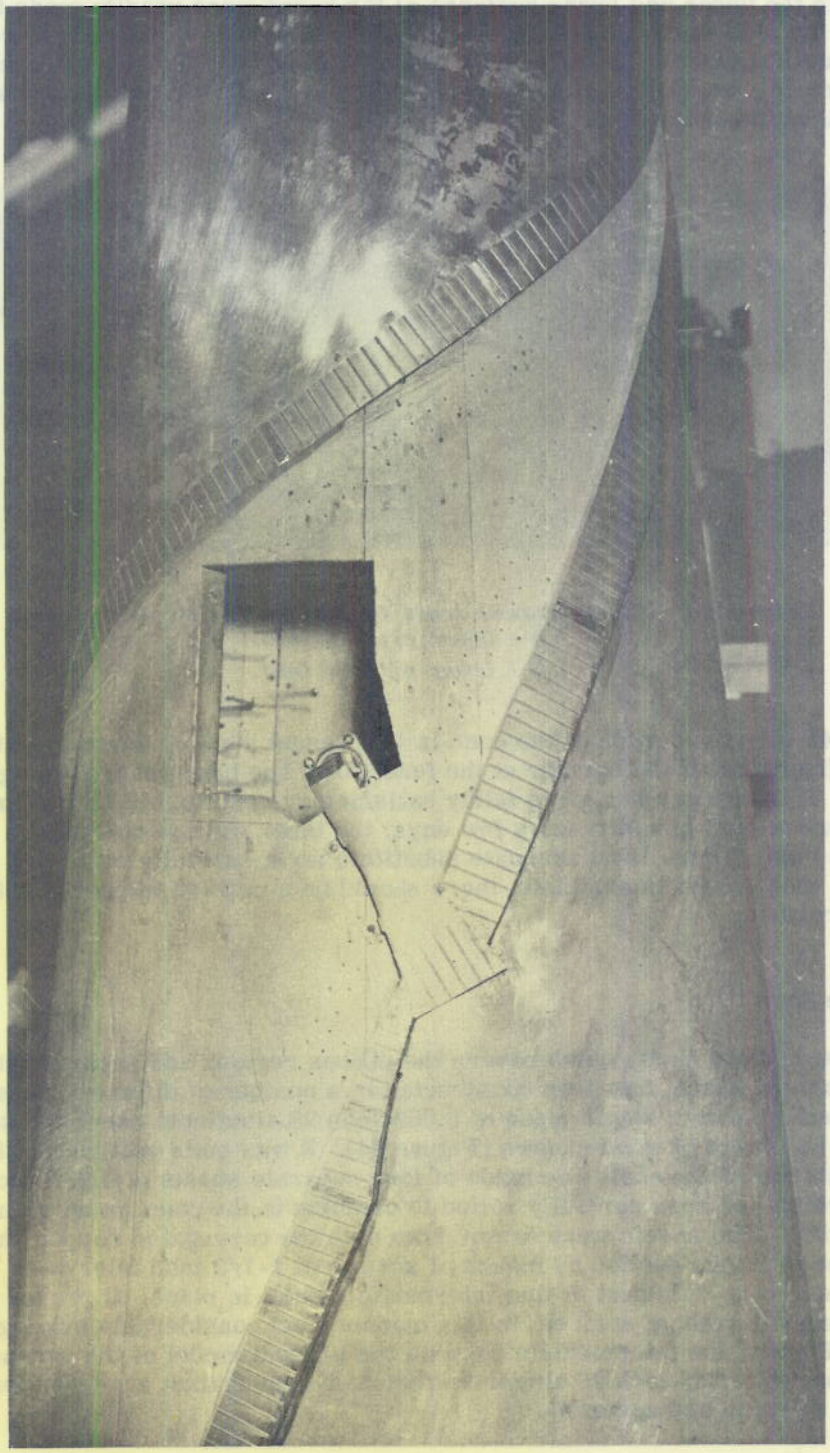

Figure 45 - Experimental inner cone with upper pillbox cover in place

The pillbox feed horns used on the original inner cone were fabricated from sheet brass. While the upper and lower surfaces of the horns were readily made to conform to the cone, the side walls could not be maintained normal to it, since they represent non-developable surfaces. Later models of the scanner have incorporated electroformed horns (Figure 46), produced on Lucite cores that were softened and shaped around the cone at the location of the feeds.

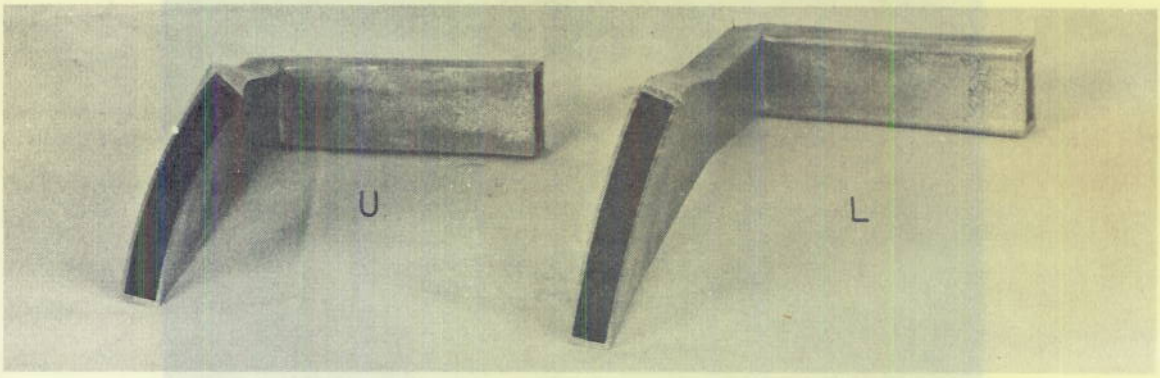

Figure 46 - Electroformed feeds for use on wooden inner cones
U - Upper pillbox feed
L - Lower pillbox feed

Figure 45 is a photograph of the cone in its present state of development, except that the configuration of the barrier at the feed horns has been changed to agree with Figure 29f. This scanner has given fairly satisfactory results, but if it is exposed to an atmosphere of high humidity for a few days, the inner cone swells enough to make the bearings bind. There is no adequate substitute for a carefully machined metal inner cone. When such a cone is available, there should be a marked improvement in the electrical performance.

Intermediate Shell

The intermediate shell, which covers the pillbox regions and separates them from the outer scanning space, has been constructed in a number of different ways. The first one was rolled up from a single piece of 0.062-inch 2S aluminum sheet and secured to the formers by means of wood screws (Figure 44). It was quite soft and easily damaged. The second intermediate shell was made of four separate sheets of 0.031-inch 24ST aluminum, which had been carefully rolled to conform to the cone, in an effort to obtain greater rigidity. The sheets were drawn down onto the corrugated copper shims described in the previous section by means of screws at 1-1/2 inch intervals. Figure 45 shows the inner cone with part of this intermediate shell in place. It proved difficult to obtain a smooth conical surface in this manner, and considerable bulging was encountered. Finally, the intermediate shell on the present model of the scanner is a one-piece sheet of 0.062 inch 2S aluminum that was spun against a wooden form to obtain greater strength and accuracy.

Interplate Support Pins

It is apparent from development drawings of the inner cone (for example, Figure 9) that the edges of the intermediate shell are unsupported for nearly a five-foot length on either side of the toothed mirror. The only practical way to avoid bowing of the edges was to anchor them with screws. In the latest model, four No. 6 flat-headed wood screws (0.138″ diam.) were used on each side at approximately 11-inch spacing. They were fitted with half-inch diameter polystyrene sleeves which maintained the proper spacing between the inner cone and the intermediate shell (Figure 47).

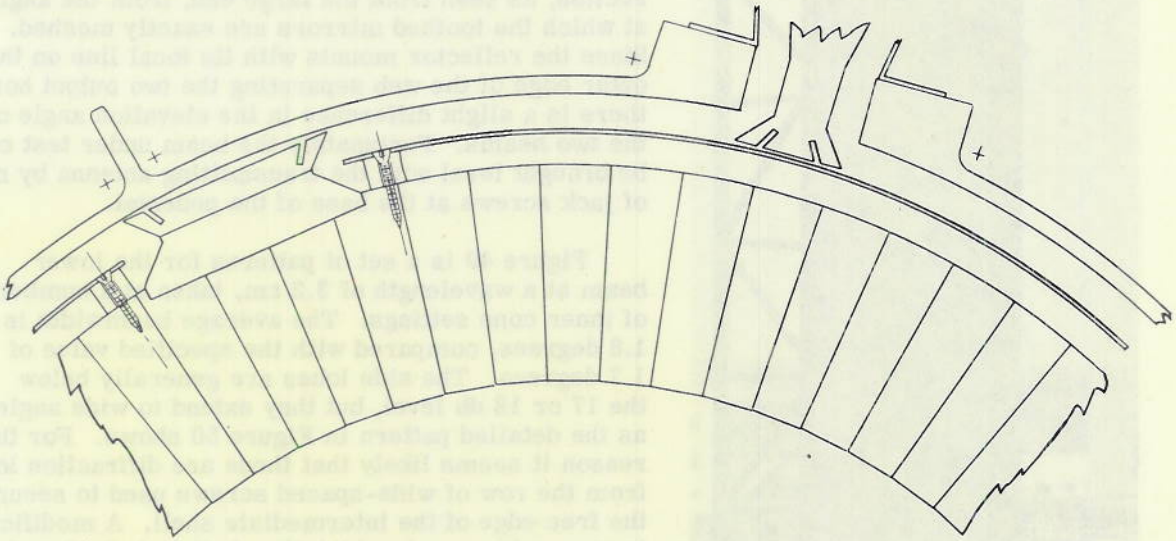

Figure 47 - Cross section of NRL scanner showing constructional details

Toothed Mirrors

The toothed mirrors were milled from bars of aluminum alloy 24 ST. The stationary mirror is shown in Figure 41. The teeth were made 0.093 inch thick and spaced 0.156 inch on centers, so that the side clearance of the teeth was only 0.031 inch. The problem of accumulative error in the tooth spacing was minimized by cutting both sets of teeth on the same milling machine.

Cylindrical Reflector

An experimental model of the cylindrical reflector is shown in Figure 48. The focal length is 18 inches, the aperture 31 inches, and the length 144 inches, some 18 inches greater than necessary. The framework was welded from aluminum alloy 61 ST angle and tubing. The skin, made of 0.050-inch 61 ST, was preformed on rollers and attached with size 00 drive screws. The effect of the round screw heads, 0.023 inch high and 0.093 inch in diameter, was assumed negligible. A tolerance of 0.031 inch was allowed on both the parabolic contours and the straightness of the elements.

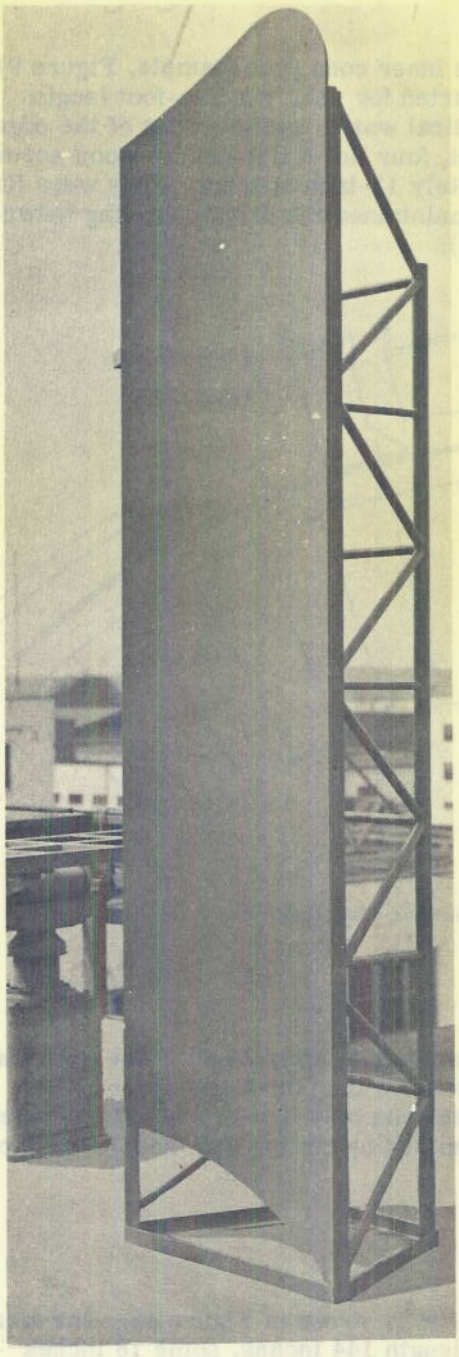

Figure 48 - Solid-sheet reflector used with NRL scanner

RESULTS OBTAINED WITH NRL SCANNER

Vertical Patterns

Vertical radiation patterns were taken with the antenna mounted on its side as shown in Figure 39. The azimuth angle between the transmitter and the normal to the reflector is labelled as the elevation angle in Figures 49 through 52. Inner cone rotation is measured in a counter-clockwise direction, as seen from the large end, from the angle at which the toothed mirrors are exactly meshed. Since the reflector mounts with its focal line on the outer edge of the web separating the two output horns, there is a slight difference in the elevation angle of the two beams. Fortunately the beam under test could be brought level with the transmitting antenna by means of jack screws at the base of the pedestal.

Figure 49 is a set of patterns for the lower beam at a wavelength of 3.2 cm, taken at a number of inner cone settings. The average beamwidth is 1.8 degrees, compared with the specified value of 1.7 degrees. The side lobes are generally below the 17 or 18 db level, but they extend to wide angles, as the detailed pattern in Figure 50 shows. For this reason it seems likely that these are diffraction lobes from the row of wide-spaced screws used to secure the free edge of the intermediate shell. A modification is now under way in which the shell is to be laced together with 1/8-inch square straps passing through every third slot in the rotating mirror. This will eliminate the screws and should effect a great improvement in the vertical patterns. It seems reasonable to expect a side lobe level of at least 20 db.

Typical upper beam patterns at 3.3 cm are shown in Figures 51 and 52. The average beamwidth is 2.5 degrees, as desired, while the side lobes do not exceed 17 db.

Scanning Angle vs. Cone Rotation

Figure 53 shows the linearity of the scan angle with cone rotation. When the antenna is mounted at the proposed tilt angle of 33 degrees, the scan will be from 1-1/2 degrees below the horizon to 79.5 degrees above. There is, however, a 0.9 degree gap in the scan at 39.5 degrees.

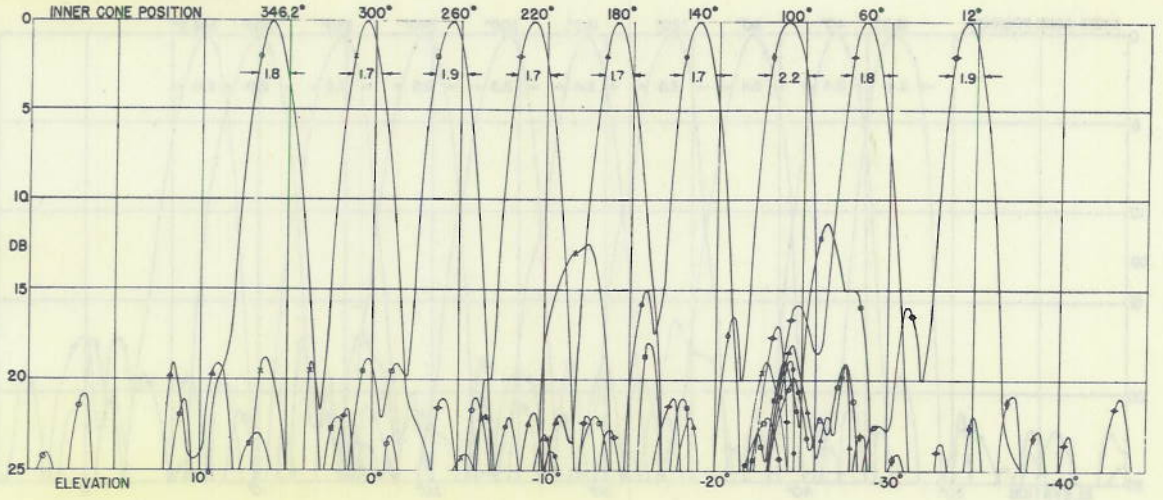

Figure 49 - Vertical plane radiation patterns from scanner upper pillbox at wavelength of 3.2 cm

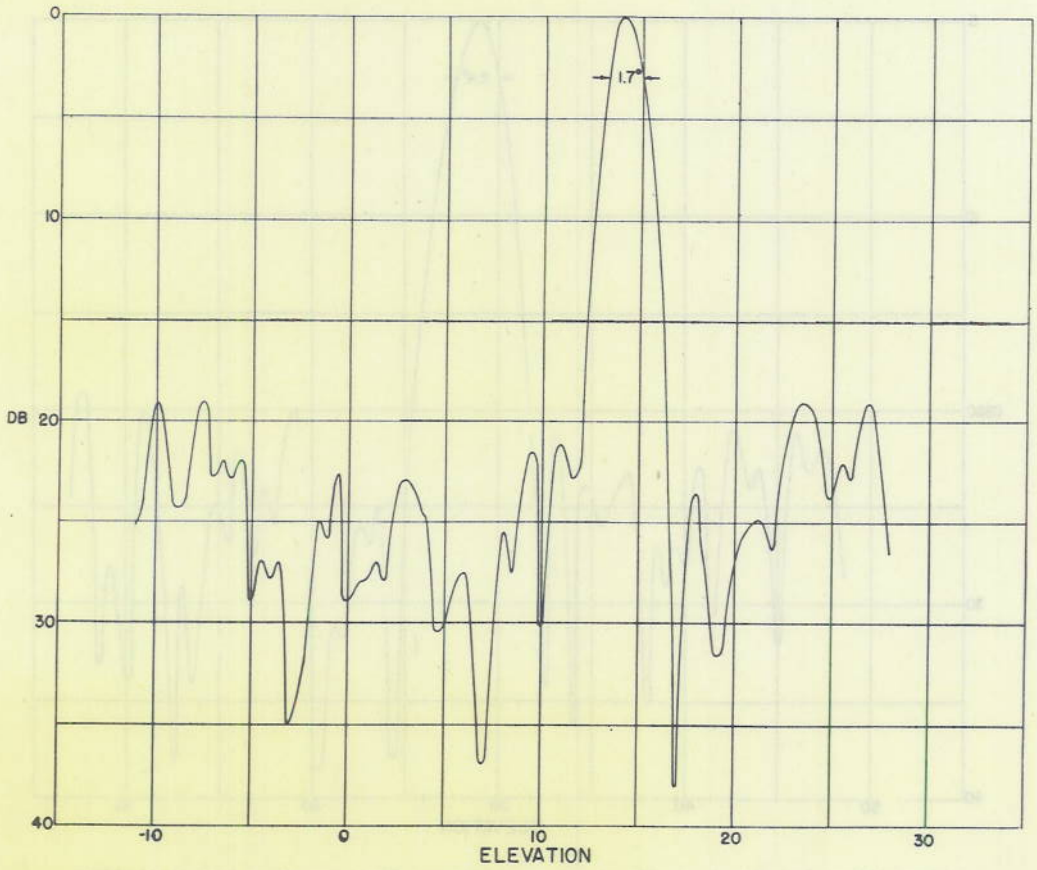

Figure 50 - Detailed vertical plane pattern from scanner upper pillbox
Inner cone rotation - 180 degrees
Wavelength - 3.2 cm

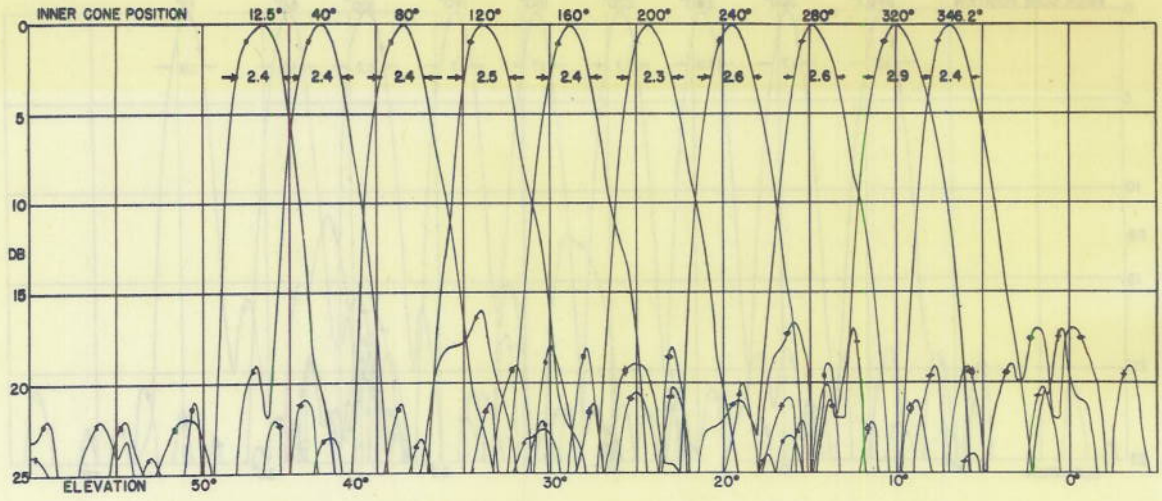

Figure 51 - Vertical plane radiation patterns from scanner lower pillbox at wavelength of 3.3 cm

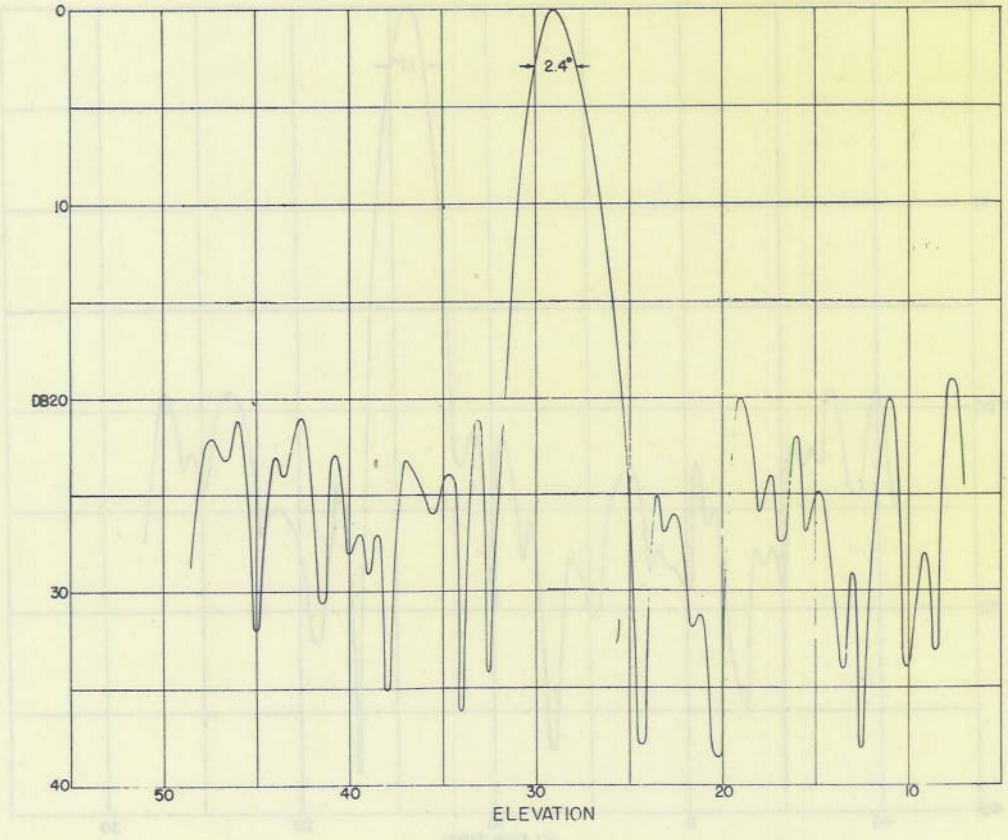

Figure 52 - Detailed vertical plane pattern from scanner lower pillbox
Inner cone rotation - 160 degrees
Wavelength - 3.3 cm

Horizontal Patterns at Overlap

Figure 40 shows the antenna tilted 6 degrees forward of the vertical to permit taking horizontal patterns of both upper and lower beams at the overlap point. The output horns seen in this photograph have an E-plane aperture of 1-11/16 inches, and are similar in cross section to a design that gave acceptable horizontal patterns from the flat pillbox. However, the results obtained with this arrangement (Figures 54 and 55) are far from satisfactory. Primary patterns of the scanner, taken with the output horns vertical, reveal that the illumination of the reflector is unsymmetrical and tapers only 8 db to the vertex edge. A new set of output horns with an E-plane aperture of 1-3/4 inches is now under construction.

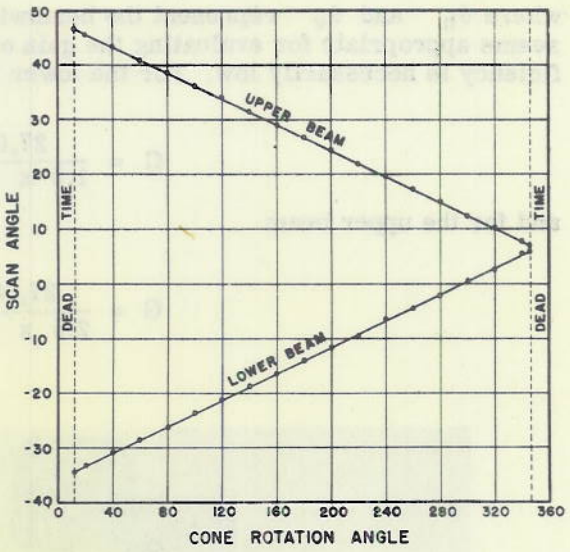

Figure 53 - Scanning schedule of NRL scanner

It is anticipated that clean horizontal patterns will be obtained as soon as the proper E-plane aperture can be determined, for the primary patterns show deep nulls at either side of the main beam. This is accomplished by means of a parallel section at the end of the output horns (Figure 56).

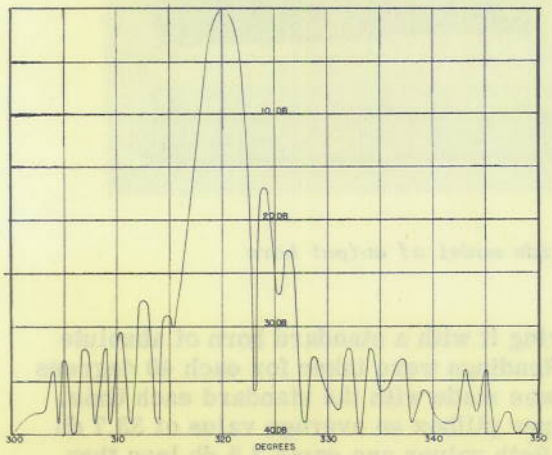

Figure 54 - Horizontal plane radiation pattern of lower beam at 3.2 cm - beam width 2.7 degrees

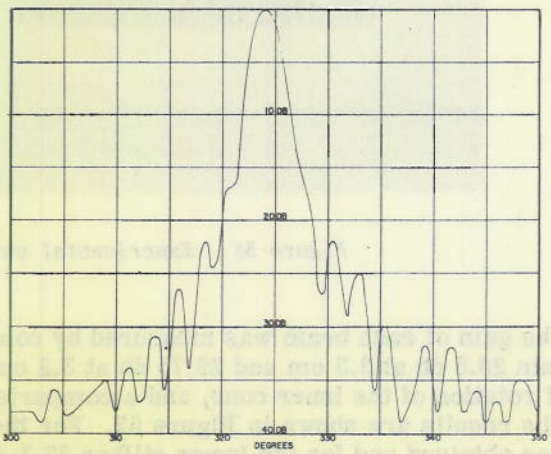

Figure 55 - Horizontal plane radiation pattern of upper beam at 3.3 cm - beam width 2.7 degrees

Gain Measurements

The well known empirical formula

$$G = \frac{27{,}000}{\theta_h \times \theta_v}, \qquad (22)$$

where θ_h and θ_v represent the beamwidths in the horizontal and vertical planes, seems appropriate for evaluating the gain of a wide-angle scanner, whose reflector efficiency is necessarily low. For the lower beam the gain should be

$$G = \frac{27{,}000}{1.8 \times 2.9} = 5175, \text{ or } 37.1 \text{ db}, \quad (23)$$

and for the upper beam

$$G = \frac{27{,}000}{2.5 \times 2.9} = 3755, \text{ or } 35.8 \text{ db}. \quad (24)$$

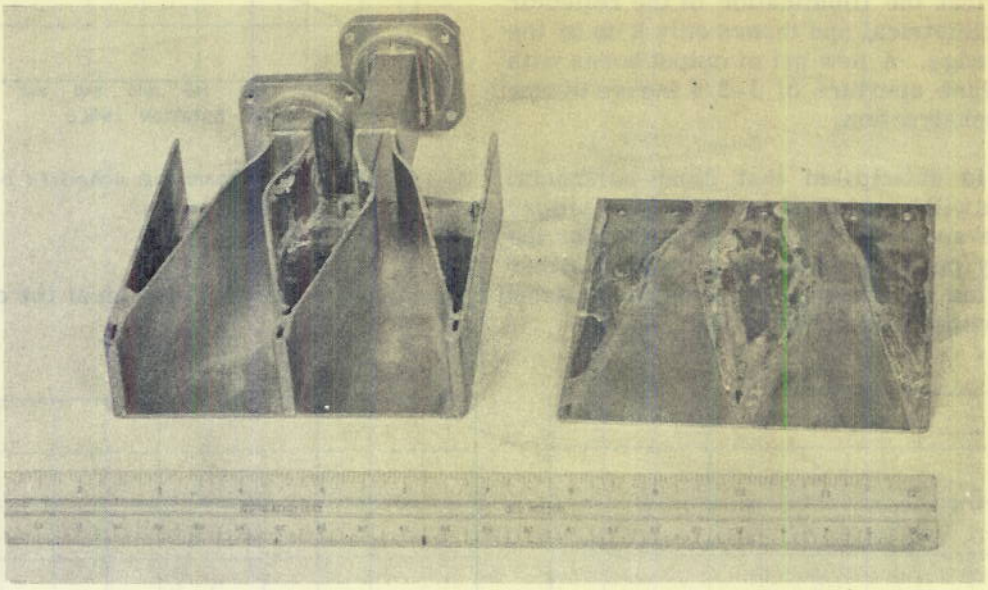

Figure 56 - Experimental waveguide model of output horn

The gain of each beam was measured by comparing it with a standard horn of absolute gain 29.5 db at 3.3 cm and 29.75 db at 3.2 cm. Readings were taken for each 40 degrees of rotation of the inner cone, and a comparison was made with the standard each time. The results are shown in Figure 57. For the upper pillbox an average value of 33.7 db was obtained and for the lower pillbox 32.3 db. Both values are some 3.5 db less than the predicted values shown by the broken lines. The reason for the low gain is not known, but it may be related to the unsatisfactory condition of the horizontal patterns or to problems of alignment.

Match Measurements

Figure 58 shows the standing wave ratio at the input to either pillbox feed horn. The match is generally satisfactory, but will be affected by the final design of the output horns. It is interesting to note that the highest standing-wave ratio for the upper pillbox occurs at a cone angle of 300 degrees, where the beam is incident normally upon the fixed mirror.

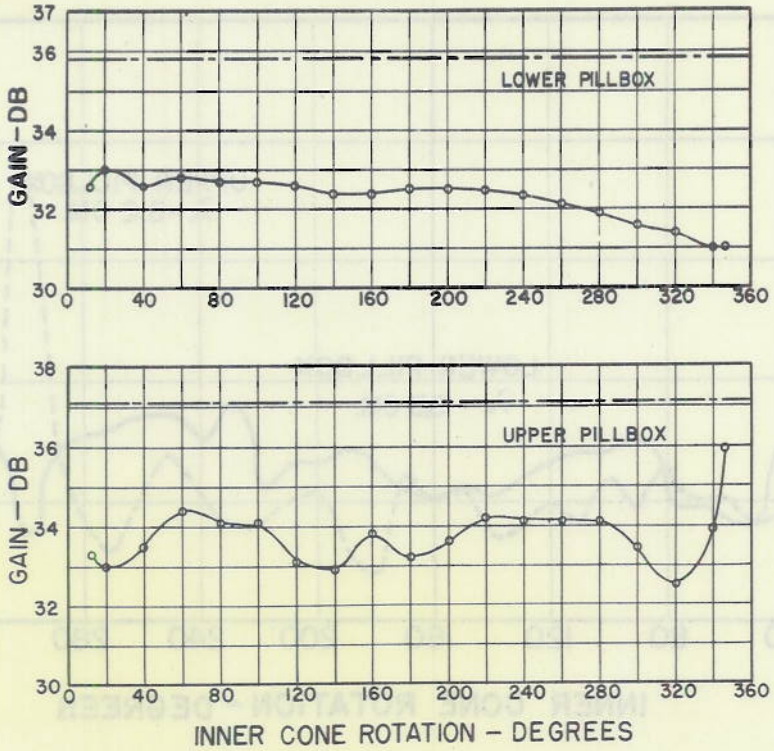

Figure 57 - Gain of NRL scanner

CONSTRUCTION OF THE PROTOTYPE ANTENNAS

Background

Early in the development of the AN/SPS-3 antenna, it became evident that high-speed operation would impose requirements on the mechanical design that would have to be taken into account in the r-f design. Accordingly in May 1947, when the electrical parameters were not yet rigidly established, the American Machine and Foundry Company of Brooklyn, N. Y., was given a contract for the construction of two prototypes of the antenna, with full responsibility for the mechanical design. The Naval Research Laboratory has supplied the electrical design information, and has attempted to work out satisfactory compromises wherever the requirements were conflicting. The prototypes will be similar in their r-f properties to the NRL scanner described above, but have been designed to meet the weight requirements, and to withstand the stresses of high-speed rotation. Figures 59 and 60 are two views of a quarter-scale model which has been used for wind testing.

Outer Cone

While the outer cone of the NRL scanner is made of cast aluminum, the American Machine and Foundry Company has used a fabricated magnesium construction, for reasons discussed earlier in this report. First the horizontal rings and vertical fins seen in Figures 59 and 60 were assembled and welded together to form a conical cage. Then a large sheet of half-inch magnesium alloy FS-1XR was rolled to conical shape, inserted into the

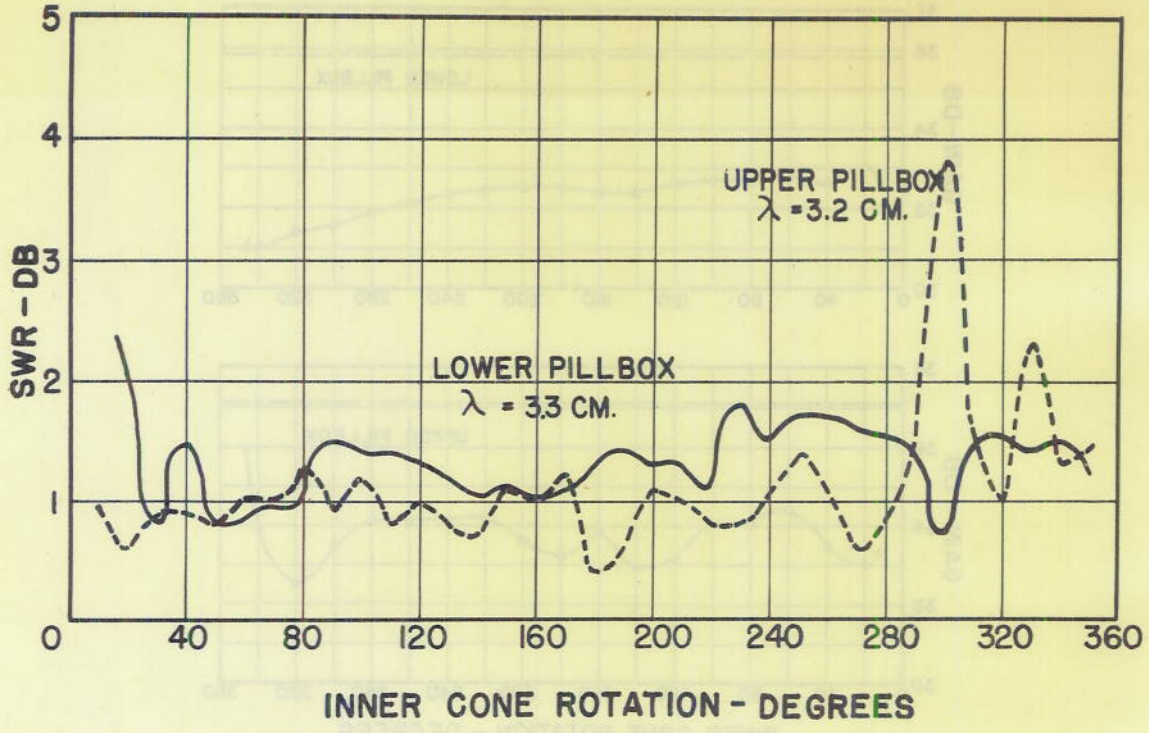

Figure 58 - Match of NRL scanner

cage, and welded into place. The inside surface was machined by mounting the cone rigidly and rotating a cutter bar that had been aligned with its axis. The cutting tool supported from this bar was provided with radial and longitudinal feeds that were properly geared to generate the cone angle.

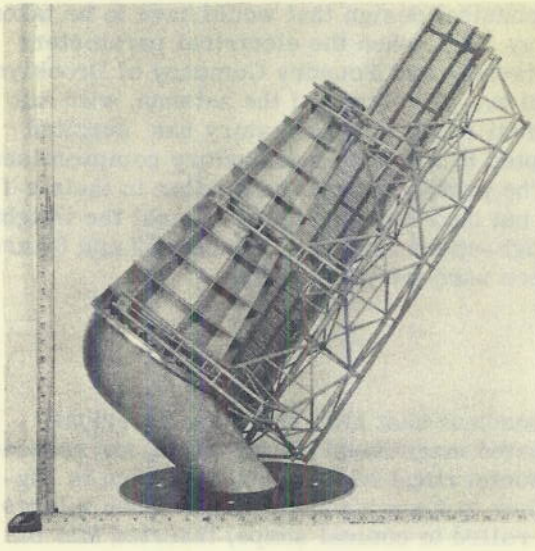

Figure 59 - End view of American Machine and Foundry Company (AMF) quarter-scale model of AN/SPS-3 antenna

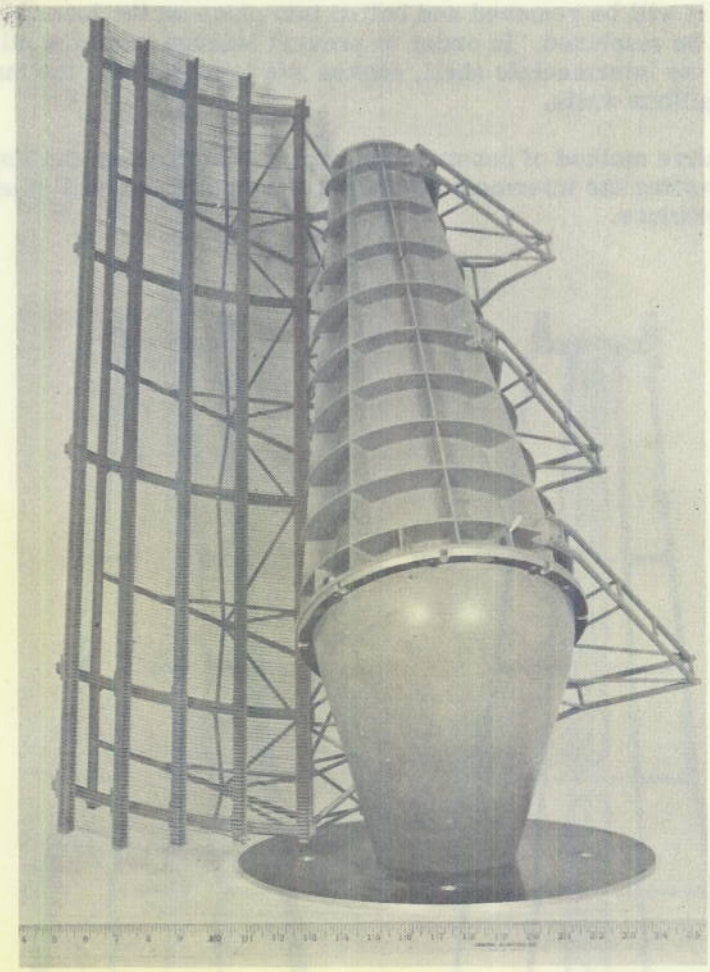

Figure 60 - Front view of AMF quarter-scale model

Inner Cone

The inner cone of the prototype is a large, hollow, internally braced magnesium casting with two pillboxes machined into its surface (Figure 61). One inner cone has been cast successfully and is ready for machining. The pillbox boundaries will be cut by mounting the cone between indexing centers and driving an end-milling cutter along the cone from a specially generated cam geared to the rotation of the cone on its axis. The cam was constructed from the pillbox coordinates—cone rotation vs. slant distance—(see Appendix II) after making a correction for the finite diameter of the cutter.

Intermediate Shell

The intermediate shell is to be rolled up from 1/8-inch magnesium sheet, tack-welded along the seam, and slid into the completed outer cone, where it will be held fast with flour paste. Then the inside surface will be machined by the same procedure used for the outer

cone. After this, it will be removed and bolted into place on the inner cone so that the outer surface can be machined. In order to prevent leakage from the pillboxes because of poor contact with the intermediate shell, chokes are to be cut into the inner cone a quarter-wave back of the pillbox walls.

As an alternative method of construction, American Machine and Foundry engineers have considered rolling the intermediate shell to its final shape and in so doing eliminating the machining procedure.

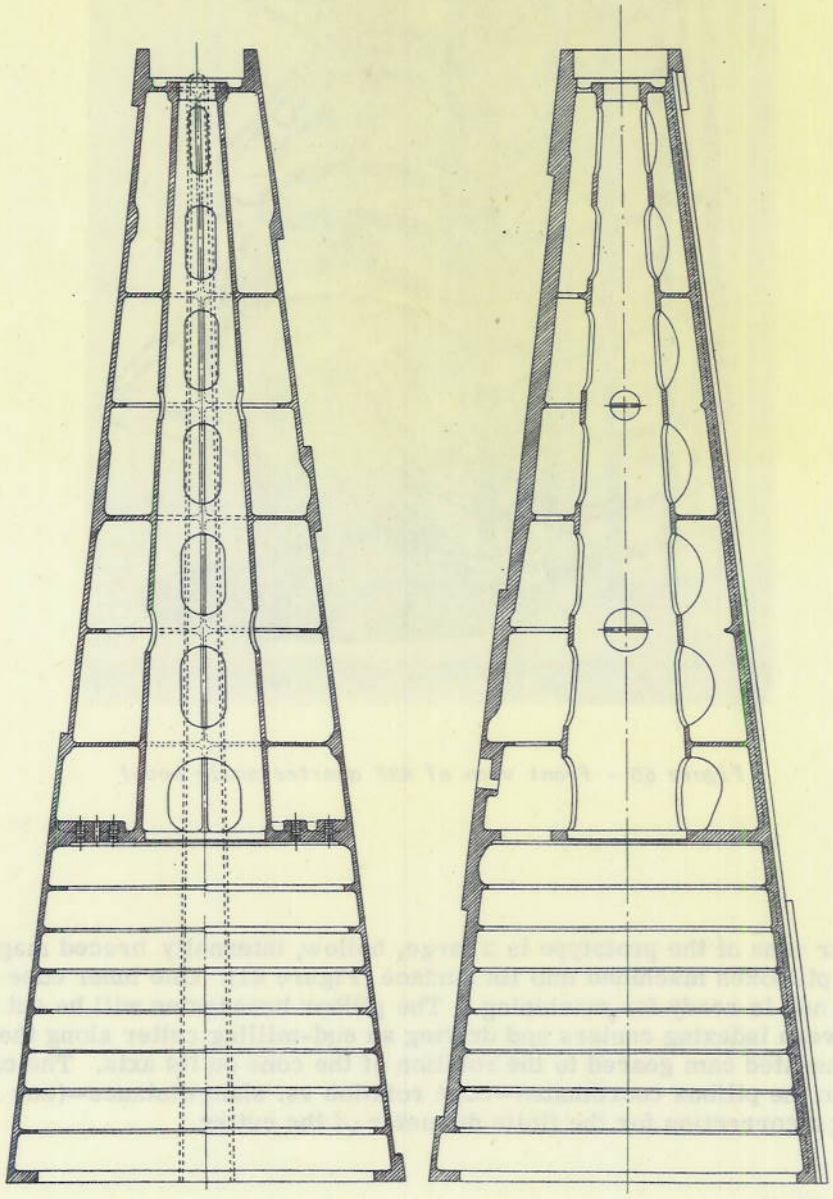

Figure 61 - Lateral section of AMF inner cone

Motor Drive

A sectional view of the scanner in Figure 62 shows the inner and outer cones, the bearings, waveguide rotating joints, drive mechanism, and oil system. The lower bearing has been located nearly half-way up the cone to permit bringing the drive mechanism within the enclosure. The motor is a two-speed, three-phase, shaftless induction type, rated at 2.2 HP at either 3600 or 1200 rpm, and operates through 2 to 1 reduction gearing. A positive pressure oil feed system, augmented by oil slingers, is used to lubricate the drive mechanism.

The surface search function of this set requires a stowing device (not shown in Figure 62) for stopping the scanner with the lower beam on the horizon. This is accomplished by means of a small motor that is coupled—through a reduction gear and a friction drive wheel—to a machined surface on the lowest internal rib of the inner cone, in conjunction with a positive locking pin which drops into a positioning hole on this same surface. A microswitch cuts off the motor and releases the pin at the proper point of the periphery. This mechanism is activated automatically whenever the scanning motor is cut off and the cone rotation drops below a certain speed.

Reflector Construction

Although it has not yet been determined whether the cylindrical reflector will be of strip or tubular construction, current American Machine and Foundry plans are for the latter type. The photographs of the scale model (Figures 59 and 60) show the general appearance of an edgewise strip reflector, as well as the method of mounting and bracing it.

Weight Estimate

The total weight of the prototype antenna is currently estimated at 1050 lbs, distributed as follows:

TABLE 5
Estimated Weight of Prototype
Scanner Components

Outer cone	200 lbs.
Inner cone, with shell	175 lbs.
Motor and gears	215 lbs.
Scanner mounting tube	120 lbs.
Reflector, with bracing	90 lbs.
Transmitters and receivers	250 lbs.
Total	1050 lbs.

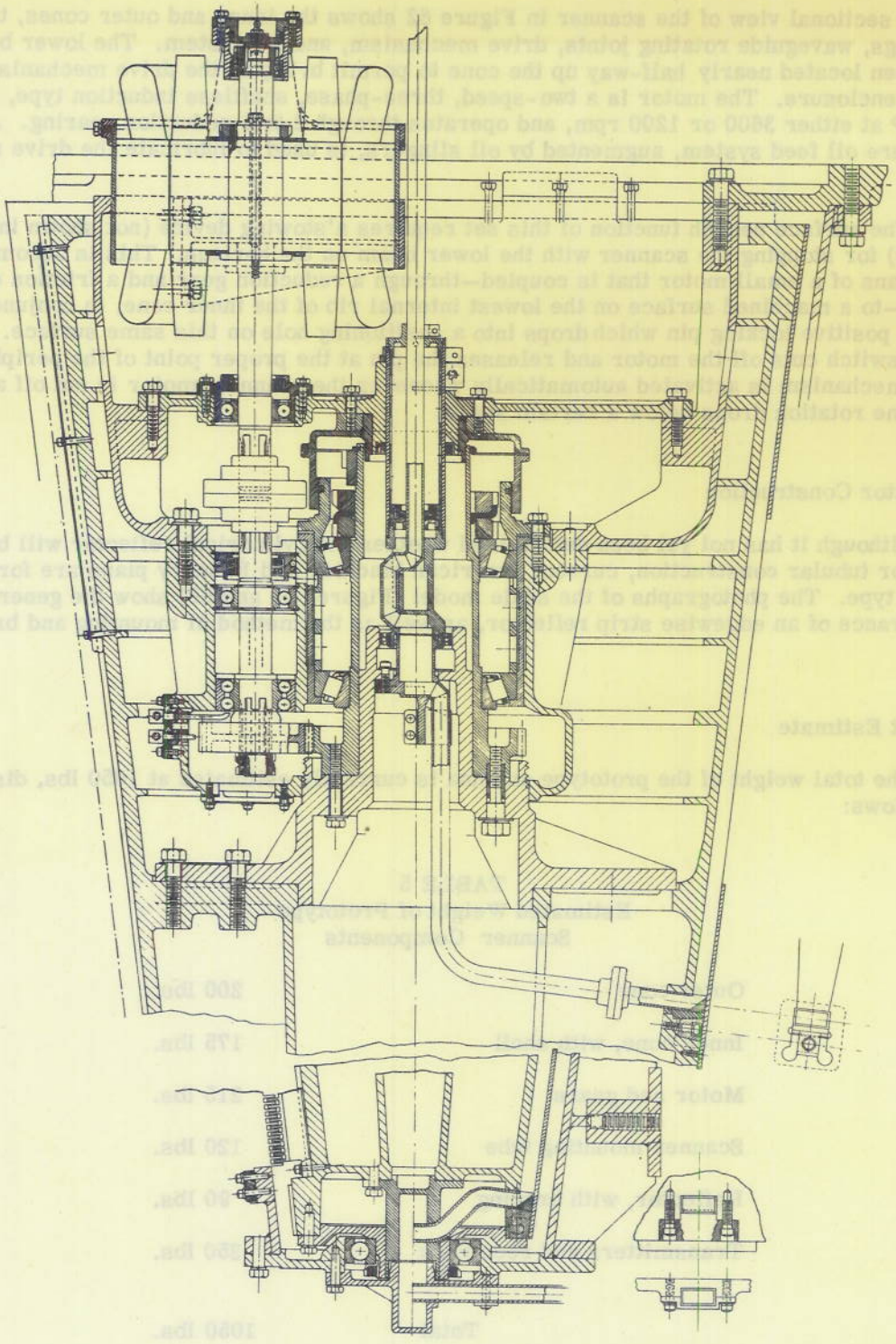

Figure 62 - Lateral section of AMF scanner showing motor drive and waveguide rotating joints

MAGNESIUM CORROSION PROTECTION

Protective Coatings

The problem of protecting the SPS-3 antenna from corrosion is unique since the coatings used internally, in addition to providing adequate protection, must have low r-f loss. Considerable research has been done on developing anticorrosive coatings for magnesium aircraft parts in marine atmosphere. The Protective Coatings Branch of the Chemistry Division at the Naval Research Laboratory has issued three reports[12] on results of salt-spray and tide-range tests on panels bearing coatings which it developed. The coatings which were found to be good will be quite suitable for use on the external parts of the scanner. However, the most suitable primers contain metallic ions, and cannot be used internally because of the r-f loss introduced. Therefore it has been necessary to conduct tests in order to find a coating with low loss and good corrosion protection. These tests included investigation of suitable surface treatments, primers, and top coatings.

It was observed by H. J. E. Seagrave that surface treatment produced a marked improvement on the adherence of the prime coating at the cost of salt water corrosion. That is, surface treated panels normally corroded sooner than panels with no surface treatment, but the prime coat scaled from the latter and did not scale from treated samples. It was concluded that surface treatment, therefore, delays the start of corrosion by increasing the adherence of the prime coating. Two surface treatments appear to be suitable for use on the Foster scanner. The first of these is the Manodyz process developed by Hanson-Van Winkle-Munning Company. This process, formerly called Consolidated-Vultee #1, is an electro-chemical deposition process. Essentially, the technique is to anodyze the magnesium in a sodium hydroxide, waterglass, and phenol bath, which results in the formation of an oxide-silicate film on the metal. Only two jobbers in this country have facilities for Manodyzing a casting as large as the inner cone, and one of these would require the Navy to provide the necessary tanks. An alternative surface treatment is the standard sealed chrome pickle (Spec: AN-M-12a), which is a chemical process.

An excellent prime coating for external use is the standard zinc chromate primer (Spec: AN-TT-P-656b). H. J. E. Seagrave found the addition of 1 percent magnesium chromate to the primer to be quite effective for use on magnesium. The presence of zinc or magnesium ions in a primer, however, precludes its use internally. A primer which can be used internally as well as externally is Woolsey's Wash Coat Primer.[13] In addition two alkyd and three vinyl base primers developed in the Protective Coatings Branch are being considered. One of these is commercially available as Bakelite Primer M1.[14]

For the top-coating, a vinyl or alkyd resin may be used, depending on the type of primer used.

---

[12] *Seagrave, H. J. E. "Anticorrosive Coatings for Magnesium III," NRL Report C-3393, 7 December 1948 (Unclassified); Cowling, J. E. "Anticorrosive Coatings for Magnesium I," NRL Report P-2835, 15 May 1946 (Unclassified); Cowling J. E. and Freriks, R. "Anticorrosive Coatings for Magnesium II," NRL Report P-3012, 10 December 1946 (Unclassified)*

[13] *C. A. Woolsey Paint & Color Company, 231 E. 42nd. St., New York, N. Y.*

[14] *Bakelite Corporttion, Bound Brook, New Jersey*

Salt-Spray Tests

In order to determine experimantally the effective corrosion protection of various coatings in salt water atmosphere, 4 x 6 inch panels of magnesium alloys FS-1a (DOW) were prepared with combinations of the surface treatments, prime, and top coatings, and submitted to exposure in a salt spraying chamber. The test panels were alternately sprayed for one minute and dried for four minutes for a period of 600 hours. The results will appear in a subsequent NRL report.

R-F Loss Measurements

For the purpose of determining the r-f loss introduced by any of these coatings, sample lengths of 1-1/4 x 5/8 inch magnesium waveguide were fabricated from magnesium sheet alloy FS-1a (DOW). The loss in untreated magnesium waveguide was measured as 0.242 db/meter. These samples were Manodyzed to determine the loss introduced by the surface treatment. However, poor coverage was obtained inside the guide, and the loss measurements were considered invalid. The Sylvania Corporation has measured the loss[15] due to Manodyz coating to be 0.258 db/meter, in 1 x 1/2 inch guide, at 3.2 centimeters. The loss due to zinc chromate has been measured at NRL as 0.66 db/meter. Magnesium waveguide has recently become commercially available and will be used for a series of r-f loss measurements on the most promising surface treatments.

ACKNOWLEDGMENTS

The authors wish to express their gratitude to Charles W. Price who made the design layouts and manufacturing drawings for the NRL scanner and its associated components.

A large number of the figures for this report were prepared by T. A. Lambert, who was also of great assistance in making measurements on the scanner and flat pillboxes.

---

[15] *Ltr. from Sylvania Corporation Electronic Division (Richard M. Walker, Development Engineer) to Naval Research Laboratory dated 21 October 1947*

* * *

APPENDIX I
Calculation for Forming Edgewise-Strip Reflector

The reflector is represented in Figure 63 as the parabolic cylinder $y^2 = 4fx'$, inclined at an angle θ to the vertical. The front edge of a typical strip conforms to the intersection of the cylinder with the X'Y plane, and P is a typical point on this curve. When the curve of intersection is projected onto the XY and YZ planes, the curves $y^2 = 4fx \sec\theta$ and $y^2 = 4fz \csc\theta$ result.

It is necessary to determine the curve $\eta(x)$ to which a strip may be cut in the XY plane such that after suitable rolling—on rollers parallel to the X-axis—it will fall into its proper position in the reflector. Evidently the rolling operation will not affect the x-coordinate of any point on the strip. This is implicit in the indicated coordinates of the point B on the flat strip corresponding to point P.

Since the strip undergoes no stretching, η is equal to the arc length of the curve $y^2 = 4fz \csc\theta$ from the origin to the point c,

$$\left.\begin{aligned} \eta &= \int_0^y \sqrt{1 + \left(\frac{dz}{dy}\right)^2}\, dy \\ &= \frac{y}{2}\sqrt{1 + \frac{y^2 \sin^2\theta}{4f^2}} + f \csc\theta \sinh^{-1}\left(\frac{y \sin\theta}{2f}\right). \end{aligned}\right\} \quad (25)$$

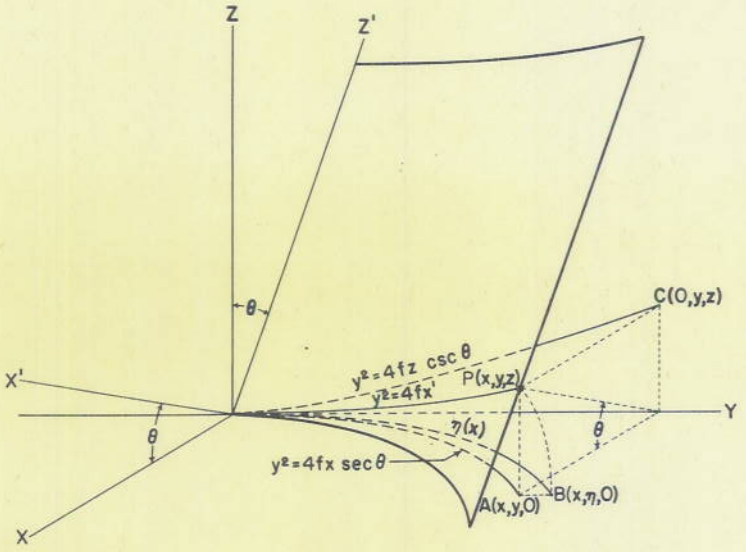

Figure 63 - Development of strips for inclined reflector

But

$$y = 2\sqrt{fx \sec \theta}, \tag{26}$$

so that

$$\eta\,(x) = x\sqrt{\tan^2 \theta + \frac{f}{x} \sec \theta} + f \csc \theta \sinh^{-1}\sqrt{\frac{x}{f} \sin \theta \tan \theta}. \tag{27}$$

* * *

APPENDIX II
Method of Calculating Templates for Pillboxes

Introduction

The process of wrapping the pillboxes onto the cone is complicated by their finite aperture in the E-plane. Evidently the surfaces of the parabolic mirrors and straight barriers must be perpendicular to the cone to conform to the TEM mode field configuration. But when a pillbox is constructed in this way, the mirror can be made truly parabolic on only one level; if it is parabolic on the lower surface, it will have a quite different shape on the upper surface. In order to keep such errors to a minimum, the pillboxes for this scanner have been defined on a "mid-surface" development, taken half-way between the two levels. The parabolic mirrors and straight barriers shown in Figure 64 must be projected onto the upper and lower level cones to obtain templates that can be used in manufacture. The upper surface template is needed to lay out the curves before machining, while the lower surface template is used to check the finished work.

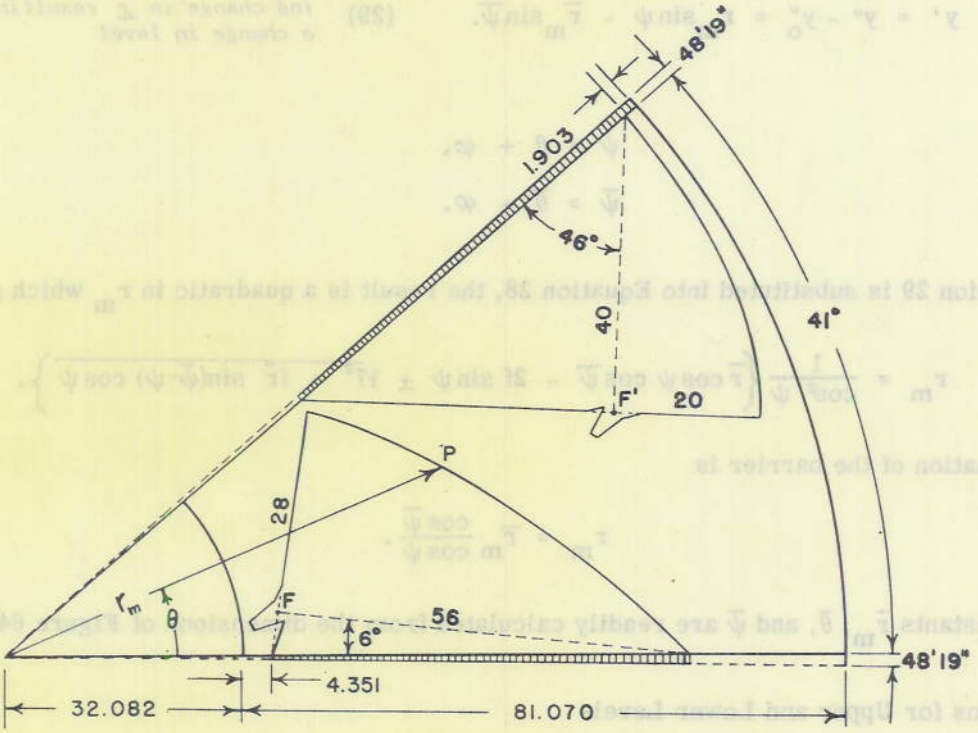

Figure 64 - Development showing location of pillboxes on mid-surface

Method of Changing Level

The projection of a given curve from one level to another is easily described in terms of polar coordinates r and θ on the developed cones. Subscripts u, m, and ℓ may be used to distinguish the radius vector for the upper, mid, and lower levels. The θ coordinate does not change along a line segment P normal to the cone (Figures 64 and 65), but r is increased or decreased by d/2 cot α in going from the mid surface to the upper or lower surface. Since d is one-half inch and $\alpha = 6^\circ\ 47'\ 51''$, the increment amounts to 2.097 inches.

Polar Equations for Mirrors and Barriers

The boundaries of the upper and lower pillboxes may be expressed in polar form with the aid of the coordinate systems shown in Figures 66A and 67A respectively, which represent mid-surface developments. The equation of either parabola is

$$x'^2 = 4f(y' - f). \tag{28}$$

This can be written in terms of x″, y″ through the relations

$$\begin{aligned} x' &= x'' - x''_o = r_m \cos\psi - \bar{r}_m \cos\bar{\psi}, \\ y' &= y'' - y''_o = r_m \sin\psi - \bar{r}_m \sin\bar{\psi}. \end{aligned} \tag{29}$$

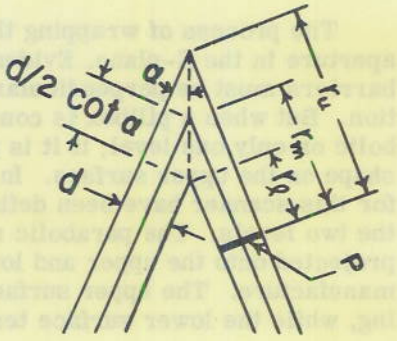

Figure 65 - Lateral section showing change in r resulting from a change in level

where

$$\begin{aligned} \psi &= \theta + \varphi, \\ \bar{\psi} &= \bar{\theta} + \varphi. \end{aligned} \tag{30}$$

If Equation 29 is substituted into Equation 28, the result is a quadratic in r_m which gives

$$r_m = \frac{1}{\cos^2\psi}\left\{\bar{r}\cos\psi\cos\bar{\psi} - 2f\sin\psi \pm \sqrt{f^2 + f\bar{r}\,\sin(\bar{\psi}-\psi)\cos\psi}\right\}. \tag{31}$$

The equation of the barrier is

$$r_m = \bar{r}_m \frac{\cos\bar{\psi}}{\cos\psi}. \tag{32}$$

The constants $\bar{r}_m$, $\bar{\theta}$, and $\bar{\psi}$ are readily calculated from the dimensions of Figure 64.

Equations for Upper and Lower Levels

The radius vector for the upper and lower levels are given by

$$\begin{aligned} r_u &= r_m + 2.097, \\ r_\ell &= r_m - 2.097, \end{aligned} \tag{33}$$

while the value of θ is unchanged. Rectangular coordinates for either of the new levels (Figures 66B and 67B) are obtained from the relations

$$\begin{Bmatrix} x_u \\ x_l \end{Bmatrix} = \begin{Bmatrix} r_u \\ r_l \end{Bmatrix} \cos\theta \,,$$

$$\begin{Bmatrix} y_u \\ y_l \end{Bmatrix} = \begin{Bmatrix} r_u \\ r_l \end{Bmatrix} \sin\theta \,. \qquad (34)$$

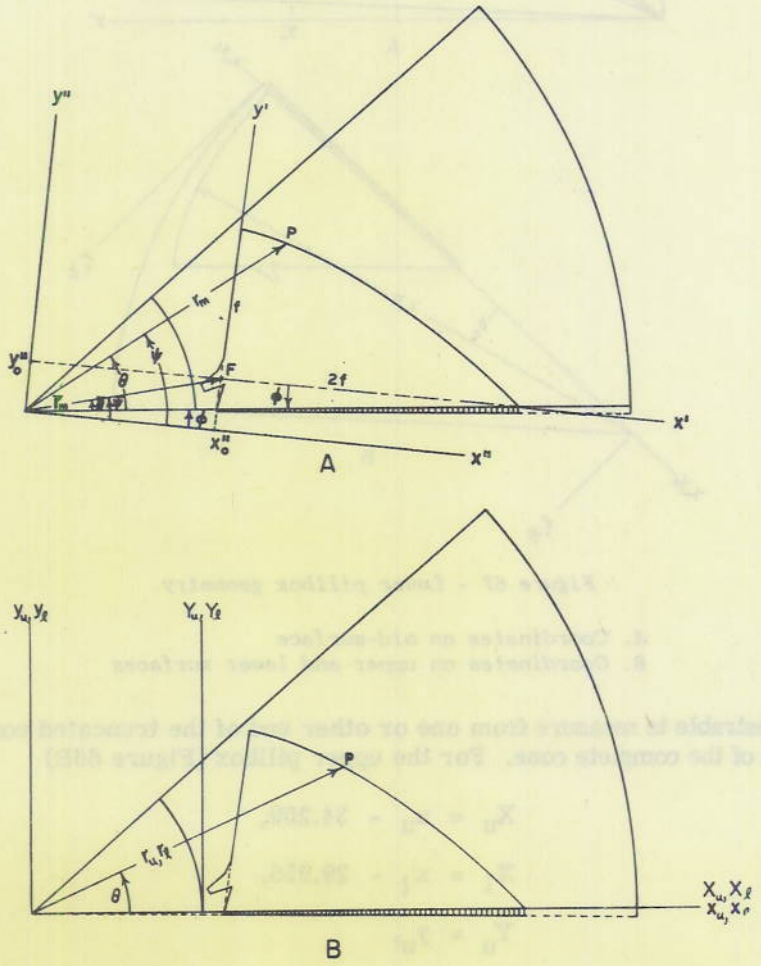

Figure 66 - Upper pillbox geometry

A. Coordinates on mid-surface
B. Coordinates or upper and lower surfaces

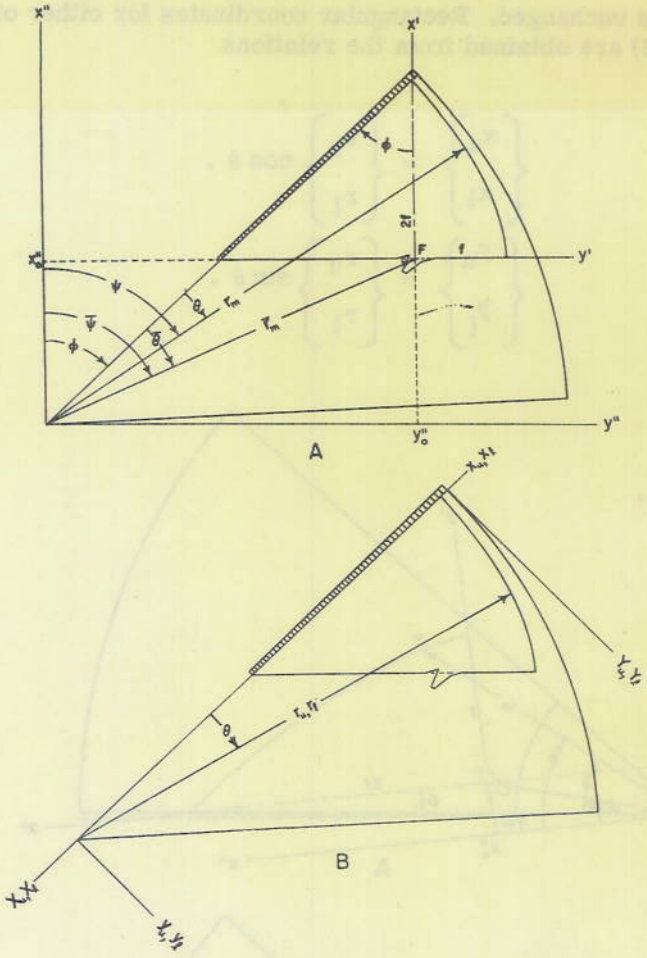

Figure 67 - Lower pillbox geometry

A. Coordinates on mid-surface
B. Coordinates on upper and lower surfaces

Finally, it is desirable to measure from one or other end of the truncated cone, rather than from the vertex of the complete cone. For the upper pillbox (Figure 66B)

$$X_u = x_u - 34.209,$$
$$X_l = x_l - 29.955,$$
$$Y_u = y_u,$$
$$Y_l = y_l, \qquad (35)$$

while for the lower pillbox (Figure 67B),

$$X_u = 115.279 - x_u,$$

$$X_l = 111.025 - x_l,$$

$$Y_u = y_u,$$

$$Y_l = y_l. \qquad (36)$$

Tables

In Tables 6, 7, 8, and 9 are listed lower-surface coordinates for the mirror and barrier of each pillbox. A sufficient number of significant figures was carried in the calculations to ensure that the results are accurate to 0.001 inch. Tables 10 and 11, together with Figure 68, is included to show the location of the feed horns.

Lower Pillbox

Contour of Parabolic Mirror

TABLE 6
Coordinates of the Parabolic Mirror of the Lower Pillbox

θ		r_m	r_l	X_l	Y_l
0°		111.2471 in.	109.1498 in.	1.8750 in.	0.0000 in.
1		111.2912	109.1839	1.8577	1.9055
2		111.3136	109.2163	1.8752	3.8115
3		111.3432	109.2459	1.9288	5.7175
4		111.3673	109.2700	2.0212	7.6222
5		111.3846	109.2873	2.1535	9.5250
6		111.3919	109.2946	2.3291	11.4243
7		111.3865	109.2892	2.5504	13.3190
8		111.3666	109.2693	2.8191	15.2073
9		111.3174	109.2201	3.1496	17.0857
10		111.2704	109.1731	3.5105	18.9577
11		111.1884	109.0911	3.9382	20.8156
12		111.0798	108.9825	4.4240	22.6588
13		110.9400	108.8427	4.9719	24.4843
14		110.7668	108.6695	5.5834	26.2895
15		110.5568	108.4595	6.2611	28.0714
16		110.3058	108.2085	7.0083	29.8263
17		110.0101	107.9128	7.8274	31.5507
18		109.6663	107.5690	8.7207	33.2406
19		109.2717	107.1744	9.6896	34.8926
20		108.8236	106.7263	10.7350	36.5025
21		108.3174	106.2201	11.8600	38.0659
22		107.1242	105.0269	14.3472	41.0373
	Vertex 23° 33′ 35″	Vertex 106.7462	Vertex 104.6489	Vertex 15.0992	Vertex 41.8287
	Focal point 19° 01′ 19″	Focal point 88.2814	Focal point 86.1841	Focal point 29.5471	Focal point 28.0900

Lower Pillbox

Contour of Straight Barrier

TABLE 7
Coordinates of the Straight Barrier of the Lower Pillbox

θ		r_m	r_l	X_l	Y_l
0°		53.6650	51.5680	59.4570	0.0000
1		54.6612	52.5642	58.4688	0.9174
2		55.7124	53.6154	57.4423	1.8711
3		56.8224	54.7254	56.3746	2.8641
4		57.9956	55.8986	55.2626	3.8993
5		59.2367	57.1397	54.1027	4.9801
6		60.5509	58.4539	52.8913	6.1101
7		61.9440	59.8470	51.6241	7.2935
8		63.4226	61.3256	50.2962	8.5349
9		64.9937	62.8967	48.9027	9.8392
10		66.6654	64.5684	47.4375	11.2122
11		68.4469	66.3499	45.8941	12.6602
12		70.3480	68.2510	44.2654	14.1902
13		72.3807	70.2837	42.5427	15.8104
14		74.5577	72.4607	40.7167	17.5298
15		76.8938	74.7968	38.7768	19.3588
16		79.4060	77.3090	36.7018	21.3092
17		82.1137	80.0167	34.5046	23.3946
18		85.0394	82.9424	32.1420	25.6306
19		88.2093	86.1123	29.6042	28.0354
20		91.6535	89.5565	26.8694	30.6301
21		95.4079	93.3109	23.9118	33.4396
22		99.5146	97.4176	20.7010	36.4933
23		104.0239	101.9269	17.2008	39.8260
	Vertex 23° 33′ 35″	Vertex 106.7456	Vertex 104.6486	Vertex 15.0995	Vertex 41.8286

Upper Pillbox

Controur of Parabolic Mirror

TABLE 8
Coordinates of the Parabolic Mirror of the Upper Pillbox

θ		r_m	r_l	X_l	Y_l
0°		92.7414	90.6441	60.6891	0.0000
1		91.4453	89.3480	59.3794	1.5593
2		90.1780	88.0807	58.0720	3.0740
3		88.9374	86.8401	56.7661	4.5449
4		87.7225	85.6252	55.4616	5.9729
5		86.5317	84.4344	54.1581	7.3589
6		85.3635	83.2662	52.8551	8.7037
7		84.2169	82.1196	51.5525	10.0079
8		83.0905	80.9932	50.2500	11.2721
9		81.9831	79.8858	48.9473	12.4969
10		80.8935	78.7962	47.6441	13.6828
11		79.8206	77.7233	46.3403	14.8303
12		78.7632	76.6659	45.0356	15.9397
13		77.7206	75.6233	43.7301	17.0115
14		76.6914	74.5941	42.4233	18.0459
15		75.6745	73.5772	41.1151	19.0432
16		74.6694	72.5721	39.8058	20.0036
17		73.6749	71.5776	38.4950	20.9273
18		72.6901	70.5928	37.1827	21.8144
19		71.7147	69.6174	35.8695	22.6652
20		70.7470	68.6497	34.5546	23.4796
21		69.7873	67.6900	33.2391	24.2579
22		68.8338	66.7365	31.9220	24.9999
23		67.8872	65.7899	30.6049	25.7062
24		66.9460	64.8487	29.2872	26.3761
25		66.0096	63.9123	27.9692	27.0105
26		65.0778	62.9805	26.6515	27.6088
27		64.1500	62.0527	25.3344	28.1713
28		63.2264	61.1291	24.0188	28.6984
29		62.3058	60.2085	22.7045	29.1897
30		61.3889	59.2916	21.3930	29.6458
31		60.4749	58.3776	20.0844	30.0667
32		59.5640	57.4667	18.7794	30.4527
33		58.6563	56.5590	17.4794	30.8042
34		57.7510	55.6537	16.1840	31.1212
35		56.8497	54.7524	14.8955	31.4047
36		55.9537	53.8564	13.6157	31.6560
37		55.0572	52.9599	12.3407	31.8721
38		54.1668	52.0695	11.0763	32.0572
39		53.2814	51.1841	9.8225	32.2112
40		52.4008	50.3035	8.5797	32.3345
	Vertex 40° 07′ 55″	Vertex 52.2849	Vertex 50.1875	Vertex 8.4165	Vertex 32.3484
	Focal point 8° 58′ 42.5″	Focal point 37.5078	Focal point 35.4105	Focal point 5.0216	Focal point 5.5263

Upper Pillbox

Contour of Straight Barrier

TABLE 9

Coordinates of the Straight Barrier of the Upper Pillbox

θ	r_m	r_l	X_l	Y_l
0°	36.4330	34.3357	4.3807	0.0000
1	36.5055	34.4082	4.4480	0.6005
2	36.5895	34.4922	4.5162	1.2038
3	36.6851	34.5878	4.5854	1.8102
4	36.7924	34.6951	4.6556	2.4202
5	36.9116	34.8143	4.7268	3.0340
6	37.0429	34.9456	4.7992	3.6528
7	37.1865	35.0892	4.8726	4.2763
8	37.3426	35.2453	4.9479	4.9052
9	37.5116	35.4143	5.0233	5.5400
10	37.6936	35.5963	5.1005	6.1812
11	37.8890	35.7917	5.1791	6.8294
12	38.0980	36.3007	5.2590	7.4850
13	38.3212	36.2239	5.3405	8.1486
14	38.5588	36.4615	5.4234	8.8208
15	38.8112	36.7139	5.5079	9.5023
16	39.0790	36.9817	5.5941	10.1935
17	39.3625	37.2652	5.6819	10.8953
18	39.6624	37.5651	5.7715	11.6083
19	39.9791	37.8818	5.8629	12.3331
20	40.3134	38.2161	5.9564	13.0707
21	40.6657	38.5684	6.0517	13.8217
22	41.0369	38.9396	6.1492	14.5870
23	41.4276	39.3303	6.2487	15.3676
24	41.8387	39.7414	6.3506	16.1643
25	42.2710	40.1737	6.4547	16.9781
26	42.7256	40.6283	6.5015	17.8103
27	43.2034	41.1061	6.6708	18.6618
28	44.7054	41.6081	6.7828	19.5338
29	44.2328	42.1355	6.8888	20.4228
30	44.7869	42.6896	7.0153	21.3448
31	45.3691	43.2718	7.1019	22.2660
32	45.9808	43.8835	7.2603	23.2547
33	46.6237	44.5264	7.3800	24.2508
34	47.2993	45.2020	7.5192	25.2766
35	48.0097	45.9124	7.6542	26.3343
36	48.7568	46.6595	7.7933	27.4258
37	49.5429	47.4456	7.9367	28.5535
38	50.3704	48.2731	8.0847	29.7199
39	51.2418	49.1445	8.2374	30.9276
40	52.1600	50.0627	8.3953	32.1797
Vertex 40° 07′ 55″	Vertex 52.2848	Vertex 50.1875	Vertex 8.4165	Vertex 32.3484

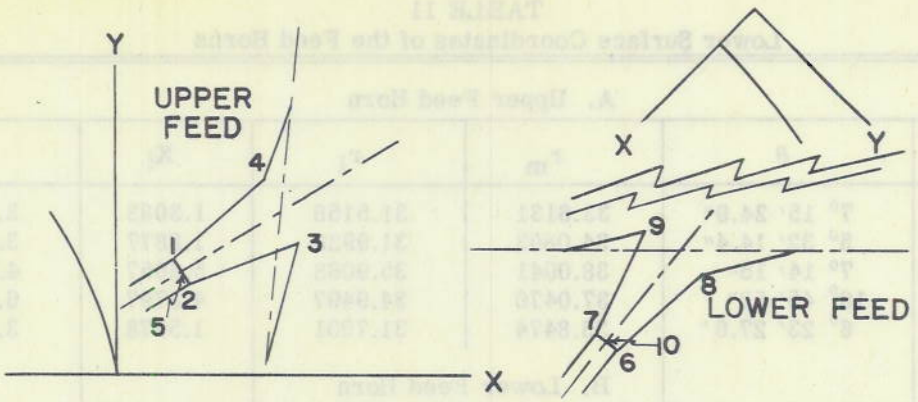

Figure 68 - Coordinates on pillbox feeds

TABLE 10
Upper Surface Coordinates of the Feed Horns

A. Upper Feed Horn

Point	θ	r_m	r_u	X_u	Y_u
1	7° 15′ 24.9″	33.6131	35.7104	1.2153	4.5109
2	5° 32′ 14.4″	34.0893	36.1866	1.8087	3.4918
3	7° 14′ 15″	38.0041	40.1014	5.5729	5.0521
4	10° 45′ 53″	37.0470	39.1443	4.2465	7.3112
5	6° 23′ 27.6″	33.8474	35.9447	1.5123	4.0011

B. Lower Feed Horn

6	20° 36′ 10.8″	85.0257	87.1230	33.7280	30.6578
7	19° 56′ 10.8″	84.4857	86.5830	33.8847	29.5227
8	19° 44′ 12″	88.8659	90.9632	29.6595	30.7181
9	18° 17′ 52″	88.0184	90.1157	29.7198	28.2923
10	20° 16′ 17.7″	84.7543	86.8516	33.8069	30.0915

TABLE 11
Lower Surface Coordinates of the Feed Horns

Point	θ	r_m	r_l	X_l	Y_l
		A. Upper Feed Horn			
1	7° 15′ 24.9″	33.6131	31.5158	1.3083	3.9810
2	5° 32′ 14.4″	34.0893	31.9920	1.8877	3.0870
3	7° 14′ 15″	38.0041	35.9068	5.6657	4.5236
4	10° 45′ 53″	37.0470	34.9497	4.3797	6.5278
5	6° 23′ 27.6″	33.8474	31.7501	1.5978	3.5342
		B. Lower Feed Horn			
6	20° 36′ 10.8″	85.0257	82.9284	33.4006	29.1817
7	19° 56′ 10.8″	84.4857	82.3884	33.5740	28.0924
8	19° 44′ 12″	88.8659	86.7686	29.3537	29.3016
9	18° 17′ 52″	88.0184	85.9211	29.4483	26.9754
10	20° 16′ 17.7″	84.7543	82.6570	33.4877	28.6382

* * *